

INFORMATION TO USERS

This manuscript has been reproduced from the microfilm master. UMI films the text directly from the original or copy submitted. Thus, some thesis and dissertation copies are in typewriter face, while others may be from any type of computer printer.

The quality of this reproduction is dependent upon the quality of the copy submitted. Broken or indistinct print, colored or poor quality illustrations and photographs, print bleedthrough, substandard margins, and improper alignment can adversely affect reproduction.

In the unlikely event that the author did not send UMI a complete manuscript and there are missing pages, these will be noted. Also, if unauthorized copyright material had to be removed, a note will indicate the deletion.

Oversize materials (e.g., maps, drawings, charts) are reproduced by sectioning the original, beginning at the upper left-hand corner and continuing from left to right in equal sections with small overlaps. Each original is also photographed in one exposure and is included in reduced form at the back of the book.

Photographs included in the original manuscript have been reproduced xerographically in this copy. Higher quality 6" x 9" black and white photographic prints are available for any photographs or illustrations appearing in this copy for an additional charge. Contact UMI directly to order.

UMI

A Bell & Howell Information Company
300 North Zeeb Road Ann Arbor MI 48106-1346 USA
313 761-4700 800 521-0600

University of Nevada

Reno

In-situ Formation of SiC in Al-Si Melt

A dissertation submitted in partial fulfillment of the requirements for the degree of
Doctor of Philosophy in Metallurgical Engineering

by

Dmitry M. Kocherginsky

Professor Ramana G. Reddy

Dissertation Advisor

May 1995

UMI Number: 9536438

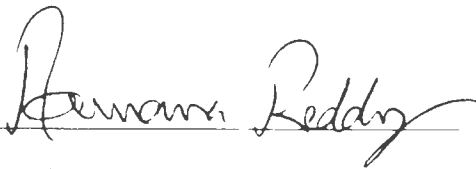
UMI Microform 9536438
Copyright 1995, by UMI Company. All rights reserved.

This microform edition is protected against unauthorized
copying under Title 17, United States Code.

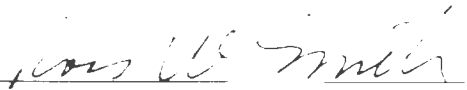
UMI

300 North Zeeb Road
Ann Arbor, MI 48103

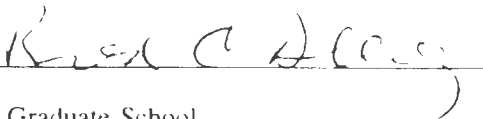
The dissertation of Dmitry M. Kocherginsky is approved



Dissertation Advisor



Department Chair



Dean, Graduate School

University of Nevada

Reno

May 1995

ACKNOWLEDGEMENTS

I would like to express my sincere gratitude and appreciation to Dr. R. G. Reddy for his guidance and encouragement during the course of this study.

I also would like to thank Dr. D. Chandra, Dr. R. Bradt, Dr. L. C. Hsu, Dr. M. Pinsky, and Dr. R. Bautista for their advise, criticism and interest in this work.

Special thanks for constant help to Mr. L. Grasseschi and Mr. D. Meredith and my friends Dr. S. Kumar and Mr. S. Brown, Mr. P. Velu, and Mr. C. Mulgrew.

Financial support by the Department of Chemical and Metallurgical Engineering, National Science Foundation and Pyrometallurgical Processing and Extraction of Metals (a consortium of metal industries) is greatly appreciated.

Finally, I would like to thank my wife for her loving support and patience.

ABSTRACT

Al/SiC composite is identified as a potential material for automotive and electronic packaging applications. Conventional method of Al-SiC composite processing includes incorporation of SiC particles into Al alloy. SiC is produced as a result of reaction between silica and carbon at temperatures higher than 2500 K for 48 hours. Because of high price of SiC the whole composite becomes very expensive.

The goal of this work was to develop a low cost method of Al-SiC processing using in-situ reactions at temperatures around 1500 K and carbon as a precursor material for SiC formation.

Thermodynamic analysis of Al-Si-C system was performed using Gibbs energy minimization method. Equilibrium species distribution diagrams were constructed for a wide range of alloys, temperatures and carbon concentrations. It was found that Al-SiC composite, containing 24-40% of SiC may be produced as a result of reaction between carbon and Al-Si alloy containing 30-50% Si.

Experimental study on in-situ formation of SiC in Al-Si alloys was conducted using three different carbon sources. Results of experiments were analyzed using X-ray diffraction, SEM-EDAX system and LECO carbon analyzer. When natural gas was introduced into the melt it decomposed into carbon and hydrogen but most of the carbon was removed from the melt by Ar which served as a carrier gas. The small quantity of SiC which formed was floated to the surface of the melt. Overall efficiency of natural gas was very low and maximum of only 3% of SiC was achieved. When graphite rod was used as a carbon source both aluminum and silicon carbides were formed. Because

of the presence of aluminum carbide the material degraded in air and decomposed into powder in a few days.

When activated carbon particles were used as a carbon source the results of experiments were successful for the specific experimental conditions. Only silicon carbide was formed and no aluminum carbide was detected in any sample. The silicon carbide formed retained the size and the shape of initial carbon. Reaction proceeded from the surface to the center of carbon particles. The rate of reaction was described using Avrami equation. Al-Si-Ca oxides present in activated carbon as ash constituents were pushed out of SiC and precipitated on the boundaries between SiC and matrix alloy.

The main goal of this work: in-situ processing of Al/SiC composite was achieved and the results of experiments may be used for development of a new industrial technology.

CONTENTS

Section	Description	Page
	ACKNOWLEDGEMENTS	ii
	ABSTRACT	iii
	CONTENTS	v
	LIST OF TABLES	viii
	LIST OF FIGURES	x
1.	INTRODUCTION	1
2.	REVIEW OF THE LITERATURE	4
2.1	Characteristics of SiC	4
2.2	Production of SiC	4
2.3	Structure and Properties of SiC	9
2.4	Al-Si Alloys	11
2.5	Aluminum-Silicon-Magnesium-Copper-Casting Alloys	11
2.6	Phase Equilibria in the Al-Si-C System	13
2.7	Reactions in the Al/SiC Composite	17
2.8	Wetting, Solidification and Microstructure of Al/SiC Composites	22
2.9	Physical Properties of the Al/SiC Composites	27
2.10	Fiber Composites	30
2.11	In-Situ Composites	34
2.12	Composites Produced by Melt Oxidation	35

2.13	Al/TiC Composites	37
2.14	SiC/MoSi ₂ Composites	39
2.15	Theoretical Possibility to Form SiC In-Situ in Al-Si Alloy	41
2.16	Conclusions	41
2.17	RESEARCH OBJECTIVES	42
3.	THERMODYNAMIC CALCULATIONS	43
3.1	Introduction	43
3.2	Pure Al with SiC	46
3.3	Al-Si Alloy with SiC	57
3.4	Al-Si Alloy with Carbon	62
4.	EXPERIMENTAL PROCEDURE	76
4.1	Chemicals and Materials	76
4.2	High Temperature Furnace Set-up	76
4.3	Preparation of alloy	77
4.4	Reactions with Natural Gas	77
4.5	Reactions with Graphite Rod	80
4.6	Reactions with Activated Carbon Particles	80
4.7	X-ray Powder Diffraction	81
4.8	SEM-EDAX analysis	81
4.9	Chemical analysis	81
5.	EXPERIMENTAL RESULTS	83
5.1	EXPERIMENTAL TRIALS	83

5.1.1	Reaction with Natural Gas	83
5.1.2	Effect of Time, Temperature and Gas Composition	83
5.1.3	Conclusions on the Experiments with Natural gas	92
5.1.4	Reaction with Graphite Rod	92
5.1.5	Conclusions on the Experiments with Graphite Rod	99
5.1.6	Reaction with Activated Carbon	99
5.1.7	Conclusions on the Experiments with Activated Carbon	105
5.2.	MECHANISM OF SiC FORMATION	108
5.2.1	Characterization of Activated Carbon	108
5.2.2	Initial Stage of Carbon Reaction with the Melt	117
5.2.3	Intermediate Stage of Reaction	129
5.2.4	Final Stage of Reaction. Characterization of In-Situ Formed Al/SiC Composite	137
5.2.5	Reaction Rate	151
6.	SUMMARY AND CONCLUSIONS	157
7.	RECOMMENDATION	159
8.	REFERENCES	160
	APPENDIX 1	175
	APPENDIX 2	197

LIST OF TABLES

No.	TITLE	PAGE
1.	List of some composite components with proven potential	2
2.	Chemical compositions and typical applications for aluminum casting alloys	12
3.	Effect of SiC/Al ratio on the equilibrium species distribution	47
4.	Effect of temperature on the equilibrium species distribution	53
5.	Effect of temperature and SiC/Al ratio on the quantity of Al_4C_3	58
6.	Effect of Si concentration in Al alloy on the formation of Al_4C_3 (Al-20mol% SiC)	60
7.	Effect of temperature and carbon addition to 30mol%Si-70mol%Al alloy on the formation of SiC and Al_4C_3	65
8.	Effect of temperature and carbon addition to 40mol%Si-60mol%Al alloy on the formation of SiC and Al_4C_3	68
9.	Effect of temperature and carbon addition to 50mol%Si-50mol%Al alloy on the formation of SiC and Al_4C_3	69
10.	Results of Al-Si alloy analysis on carbon after reaction of 70wt%Al-30wt%Si alloy with natural gas at 1273K	85
11.	Results of Al-Si alloy analysis on carbon after reaction of 70wt%Al-30wt%Si alloy with natural gas (Ar-10%CH ₄) at 1473K	86
12.	Results of experiments on reaction between 70wt%Al-30wt%Si alloy and graphite rod at 1773K	100

13.	Results of experiments on reaction between 70wt% Al-30wt% Si alloy and activated carbon at 1573K	106
14.	Results of experiments on reaction between 60mol% Al-40mol% Si Alloy and activated carbon	152
15.	K and n values in Avrami equation	152

LIST OF FIGURES

No	TITLE	PAGE
1.	Structure of SiC: (a) cubic or β -SiC, (b) tetrahedral or α -SiC type 6H	10
2.	Al-Si phase diagram	14
3.	Al-C phase diagram	15
4.	Si-C phase diagram	16
5.	Al-Si-C phase diagram at 1273K	18
6.	Typical microstructure of the Al-SiC composite. Black particles - SiC, white matrix - Al alloy	26
7.	(a) Cross-sectional SEM micrograph of the SCS-6 fiber	31
	(b) Schematic drawing of the fiber microstructure	31
8.	SEM micrograph of the Al alloy composite reinforced with SiC fibers	32
9.	Effect of temperature on the silicon concentration in the melt	45
10.	Effect of SiC/Al ratio on the equilibrium species distribution in the system at 1073K	48
11.	Al-Si-C phase diagram with compositional path corresponding to addition of SiC to pure Al at 1073K	50
12.	Optical micrograph of an Al-SiC sample after reaction for 1h at 1270K	52
13.	XRD specter of Al-SiC sample reacted at 1270K for 1h	54
14.	Effect of temperature on the equilibrium species distribution.	

	initial SiC/Al=1	55
15.	Effect of temperature on the Al-Si-C phase diagram and compositional path corresponding to addition of SiC to pure Al	56
16.	Effect of SiC/Al mol ratio and temperature on the equilibrium mol fraction of Al_4C_3	59
17.	Effect of temperature and initial Si concentration in Al alloy on the equilibrium mol fraction of Al_4C_3	61
18.	Effect of silicon alloying of aluminum on the compositional path corresponding to addition of SiC to alloy at 1073K	63
19.	Optical micrograph of SiC particles heated for 1h at 1270K in the presence of Al-Si alloy containing 20mol% Si	64
20.	Effect of carbon addition to the 70mol%Al-30mol%Si alloy on the equilibrium species distribution in the system at 1473K	66
21.	Effect of initial Al-Si alloy composition and carbon addition to the alloy on the formation of SiC and Al_4C_3 at 1473K	70
22.	Effect of Si concentration in Al alloy on the compositional path corresponding to in-situ formation of SiC at 1473K	72
23.	Effect of temperature and carbon addition to the 70mol%Al- 30mol%Si alloy on the formation of SiC and Al_4C_3	73
24.	Effect of temperature on the Al-Si-C phase diagram and compositional path corresponding to addition of carbon to 70mol%Al-30mol%Si alloy	74

25.	Temperature profile of the furnace	78
26.	Experimental setup	79
27.	X-ray diffraction pattern of the sample with 0.3wt% carbon after 1 hour of reaction of natural gas with 70wt% Al-30wt% Si alloy	84
28.	Effect of reaction time and partial pressure of natural gas on carbon concentration in the melt at 1273K	87
29.	Typical SEM images of the sample after the reaction of natural gas with 70wt% Al-30wt% Si alloy	89
30.	Effect of reaction time and temperature on carbon concentration in the melt for 90% Ar - 10% CH ₄ gas mixture	90
31.	Effect of temperature on the species distribution in the C-H system for 100% CH ₄ gas	91
32.	SEM image in backscattered electrons of the reaction zone on the graphite rod with magnification 15X	93
33.	SEM image in backscattered electrons of the reaction zone on the graphite rod with magnification 140X	94
34.	SEM image in backscattered electrons of the reaction zone on the graphite rod with magnification 350X	95
35.	EDS spectra corresponding to the average concentration of the reaction zone (Fig. 34) on the graphite rod	96
36.	EDS spectra of the reaction zone (Fig. 34) on the graphite rod at point 1	97

37.	EDS spectra of the reaction zone (Fig. 34) on the graphite rod at point 2	98
38.	SEM image in backscattered electrons of a SiC particle	101
39.	Energy spectra of the SiC particle	102
40.	SEM image in backscattered electrons of several SiC particles	103
41.	SEM image in backscattered electrons of a non-completely reacted particle with a carbon core	104
42.	A photograph of as received activated carbon particles	109
43.	SEM image in backscattered electrons of an activated carbon particle, magnification 200X	110
44.	SEM image in backscattered electrons of a pore in activated carbon particle, magnification 1000X	111
45.	SEM image in backscattered electrons of a dense part of activated carbon particle, magnification 1000X	112
46.	EDS spectra of an activated carbon particle	113
47.	Schematic representation of the microstructure of activated carbon	116
48.	Microstructure of the alloy after incorporation of carbon at 1473K for 1 hour, SEM image in backscattered electrons	118
49.	Microstructure of the alloy after incorporation of carbon at 1473K for 1 hour, SEM image in secondary electrons	119
50.	SEM image in secondary electrons of one carbon particle after reaction at 1473K for 1 hour	120

51.	SEM image in backscattered electrons of one carbon particle after reaction at 1473K for 1 hour	121
52.	Microstructure of the interface between the carbon and matrix alloy after reaction at 1473K for 1 hour, SEM image in backscattered electrons	122
53.	Microstructure of the interface between the carbon and matrix alloy, after reaction at 1473K for 1 hour, SEM image in secondary electrons	123
54.	The microstructure of Al-Si eutectic in the matrix alloy after reaction at 1473K for 1 hour, SEM image in secondary electrons	124
55.	EDS spectra of primary Si crystals from Figure 54	125
56.	EDS spectra of Al-Si eutectic mixture from Figure 54	126
57.	EDS spectra of Si crystals in eutectic mixture from Figure 54	127
58.	EDS spectra of aluminum crystals in eutectic mixture from Figure 54	128
59.	A micrograph of several partly reacted carbon particles after reaction at 1373K for 6 hours, SEM image in backscattered electrons	130
60.	A micrograph of several partly reacted carbon particles after reaction at 1373K for 6 hours, SEM image in secondary electrons	131
61.	Partly reacted carbon particle after reaction at 1373K for 6 hours, SEM image in backscattered electrons	132
62.	Reaction zone on the partly reacted carbon particle after reaction at 1373K for 6 hours, SEM image in backscattered electrons	133
63.	A micrograph of the interface between carbon and matrix alloy	

51.	SEM image in backscattered electrons of one carbon particle after reaction at 1473K for 1 hour	121
52.	Microstructure of the interface between the carbon and matrix alloy after reaction at 1473K for 1 hour, SEM image in backscattered electrons	122
53.	Microstructure of the interface between the carbon and matrix alloy, after reaction at 1473K for 1 hour, SEM image in secondary electrons	123
54.	The microstructure of Al-Si eutectic in the matrix alloy after reaction at 1473K for 1 hour, SEM image in secondary electrons	124
55.	EDS spectra of primary Si crystals from Figure 54	125
56.	EDS spectra of Al-Si eutectic mixture from Figure 54	126
57.	EDS spectra of Si crystals in eutectic mixture from Figure 54	127
58.	EDS spectra of aluminum crystals in eutectic mixture from Figure 54	128
59.	A micrograph of several partly reacted carbon particles after reaction at 1373K for 6 hours, SEM image in backscattered electrons	130
60.	A micrograph of several partly reacted carbon particles after reaction at 1373K for 6 hours, SEM image in secondary electrons	131
61.	Partly reacted carbon particle after reaction at 1373K for 6 hours, SEM image in backscattered electrons	132
62.	Reaction zone on the partly reacted carbon particle after reaction at 1373K for 6 hours, SEM image in backscattered electrons	133
63.	A micrograph of the interface between carbon and matrix alloy	

74.	EDS spectra at point 2 of Figure 71	146
75.	EDS spectra at point 3 of Figure 71	147
76.	Microstructure of SiC. SEM image in secondary electrons	148
77.	Microstructure of the interface between SiC and matrix alloy with low concentration of oxides after reaction at 1573K for 6 hours. SEM image in backscattered electrons	150
78.	Transformation kinetics of carbon into silicon carbide	153
79.	Effect of time and temperature on the transformation of carbon into silicon carbide	155
80.	Correlation between $\ln K$ and $1/T$	156
81.	Activity of Si in dilute Al-Si solution	197

1. INTRODUCTION

Composite materials are defined as material systems combining two or more dispersed material phases, each of which maintains its own distinct volumetric region and properties [1].

Discontinuously reinforced aluminum composites are aluminum based materials reinforced by particles, whiskers, or short fibers [2]. They are rapidly emerging as new commercial materials for aerospace and other high-performance markets. In many stiffness-, strength-and weight-critical applications, they can offer higher performance than traditional aluminum alloys at potentially low cost than organic matrix composites [3]. The most inexpensive composites and, therefore, those of most interest to the industry are produced via molten metal routes [4].

Metal matrix composites (MMCs) have tremendous potential for the future. They are an important class of materials with a long history of commercial applications. Particulate MMCs have been used in internal combustion engines. Toyota is using alumina discontinuous fibers in aluminum for diesel engine pistons. Suzuki used SiC whiskers in aluminum for outboard engine pistons. Honda is using discontinuous fibers of carbon and alumina in aluminum for automotive engine blocks [1]. These and other applications are listed in Table 1 [5].

The interface between reinforcements and the matrix is undoubtedly one of the most important features in a composite system. It affects the mechanical properties of the composite through mechanisms such as debonding, stress damping, crack deviation, and grain boundary pinning [6]. From a thermodynamic point of view, it is extremely

Table 1 List of some composite components with proven potential [5]

Composite	Components	Benefits	Manufacturers
Al-SiC(particles)	Piston	Reduced weight, high strength and wear resistance	Duralcan, Martin Marietta, Lanxide
	Brake rotor, caliper, liner	high wear resistance and reduced weight	Duralcan, Lanxide
	Shaft	Reduction of weight and high specific stiffness	GKN, Duralcan
Al-SiC(whiskers)	Connecting rod	Reduced mass, high specific strength, stiffness and low CTE	Nissan

difficult to design a composite in which the matrix-reinforcement interfaces will remain stable under all possible conditions [7]. During its entire life, a composite member may encounter fabrication and service temperatures in the range of 0-1000K, and, hence, may exhibit phase transformations, significant changes in solubility, differential dilations, or chemical interaction between the matrix and the reinforcement members, all of which can cause the interface to be unstable. Since it is unlikely that any number of candidate composite materials will produce a composite in which the interfaces are stable, materials must be chosen for interfacial stability [7].

During the design of high-temperature metal-matrix composites, both the thermodynamics and the kinetics of the proposed system should be considered. Thermodynamic phase-equilibria data can aid in identifying matrix and reinforcement materials that are interfacially more stable than other candidate materials, whereas reaction kinetics data can be employed to estimate the rate of any reaction that may occur at interfaces [7].

To control the extent of interfacial reaction, common practices include shortening processing time, coating reinforcements with materials of different reactivities, and adding alloying elements to the matrix [5].

Naturally stable composites are those produced in-situ. The in-situ processing for non-ferrous and intermetallic systems eliminates interface incompatibility of matrices with reinforcements by creating more thermodynamically stable reinforcements based on their nucleation and growth from the parent matrix phase [8]. By controlling reaction chemistry, a hierarchical range of carbides, nitrides, oxides, borides, and even silicides

can be generated. One of the major, fundamental scientific challenges lies in controlling the materials synthesis through optimized reaction kinetics and interfacial design [8].

The objective of this work was to study the fundamentals of processing of Al-Si alloy composite reinforced with in-situ produced silicon carbide. This work includes thermodynamic analysis of Al/SiC composite and experimental verification of the findings. These aspects are discussed in details in the following sections.

2. REVIEW OF THE LITERATURE

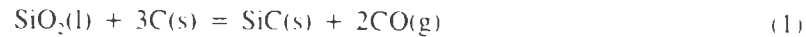
2.1 Characteristics of SiC

Silicon carbide is an optimal reinforcement for aluminum because it has density only slightly higher than aluminum, a high modulus and strength, and is readily available [9]. The SiC is best known for its hardness (9-10 on Mohs scale, or 25GPa indentation hardness), but it is also a good electrical and thermal conductor [10]. Annual world production of silicon carbide is today in the region of 500,000 tons. Much of this is used as the basis for grinding, cutting and abrasive materials, but significant quantities are now also being used in the manufacture of refractory brick materials. A lot of research has been done in recent years on the potential use of SiC in the high temperature gas-turbine engine.

2.2 Production of SiC

Silicon carbide is produced commercially by reaction of a mixture of sand (silica)

and coke (carbon) in an electric resistance furnace (Acheson process)[11]:

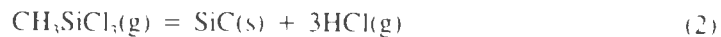


The composition of the mixture may be, for instance, coke 40%, silica 50%, sawdust 7%, and common salt 3% [12]. The furnace is not usually shielded from air, and employs a centrally mounted core of graphite and coke as the electrical heater element. The reaction mixture is filled around this core, between removable walls. The temperature of the central core is first raised to about 2200K, after which it is more slowly increased to reach maximum value of about 3000K. The temperature is then lowered and kept a little over 2300K for about 30 hours, after which the furnace is allowed to cool down and the silicon carbide is removed, washed, dried and graded according to size. The best grades are found near the core. The exact temperature-time cycle varies from furnace to furnace, depending on its geometry. The particles, as a result of the way they are produced are highly defective. A typical particle has many microtwins and stacking faults [9].

Coarser grades ($>10\mu\text{m}$) of silicon carbide powder cannot be sintered to high density. For refractory applications, compacted SiC grid in the required shape is bonded using a bonding phase of, for example, silicon nitride or nitride oxide, aluminosilicate glass, or selfbonded carbon or silicon. For electric heating element material, high-purity size graded silicon carbide grits are sintered alone at temperatures in the region of 2700K.

Silicon carbide is also produced on a small scale by the decomposition in an inert atmosphere of gaseous or volatile compounds of silicon and carbon, allowing the reaction

products to deposit the carbide on a suitable hot substrate. An example of this process, known as chemical vapor deposition (CVD), is shown in Equation (2):



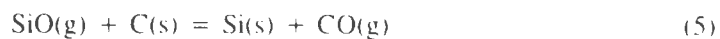
The detailed consideration of CVD process was given by Cagliostro and Riccitiello [13,14].

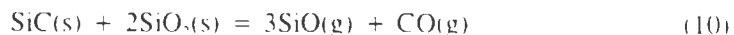
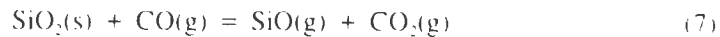
Finally, since carbon has an appreciable solubility in liquid silicon, the carbide can be obtained by high temperature (1923K) crystallization from a carbon rich silicon melt which is supersaturated with respect to SiC:



This last reaction forms the basis of the well-established self- or reaction bonding technique for binding fine-grain silicon carbide powders. The reaction between silicon and carbon was used to develop silicon carbide radiant tube materials [15]. The powders of particulate silicon, coarse grain SiC or coarse graphite were loaded into the induction furnace. After loading the powders were fired using moving hot zone. The hot zone moved from top to bottom melting the silicon and allowing it to infiltrate silicon carbide or graphite. As a result of reaction between graphite and carbon small amount of silicon carbide was formed.

Recently Krstic [16] developed a low temperature process of SiC formation. The overall reaction of SiC formation was broken into the following steps:

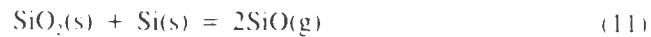




It was shown that to form SiC at a reasonable rate it is necessary to promote reactions (4) and (5) and retard reactions (6) and (7). Submicrometer SiC powders were synthesized by reacting silica and carbon black at temperatures between 1723 and 2073K. Simultaneous application of vacuum and mixing provided the condition for full conversion of silica to SiC. It was shown that two different reaction mechanisms are possible, depending on the reaction temperature and the partial pressure of CO. At lower temperatures (below approximately 1673K), the dominant mechanism is the reaction between gaseous SiO and C. Above 1673K, the rate of SiC formation is controlled by the rate of SiO formation. In as-synthesized form, the SiC powders typically contained 0.2wt% of unreacted silica and free carbon in the range between 6 and 15 wt%. Precise control of partial pressure of CO in the reaction chamber and continuous mixing of the reactants provided the conditions under which the rate of silicon carbide formation could be increased by one order of magnitude. The process is suitable for large-scale commercial production of SiC, requiring no postfabrication acid leaching or major milling.

Because the effectiveness of SiC formation is strongly diminished by formation of CO during reactions (4),(5),(8), and (10) Ledoux et. al. [17,18] developed a new process in which SiC was produced in two steps. In the first step SiO(g) was formed by

reaction of silica with silicon metal.



and then SiO(g) was pumped to react with carbon according to reaction (8). Activated carbon was used as a carbon source and as a result high surface area SiC was produced at temperatures around 1473K.

Preparation of silicon carbide fiber from activated carbon fiber and gaseous silicon monoxide was suggested by Okada et. al. [19]. The SiO vapor diffused into activated carbon fiber through its micropores. The vapor reacted with the carbon, and, under proper conditions, activated carbon fiber was completely converted to SiC fiber. Complete conversion was achieved in ten hours at 1473K and two hours at 1573K. SEM micrograph of incompletely reacted fiber showed that the formation of the carbide occurred from the outer surface of the fiber toward its center. The reacted fiber consisted mainly of SiC with an oxygen content of 1.21 wt%. Fiber densification was achieved by heat treatment in nitrogen at 1873K. The XRD pattern and TEM micrograph showed the crystalline character of the fiber.

Thermodynamics of Si-C-O system is critical in a number of areas. These include carbothermic reduction of silica and growth of silica scales on SiC. The predominance diagram for this system was constructed by Jacobson and Opila [20]. Kinetic analysis of silicon carbide growth is given by Jha [21]. Other aspects of this system are discussed in [22-27]. Diffusion coefficients of Si and C in SiC were determined by Hon et. al. [28, 29].

2.3 Structure and properties of SiC

SiC crystallize in a number of different modifications, called polytypes, in all of which two dimensions of the unit cell are the same while the third is a variable integral multiple of a common unit [12]. The different polytypic modifications can be regarded as built up of layers of structure stacked parallel to each other at constant intervals along the variable dimension. The two unit cell dimensions parallel to these layers are the same for all the modifications. The third dimension depends on the stacking sequence, but is always an integral multiple of the layer spacing. Hexagonal and rhombohedral polytypes are denoted as α -SiC, while cubic modification as β -SiC. The hexagonal unit cell has dimensions $a=b=3.078\text{\AA}$ while c is a variable integral multiple of 2.518\AA . β -SiC is a metastable low temperature modification forming around 2100K. It can exist only at temperatures below about 2300K, transforming irreversibly into α -SiC type "6H" at higher temperatures. This 6-layered hexagonal polytype is the most common modification of the compound. The structure of SiC is shown in Figure 1.

Atomic-level characterization of SiC was done by Tsong [30]. For electronic purposes Du et. al. studied the chemistry and structure of SiC implanted with aluminum [31].

The oxidation resistance of SiC was considered by Jacobson [32]. The SiC is inherently unstable in air and forms a thin layer of silicon dioxide (SiO_2) in an oxidizing environment. The SiO_2 has the lowest permeability to oxygen of any of the common oxides and forms an effective reaction barrier.

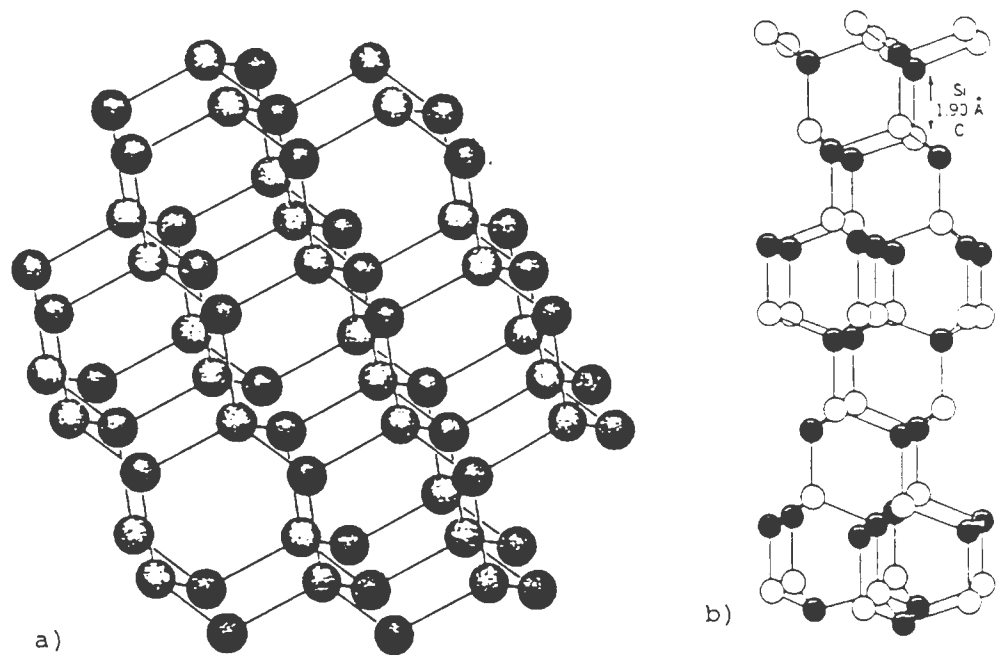


Figure 1 Structure of SiC: (a) Cubic or β -SiC. (b) Tetrahedral or α -SiC type 6H. Black balls represent C atoms and white balls represent Si atoms [12].

2.4 Al-Si alloys

The Al-Si alloys are preferred matrix for SiC because as described later in the text Si prevents formation of aluminum carbide. Table 2 [33] gives the composition and application of some Al-Si alloys. They have comparatively high fluidity in the molten state and mostly used as casting alloys.

Binary Al-Si alloys are not considered heat-treatable since only a small amount of silicon is soluble in aluminum (1.65 wt% maximum) and since the silicon that does reprecipitate from solid solution causes very little hardening.

The Al-Si system is simple eutectic type with the eutectic composition at 12.6 wt%Si. During solidification of 443 alloy (Al - 5 wt%Si) dendrites of almost pure Al solidify first. The spaces between these dendrites are then filled with aluminum silicon eutectic. When the eutectic freezes it decomposes into almost pure aluminum and silicon. As the solidification rate is increased, the dendrite cells become smaller and this increases alloy strength.

The eutectic structure of sand cast Al-Si alloys can be greatly refined by the addition of small amounts of sodium (0.025 wt%), either as metallic sodium or as sodium salts just before casting. Sodium modification of aluminum sand castings leads to higher tensile strengths.

2.5 Aluminum-silicon-magnesium-copper casting alloys

The strength properties of cast aluminum-silicon binary alloys can be improved by the addition of small amounts of magnesium (about 0.35 wt%). The most important

Table 2 Chemical compositions and typical applications of aluminum casting alloys [33]

Alloy designation	Si wt%	Cu wt%	Mg wt%	Typical applications
354	9	1.8	0.5	general-purpose alloy used for engine parts, meter housings, aircraft, missile
A356	7	-	0.3	intricate castings requiring good strength and ductility; transmission cases, truck wheels, cylinder blocks, marine hardware, cylinder heads
A357	7	-	0.5	aircraft and missile parts
A332	12	1	1	automotive pistons, diesel engine pistons, engine parts operating at elevated temperatures
A360	9.5	-	0.5	general purpose castings
A380	8.5	3.5	-	general purpose castings

aluminum casting alloy of this type is 356, which contains 7 wt% Si for castability and 0.35 wt% Mg to make the alloy heat-treatable. The magnesium silicide (Mg_2Si) content of the alloy is in the range 0.5 to 0.6 wt% and the precipitation strengthening is attributed to a metastable phase of Mg_2Si . Addition of copper reduces the ductility but increases the hardness of the alloys. Together copper and magnesium improve machinability and strength on heat treatment [34].

2.6 Phase equilibria in the Al-Si-C system

The binary subsystems Al-Si, Al-C, and Si-C (Figures 2-4) are well known [35]. The Al-Si system shows a simple eutectic at 850K and 11.3 at. pct Si, with very limited terminal solid solubility. The Al-C system shows a single intermediate phase at Al_4C_3 that decomposes peritectically at 2429K to yield solid carbon and a liquid phase containing about 20 at. pct C. The solubility of carbon in liquid Al at temperatures less than 1800K is negligible. The Si-C system shows a single intermediate phase at SiC that decomposes peritectically at 3103K to yield solid carbon and a liquid phase containing about 19 at. pct C.

The high temperature phase relations in the Al-Si-C were studied extensively in connection with aluminum carbotermic reduction [36-38] and liquid phase sintering of silicon carbide [39]. Related phase diagrams are summarized [40].

The phase equilibria in the Al-Si-C system was studied by Viala et al. [41,42]. Liquid aluminum was equilibrated with silicon carbide and reaction products were determined using chemical analysis. On the base of results obtained the phase diagram

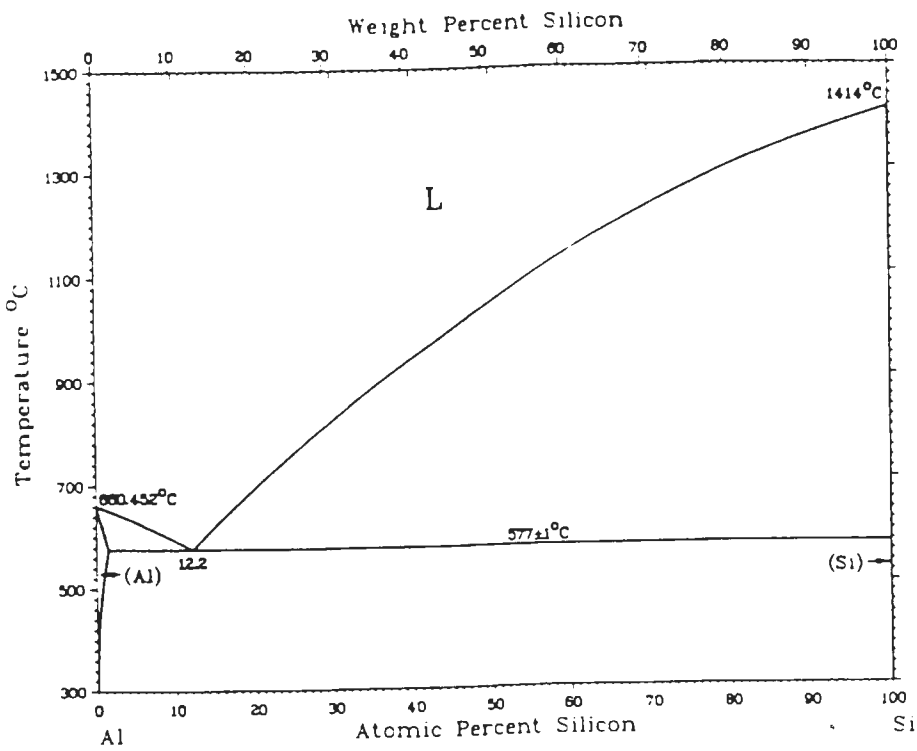


Figure 2 Al-Si phase diagram [35].

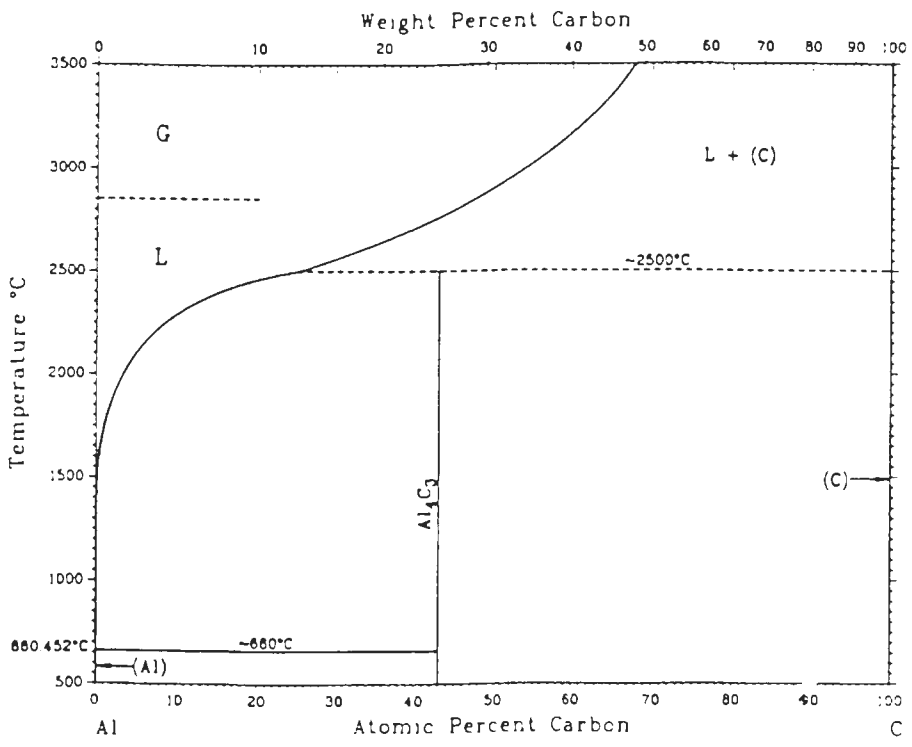


Figure 3 Al-C phase diagram [35].

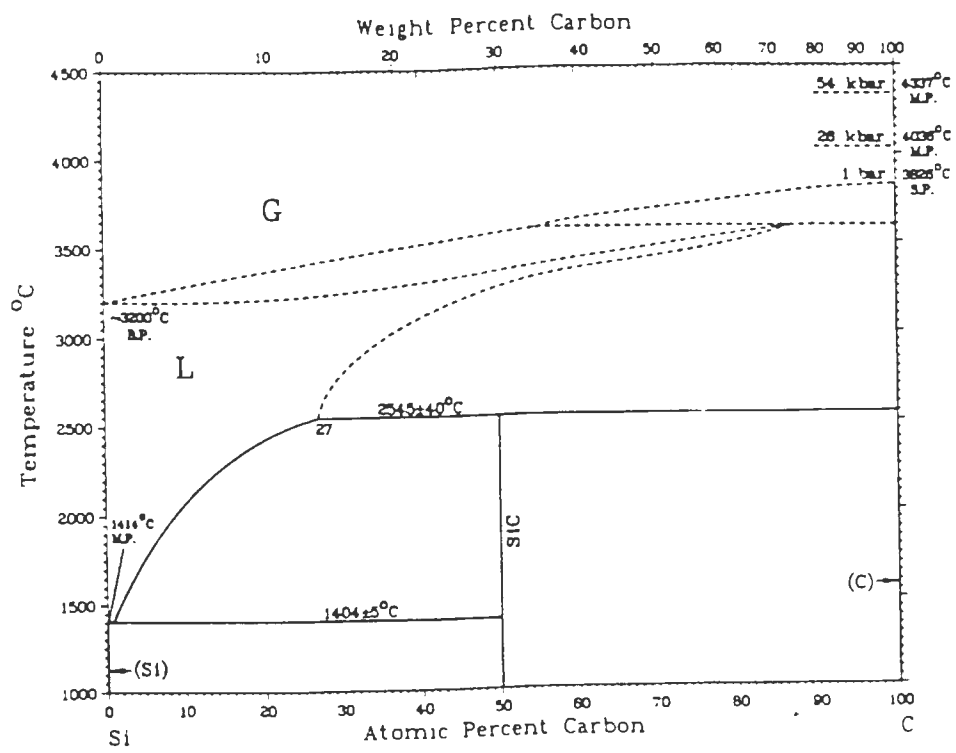
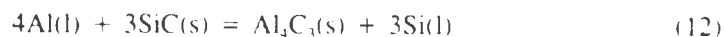


Figure 4 Si-C phase diagram [35].

of Al-Si-C system for the temperature interval 973-1473K was constructed. The Al-Si-C phase diagram at 1273K is presented in Figure 5. The calculation of the phase diagram for the same temperature range using activity coefficients for Al-Si liquid was performed by Handwerker et al. [43]. But the results of their calculations differed substantially from their own experimental data.

2.7 Reactions in the Al/SiC composite

During the Al-SiC composite fabrication involving the contact between molten Al and SiC, Al_4C_3 can form on the interface and this carbide is responsible for degradation of the mechanical properties of the material [44]. Although a large number of publications are available on Al_4C_3 formation only a few give quantitative description of the processes taking place. Iseki et. al [45] studied the extent of the following reaction



for mole ratio $SiC/Al = 3/4$ at different temperatures and treatment times. A thin reaction layer was detected which consisted of Al_4C_3 particles and aluminum metal. It was observed that $(111)_{Al}$ and $(0001)_{Al_4C_3}$ planes were parallel to the interface. Quantitative analysis done by X-ray diffraction showed that the extent of reaction (12) increased from 973K to 1273K but was practically the same for 1273 and 1473K. It was also found out that additions of free silicon to aluminum melt could substantially decrease the extent of reaction (12) or even stop it. Lloyd and Jin assessed the reactivity between SiC and molten Al for $SiC/Al = 0.3$ at 973 to 1173K [46]. After one hour exposure 4.5 wt pct Si in the composite was observed at 948K, 6.5 wt pct at 1073K and 8.2 wt pct at

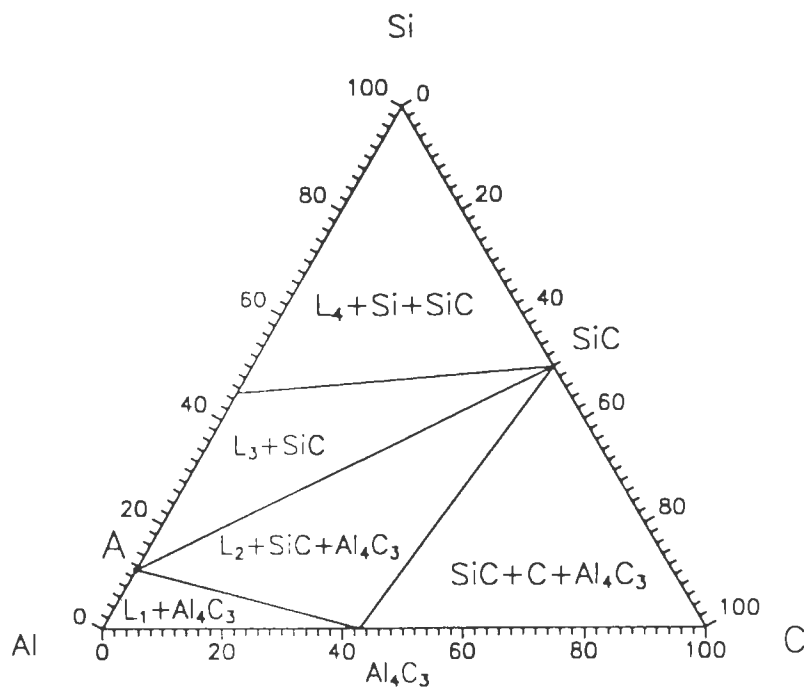


Figure 5 Al-Si-C phase diagram at 1273K [42].

1173K. The reaction products at 1073K and $\text{SiC}/\text{Al} = 7.46$ were studied by Hughes et al. [47]. The authors of this paper also performed equilibrium calculations for Al-SiC system but ideal solution model used for Al-Si solution is not adequate in this case because of the big positive deviations of Si from ideal behavior.

Mechanism and kinetics of the chemical interaction between liquid aluminum and silicon-carbide single crystals was studied by Viala et. al. [48]. This work showed that chemical interaction at temperatures ranging from 930 to 1100K between liquid aluminum and hexagonal α -SiC crystals always proceeds via a dissolution-precipitation mechanism. This mechanism involves the migration of carbon atoms by liquid-phase diffusion from places where the SiC surface is in direct contact with the metal matrix to the growing faces of Al_4C_3 crystals located at or near the metal carbide interface. The silicon liberated in this reaction dissolves in aluminum, forming a liquid Al-Si alloy.

The rate at which such a decomposition reaction proceeds, as well as the morphology of the resulting reaction zone, greatly depends on the polarity of the substrate surface exposed to aluminum attack. The (0001) Si face and the randomly oriented faces behave in a similar manner. These faces dissolve at a rather fast rate in aluminum and, Al_4C_3 crystallites nucleate onto the SiC surface with their c-axis preferentially oriented in a direction parallel to the c-axes of the substrate. Lateral extension of these crystallites results in the formation of an adherent and continuous layer of Al_4C_3 crystals that very efficiently protect the underlying substrate from further decomposition. Due to these preferential germination and growth orientations, passivation takes place sooner at the Si face than at randomly oriented faces. As for the (0001) C

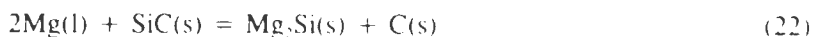
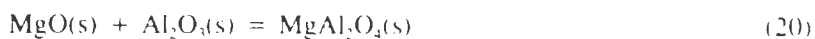
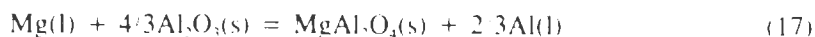
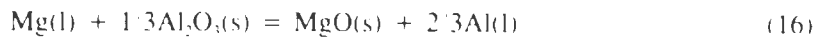
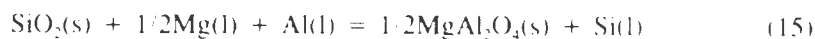
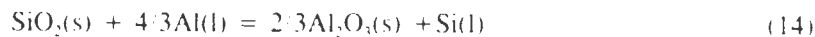
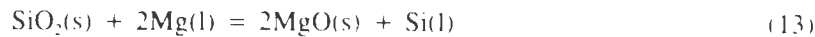
face, it exhibits a very particular behavior: it dissolves at a much slower rate than any other face (six to ten times slower); but as Al_4C_3 crystals cannot nucleate or remain fixed onto this face, passivation never occurs. Consequently, if exposed for a very long time to aluminum attack, the C face will appear more damaged than any other face. The Si face must be considered more reactive, although the C face may be severely damaged under special conditions (long time or high temperature reactions).

Lloyd et. al. [49,50] studied the kinetics of reaction (12) by monitoring the intensities of the Al_4C_3 and silicon X-ray peaks. In these experiments, SiC MMCs were remelted and held at different temperatures above the liquidus for various times. The melts were then solidified, ground to powder and examined by X-ray diffraction. The reaction rate in AA2014-20vol.% SiC (wrought alloy) was high initially but dropped to a low level after about 1 hour. This fast drop was explained by shielding effect of aluminum carbide on SiC particles. The extent of reaction increased with increasing the temperature. Reaction kinetics was not greatly affected by the volume fraction of the reinforcement. In case of A356 alloy (casting alloy) which has 7% Si no significant reaction was detected at 998K, but the reaction was observed at 1073K. It was summarized that unprotected SiC is thermodynamically unstable in the wrought alloys, and any melt processing has to be very carefully controlled if excessive Al_4C_3 formation is to be avoided. However, the high silicon casting alloys are much more resistant to Al_4C_3 formation and SiC composites based on these alloys are more stable in the molten state.

The rate of SiC particle degradation in aluminum-based composites was

established by Carotenuto et. al. [51].

Formation of magnesium spinel was studied by Wang et. al. [52]. The composite was supplied by Alcan International Ltd. Aluminum alloy (A356) with a nominal composition of 92.7 wt pct Al, 7 wt pct Si, and 0.3 wt pct Mg was employed as the matrix material. This alloy was reinforced by 15 vol pct SiC particulates with an average size of 5 to 10 μm . Based on available thermodynamic data it was proposed that in addition to reaction (12) the following reactions may take place:



Using SEM-EDAX patterns it was shown that reaction product on the boundary between Al and SiC was MgAl_2O_4 .

Ratnaparkhi and Howe [53] studied diffusion bonded interface between Al-Mg alloy and SiC using high resolution and analytical electron microscopy. Diffusion bonding was performed at 834K under pressure. The following reaction products were

observed: Mg_2Si , MgO , $MgAl_2O_4$ and Al_6Mg_5 .

Chernyshova and Kobeleva studied the interaction between Al-Si alloy and carbon fibers [54]. Formation of both Al_4C_3 and SiC was observed at the interface.

To reduce the degradation of SiC particles by liquid aluminum treating or coating of SiC particles may be used. Several methods involving the presence of oxides around the SiC particles have been proposed recently [55]: these are oxidation of the particles, production of oxide coatings by the sol-gel technique, and deposition of oxide particulates at the surface of the SiC particles by a dry mixing technique.

2.8 Wetting, solidification and microstructure of Al/SiC composites

Wettability of SiC by aluminum and Al-Si alloys was studied by Laurent et al. by measuring the contact angle formed by molten metal or alloy on a single crystal of SiC [56]. It was found that contact angle dropped with time. After two hours of exposure the contact angle became constant and the temperature increase from 950 to 1050K led to the contact angle decrease from 75 to 50 degrees, meaning improved wetting for higher temperatures. Also slight improvement in wetting was observed for increase of silicon concentration in aluminum alloy from 0 to 18 wt pct. Oh et. al. [57,58] studied wettability of SiC by aluminum alloys measuring threshold pressure for infiltration. Near equilibrium wetting was achieved in 5 to 10 minutes. The results on effect of temperature and silicon concentration were found to be similar to those of Laurent et. al. [56].

Kobashi et. al. [59,60] measured the time required for the SiC particles to be incorporated into Al alloy. The particles first formed agglomerates and only then were

incorporated into the melt. The incorporation time was substantially decreased with temperature increase from 993 to 1223 K. Also titanium and magnesium shortened the incorporation time. Effect of Mg and Ti was explained by formation of silicides or carbides. Reaction products were identified as Mg₂Si and TiC respectively. Copper and zinc, which have weak affinity for SiC and do not form silicides or carbides, prolonged the incorporation time. Addition of silicon also increased incorporation time. Although all three Li, Pb and Bi decrease the surface energy of liquid only Li addition decreased the incorporation time. Large reaction products were found in this case. The model of particle pushing/entrapment transition during directional solidification of Al-SiC composites was developed by Stefanescu et. al. [61].

The evolution of the composite microstructure during directional solidification was studied by Rohatgi et. al. [62]. It was found that the presence of silicon carbide particles disturbs the orderly aligned arrangement of dendrites observed in the base alloy, under similar solidification conditions, except near the chill surface where a particle-free zone was observed due to probable pushing of particles by the microscopic solidification front with cell spacing finer than the particle size. During the entire range of solidification conditions studied, the silicon carbide particles were pushed by growing dendrites of α aluminum into the last freezing eutectic liquid.

Recently Rohatgi [63] also proposed a new type of composite. Aluminum alloy was reinforced with fly-ash particles, which are a waste by-product of coal-based power generation. Incorporation of fly-ash particles reduced the cost of aluminum castings by acting as filler; decreased the density of the composite and increased its hardness.

abrasion resistance, and stiffness.

Effect of solidification parameters and melt cleanliness on the properties of the composite was discussed by Samuel et. al. [64,65]. The specific gravity of most of the reinforcements used in aluminum MMCs is usually higher than that of molten aluminum, which leads to settling or "sedimenting" in the melt. In Al/SiC composites sedimentation of the SiC particles to the bottom of the melt crucible normally occurs during remelting once the melt material reaches the mushy zone. As the temperature of the melt rises, the sedimentation increases with increasing fluidity of the molten material. Also, with settling, the upper regions of the melt become denuded of reinforcement, which can result in large differences in melt viscosity and temperature in different parts of the melt. Therefore, it is important that mechanical stirring be commenced as soon as the metal is sufficiently fluid. Prior to that the melt should be stirred manually, to ensure homogeneous mixing of SiC particles throughout the crucible. Another factor contributing to SiC sedimentation is the "dead time" between castings, when there is no mechanical stirring. This can be avoided by manual stirring for very short times prior to and after casting. It was observed that higher solidification rates provided refinement of the microstructure with more uniform SiC particle distribution and higher tensile properties, whereas lowering the solidification rate led to clustering of the SiC particles in the interdendritic regions and lowering of the tensile strength.

Fluxing changed the chemical composition of the matrix alloy by removing the alloying elements magnesium and strontium from the melt and by introducing sodium and potassium into the melt. The removal of magnesium softens the composite matrix by

reducing the amount of the Mg_2Si -phase precipitate. This results in significant degradation in the mechanical properties of the composite. Therefore, flux treatment using alkali chlorides cannot be applied to composites containing magnesium and/or strontium in their matrix.

Typical microstructure of Al alloy/SiC composite is shown in Figure 6 [50]. Many of the Si particles nucleate at the SiC-matrix interfaces and grow toward the aluminum matrix [66]. The average SiC particle size was about $12 \mu m$. It was proposed that during solution treatment the Si particles undergo changes in size and in shape. In the initial stages of solution treatment, unmodified Si particles undergo necking and separate into segments that retain their original morphology. Because of the separation, the average particle size decreases, and the fragmented segments are eventually spheroidized. Most of the investigators agree that the precipitated phase in Al-Si-Mg alloys subjected to artificial aging is Mg_2Si and have suggested the following process:

- (1) precipitation of Guinier-Preston (GP) zones;
- (2) intermediate-phase β - Mg_2Si , together with a homogeneous precipitation if the aging temperature is above the GP zone solvus; or intermediate-phase β - Mg_2Si , together with a heterogeneous precipitation; and
- (3) equilibrium-phase β - Mg_2Si , fcc structure.

Microscopic examination of the interface region in Al/SiC composite reinforced with as-received and oxidized SiC particles was done by Ribes et. al. [67]. No reaction between the SiC particles and molten aluminum was observed because short periods of time and low temperatures were involved during fabrication.

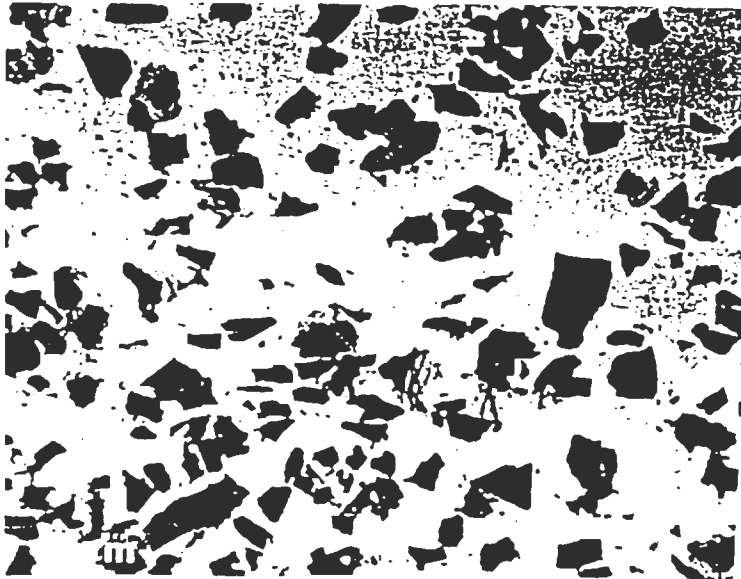


Figure 6 A typical microstructure of the Al/SiC composite. Black particles - SiC, white matrix - Al alloy [50].

Yan et. al. [68] investigated the microstructure of SiC reinforced A356 cast Al metal-matrix composite by means of transmission electron microscopy and energy-dispersive X-ray analysis. It is claimed that several phases were observed in the composite for the first time:

- Spherical-shape amorphous phase with chemical composition $Al_7Si_4Ca_2$.
- γ -SiC, a new variant of SiC. It is lath-like with a triclinic crystal structure having $a=0.308\text{nm}$, $b=0.305\text{nm}$, $c=1.262\text{nm}$, $\alpha=93.8^\circ$, $\beta=90.0^\circ$ and $\gamma=60.0^\circ$.
- J phase, which is a newly discovered constituent phase. It is bulk-like with a C-face-centered orthorhombic crystal structure having $a=0.680\text{nm}$, $b=1.170\text{nm}$ and $c=0.826\text{nm}$.

2.9 Physical properties of the Al/SiC composites

Chiou and Chang [69] fabricated SiC whisker reinforced aluminum composite by vacuum infiltration of liquid aluminum into a porous whisker preform under an argon gas pressure, using an infiltration temperature of 938K. The volume fraction of whiskers ranged from 11 to 37 pct. The whisker diameter was 1-3 μm , the whisker length was 30-200 μm . The SEM study of fracture surface showed that there was no whisker pull-out. The greater was the volume fraction of whiskers, the higher were the tensile strength and the tensile modulus and the lower was the ductility. In particular, for a volume fraction of 37 pct the tensile strength was increased by 474 pct and the modulus was increased by 108 pct, compared to the corresponding values of unreinforced metal. At the same time ductility decreased from 29 to 4 pct. Coefficient of thermal expansion at

373K also reduced from 21.3 to $11.8 \times 10^6 \text{ K}^{-1}$.

Comparison study of mechanical behavior of SiC/Al composite and matrix A356 alloy was done by Wang and Zhang [70]. The elastic constant and yield strength of the composite material were found to be higher than those of the control alloy, but the ultimate tensile strength (UTS) and the ductility were lower. Particle-matrix interface debonding, particle cracking, and void formation in the metal matrix were considered to be responsible for the low ductility.

Three possible types of fracture behavior are possible in particulate composites [66]. If the particle-matrix interface is weak, the crack will propagate through the interface, but if the interface is strong, together with a strong matrix, the particles will be loaded to their fracture stress and crack. In the case that the matrix is weak relative to the interfacial and particle strengths, the fracture will occur in the matrix by normal void nucleation and growth.

Kim et al. [71] studied fracture mechanisms in aluminum alloys reinforced with whiskers. The fractographic results showed that the presence of the brittle cleavage-like fracture facets originated from the coarse manganese-containing intermetallic particles which might have been formed during the composite powder metallurgy processing, although fracture occurs mostly by the ductile dimpled mode. From the in-situ SEM observation of fracture processes of the composite, coarse intermetallic particles are cleaved first to form microcracks at relatively low stress levels and act as local stress concentrators which facilitate the void formation at the near by whisker ends.

Similar observations were made by Lee et. al. [72] during in-situ analysis of the

microfracture process using SEM technique. In the 2124-T6P composite microcracks initiated preferentially at coarse manganese-containing particles in the initial loading stage. In addition, at the tip of a growing crack, such intermetallic particles, together with whisker clusters or residual pores, provided potential crack initiation sites. Thus, in the 2124-T6P composite showing a ductile rupture mode, coarse manganese-containing particles cleaved first to form microcracks, and shear bands tended to form along these discrete cracks. Subsequently, a main crack propagated along the shear bands; local whisker breakage and void formation at whisker ends within the shear-band regions may have contributed to the main crack growth. Conversely, in the 2009-T6P composite where coarse and brittle manganese-containing intermetallic particles are almost absent, microcrack formation was not observed in the initial loading stage. In this case, microcracks appeared mainly at whisker clusters along which shear bands seemed to form, suggesting that whisker clusters played an important role in initiating fracture. In the 2009-OA composite broken whiskers acted as additional strong fracture initiation sites. In the 2124-T6P composite, most of voids were initiated at whisker ends by the decohesion of whisker-matrix interfaces.

Sugimura and Suresh [73] studied the effect of SiC content on fatigue crack growth in aluminum alloys reinforced with SiC particles. It was found that an increase in SiC concentration results in an apparent increase in the rate of fatigue crack growth under conditions where primarily particle fracture and matrix void growth occur. The propensity for particle fracture increased with increasing stress intensity factor range, increasing volume fraction of the reinforcement, and increasing particle size. At the same

time when alloys were reinforced with brittle whiskers there was little or no contribution to overall fracture from reinforcement fracture or interfacial debonding. As a result these metal-matrix composites exhibited a superior resistance to fatigue crack growth as compared to the unreinforced matrix alloy.

The review of toughening and strengthening mechanisms through discontinuous reinforcement was given by Xia and Langdon [74].

2.10 Fiber composites

Precipitation or dispersion hardening of a metal can result in a dramatic increase in the yield stress and/or the work hardening rate. The influence of these obstacles on the elastic modulus is negligible. This is so because the intrinsic properties of the strong particles (the high elastic modulus) are not utilized. Their only function is to impede dislocation movements in the metal. The improvement in stiffness can be obtained by incorporating high modulus fibers in a metal matrix [44]. In a metal-matrix composites the strength is generally determined by the ceramic fibers while the fracture properties are controlled by the metallic component [75].

SiC fibers are of considerable interest as reinforcements for metal-matrix and ceramic-matrix composites. Basically they are produced by chemical vapor deposition of SiC on a continuous carbon fiber. Typical microstructure of the SCS-6 fiber is shown in Figure 7 [75]. Typical microstructure of the Al/SiC composite is shown in Figure 8 [76].

One of the major factors which limits the successful application of the composites at high temperature environments is the occurrence of chemical reactions between the

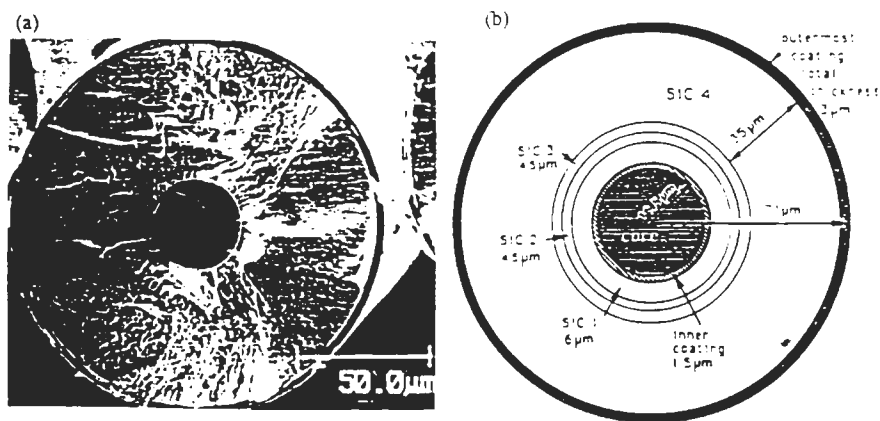


Figure 7 (a) Cross-sectional SEM micrograph of the SCS-6 fiber.

(b) Schematic drawing of the fiber microstructure [75].

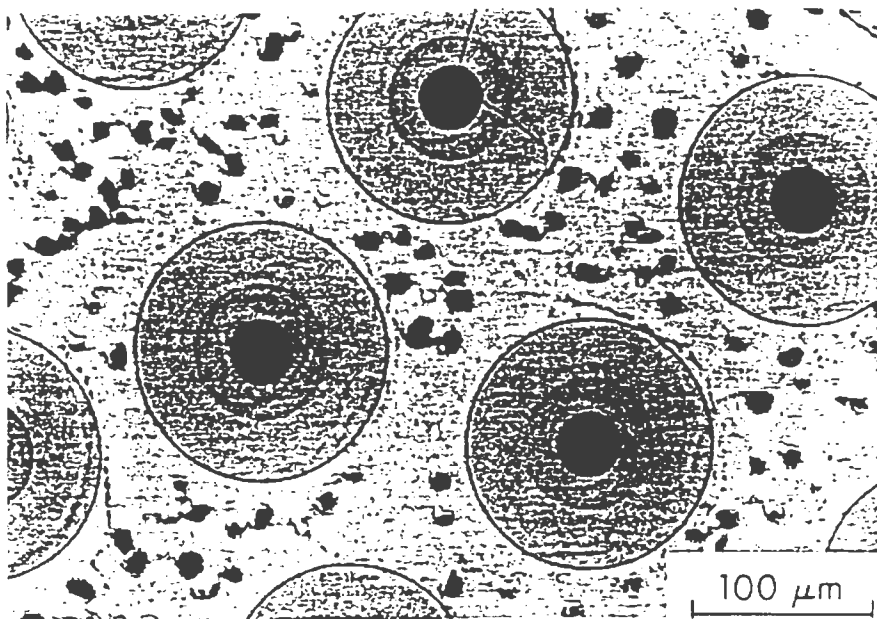


Figure 8 SEM micrograph of the Al alloy composite reinforced with SiC fibers [76].

reinforcement and the matrix [77]. These reactions are generally diffusion controlled and occur during composite fabrication, as well as during service. Although the development of an interaction zone at interfaces is desirable for establishing a sound fiber/matrix bonding, overgrowth of the interaction layer is detrimental to the properties of the composite. The tensile strength, fracture, fatigue, and crack growth behavior are all influenced by the thickness of the interfacial reaction zone. Therefore, it is important to understand the nature and severity of interfacial reactions between potential matrix alloys and various reinforcements.

The study of interface reactions between Ni₃Al matrix and SiC fiber was conducted by Yang et. al. [77]. It was found that SiC fiber reacts with nickel aluminide to form a banded structure on the SiC side and complex reaction products on the matrix side. The following reaction zones were identified: zone 1 - Ni₃Si + C, Ni₃Si₂, zone 2 - Ni₂(Si,Al) + C, zone 3 - Ni₂(Si,Al), zone 4 - Cr-rich carbide, Ni₂(Si,Al), zone 5 - Cr-rich carbide, Ni₃(Al,Si), Ni₁₀(Zr,Al,Si)-, zone 6 - Cr-rich carbide, Ni₃(Al,Si), Ni₁₀(Zr,Al,Si)-. It was concluded that diffusion barrier coating on the fiber is needed to minimize the interfacial reaction.

Thermal stability of interfaces in Ti-6Al-4V composite reinforced by SiC fibers was studied by Badini et. al. [78]. It was shown that the protective coating on the fibers made of TiB₂ allows to improve the lifetime of the fibers.

Krishnan and Kaufman [79] studied the interface reactions in NiAl composite reinforced with molybdenum fibers. To prevent interdiffusion between NiAl and Mo they formed an interface layer of Mo₂C by alloying NiAl with small additions of carbon

Extensive study of $\text{Ni}_3\text{Al}/\text{Al}_2\text{O}_3$ and $\text{Ni}/\text{Al}_2\text{O}_3$ composites was done by Nourbakhsh et al. [80].

2.11 In-situ composites

Although the advantages of advanced composites as structures in aerospace and other demanding applications are well known, they have found few applications outside the military arena. A primary detriment to the use of these materials for commercial applications is their high cost. Typically, processing of advanced composites involves embedding strong, stiff fibers, which can cost hundreds or thousands of dollars per pound, in whatever matrix is being used for the monolithic component by a series of cost intensive steps. Since composites are, by definition, man-made materials, their constituents are rarely thermodynamically compatible. Consequently, either during processing or extended high temperature operation, extensive fiber-matrix interaction can occur. The usual method for avoiding such reactions and to provide required interfacial properties is applying one or more interfacial coatings as diffusion barriers. Such coatings can add additional hundreds of dollars per pound to material cost. In-situ composites, materials in which reinforcements, matrices, and desired interfaces are formed during processing, are an attractive route to cost-effective structures. In the hierarchy of structural materials, in-situ composites can be considered to be intermediate between monolithics, which contain natural multiphases and are cheap but have limited mechanical property flexibility and artificially reinforced composites which contain artificial reinforcements and are expensive but offer great property flexibility. In-situ

composites take advantage of synthetic multiphases for property flexibility, but should have costs nearly those of monolithics. An attractive processing route to obtain synthetic multiphases, as well as desirable matrices and interphases, takes advantage of solid-solid and solid-liquid displacement and internal reduction reactions to form desirable phases [81]. The work of a number of recent investigations using this approach is discussed below.

2.12 Composites produced by melt oxidation

Lanxide Corporation developed Al_2O_3 Metal Composites by the directed oxidation of Molten Aluminum-Magnesium-Silicon Alloys [82]. The growth of Al_2O_3 metal composites by the directed oxidation of molten Al-Mg-Si alloys proceeds through four distinct stages. The first stage encompasses the early heating of the alloy ignot, melting, and continued heating to between 1123 and 1173K. In this latter temperature range, the molten alloy surface rapidly oxidizes to form a MgO-covered MgAl_2O_4 layer. During further heating and initial soak at the composite growth temperature (1173 to 1573K), the duplex layer slowly thickens (second stage). The start of the third stage, growth initiation, is marked by the spread of a metal-rich zone over the duplex layer; this metal-rich zone is believed to be connected to the molten alloy through microcracks in the thickened $\text{MgO}/\text{MgAl}_2\text{O}_4$ layer. Small nodules of the oxide-metal composite nucleate from the metal reach layer. During the final rapid growth stage, the small composite nodules grow and coalesce to form a macroscopically planar growth front, which persists until growth is complete. Throughout the growth process, the external surface of the

Al_2O_3 -metal composite is covered by a thin MgO layer. Immediately under this external layer and separating it from the Al_2O_3 is a thin layer of molten metal.

The growth kinetics of an Al_2O_3 -metal composite by the directed oxidation of an aluminum alloy (10 wt pct Si, 3 wt pct Mg, balance Al) was measured as a function of temperature (1398 to 1548K) and oxygen partial pressure in O_2 /Ar gas mixtures [83]. The growth rate exhibited an activation energy of 370 kJ/mol and a dependence on oxygen partial pressure consistent with a $P_{\text{O}_2}^{1/4}$ relationship. A dissolution-precipitation growth mechanism was proposed in which the growth rate is controlled by the electronic conductivity of an external Al_2O_3 -doped MgO surface layer in conjunction with grain boundary diffusion of magnesium.

Also alumina-matrix composites with SiC particulates have been produced by directed melt oxidation of a multicomponent Al alloy [84]. The microstructure consisted of three interpenetrating phases: the SiC preform, a continuous Al_2O_3 matrix, and a network of unoxidized metal. The volume fraction of metal within the oxidation product decreased with increasing processing temperature, and its distribution was less uniform when a preform was present. The preform did not show evidence of degradation by the molten alloy, but the growth front tended to climb up particles, increasing the oxidation area and enhancing the rate of composite formation. The total porosity of the composite was found to increase with increasing Mg content, processing temperature, and or SiC particle size. Porosity within the channels was associated primarily with insufficient metal flow to feed the solidification shrinkage. A historical overview of the development of Lanxide™ composites is given by Lewis and Singh [85].

2.13 Al/TiC composites

An in-situ process for making composites comprising a refractory material dispersed in a solid matrix was suggested by Koczak and Kumar [86]. According to the description of the patent a molten composition comprising a matrix liquid, and at least one refractory carbide-forming component are provided, and a gas is introduced into the molten composition. A reactive component is also provided for reaction with the refractory material-forming component. The refractory material-forming component and reactive component react to form a refractory material dispersed in the matrix liquid, and the liquid composite is cooled to form a solid composite material. In one embodiment, the reactive component is a carbonaceous component in the form of a component of the gas, a solid in the gas or the molten composition, or both. The carbonaceous component is provided for reaction with a refractory carbide-forming component to yield a refractory carbide. In a preferred embodiment the matrix liquid is molten aluminum and the refractory carbide forming component is tantalum. In other embodiments, refractory borides or refractory nitrides are formed in situ in the matrix liquid.

This method was mostly used for in-situ growth of TiC. In initial work of Sahoo and Koczak [87] carbonaceous gas was bubbled through Al-Ti melt and fine (0.1 to 2 μm) TiC platelets were produced. Longer processing times and larger bubble size increased the average TiC size slightly. When graphite particles were used as carbon source the final TiC ranged from sub micron to several (5-10) microns in size regardless of the initial graphite size. The results of this work were summarized by Koczak and Premkumar [88].

The work on in-situ formation of TiC was continued by Premkumar and Chu [89,90]. It was found that when carbon particles were mixed with Al-Ti alloy and heated they reacted forming TiC. Neither unreacted cores nor surface reaction zones in the carbon particles were observed. Fine (0.5 μm) TiC particles were not only round in shape but also were relatively uniform in size. It was suggested that the formation of TiC was achieved via a mechanism of multiple nucleation and growth of TiC in situ from the carbon-saturated Al-Ti melt during isothermal holding. The presence of fine submicron-size carbides with a narrow size distribution meant that nucleation was easier than growth. At the same time when natural gas was used as a carbon source increasing reaction time from 5 to 30 minutes led to the increase of particle size from 2 to 10 μm .

Recent developments of in situ formation of TiC are discussed in [91,92]

Jarfors et. al. [93] studied the reactions taking place during infiltration of graphite fibers by Molten Al-Ti alloy. Three reactions



were observed to take place simultaneously. The reaction products consisted of partly reacted graphite fibers covered by two layers: Al_4C_3 and TiC. TiC was also present in the form of small crystals randomly distributed in the matrix alloy. The results of experiments were explained using Al-Ti-C phase diagram developed by Svendsen and Jarfors [94].

Formation of TiC in Al-Ti melt with the intention of grain refinement of

aluminum alloys was studied by Banerji and Reif [95]. Reaction zones on separate graphite particles showed that they represented aggregates of small TiC particles. Also it was also found that aluminum carbide could form a layer on TiC. The results of this work were explained in terms of relative thermodynamic stabilities of Al_4C_3 and TiC. Later thermodynamic analysis made in this paper was revised by Fine and Conley [96], Rapp and Zheng [97], and Yokokawa et. al. [98]. But the reasons behind the formation of layers of TiC and Al_4C_3 remained unclear.

Thermodynamic assessment of Al-Ti system was done by Cattner et. al. [99], and diffusion of carbon in titanium carbide was studied by van Loo and Bastin [100].

Formation of ternary compound Ti_3SiC_2 or the mixtures of SiC and TiC was studied using combustion sintering by Klemm et. al. [101] or by chemical vapor deposition by Touanen [102]. Thermodynamic analysis of chemical vapor deposition of Ti_3SiC_2 was done by Racault et. al. [103].

Chrysanthou et. al. [104] prepared Cu/TiC composites by maintaining Al-Ti melt with carbon black at 1773K for 1 hour. After melting of the alloy, carbon black was observed to rise to the surface of the melt and gradually disappeared as it reacted with Ti. It took approximately 40 min. for complete reaction. The size of the particles in Cu-12%TiC composite was of the order $1-3\mu m$, while in Cu-55%TiC it was about $15\mu m$. The finely dispersed particles were almost spherical in shape.

2.14 SiC/MoSi₂ composites

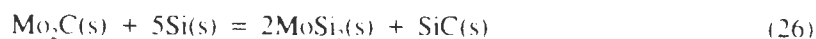
Molybdenum disilicide ($MoSi_2$) is a promising intermetallic compound for high

temperature structural applications in oxidizing atmospheres [105]. It has a higher melting point (2293K) than aluminides of iron, nickel, and titanium; furthermore, it has excellent oxidation and hot corrosion resistance approaching that of SiC. Its outstanding oxidation resistance is due to the formation of a glassy silica (SiO_2) layer which acts as a protective film at high temperatures. However, like most of the intermetallics, the major problems impeding the use of MoSi_2 are its extreme brittleness and poor impact strength at low temperatures. It exhibits a brittle-to-ductile transition at approximately 1173-1273K. Above this temperature, MoSi_2 behaves more like a metal, showing yielding and stress-relieving characteristics. The strength of MoSi_2 at elevated temperatures is relatively low since it undergoes creep and plastic deformation at temperatures above the transition temperature. Therefore, to make MoSi_2 a viable structural material, it is necessary to improve the room-temperature fracture toughness, elevated-temperature strength, and creep resistance.

The study of SiC whisker-reinforced MoSi_2 composite showed that the addition of 20 vol% SiC whisker did not result in significant improvement in either the flexural strength or fracture toughness. The composite exhibited a brittle fracture behavior across the fracture surface. No whisker pull out was observed on the fracture surface. This suggested that the bonding between the whisker and the matrix was strong. Because of this strong bond propagating cracks could not be deflected. A thin reaction layer was found at the interface of SiC-fiber/ MoSi_2 composites. It is thought that the outer C-rich layer reacted with MoSi_2 to form SiC.

A solid state displacement reaction between Mo_2C and Si was used to synthesize

a MoSi₂/SiC composite by Henager and Brimhall [106]. Composite was produced by vacuum hot pressing of powder compacts of blended Si and MoC₂. Using X-ray diffraction and quantitative metallography it was determined that in the interval 1973-2073K the following reaction takes place:



Traces of Mo₅Si₃C were present in the final composition. The following product sequence and reaction mechanism was determined: initially Mo₅Si₃C forms followed by the MoSi₂ phase. SiC was observed to grow at the interface between the ternary Mo₅Si₃C phase and MoSi₂. The initial SiC morphology was plate-like with an aspect ratio of ~ 20 but then the plates underwent pinch-off into discrete particles approximately 1 μm in diameter. Thermochemical evaluation of combustion synthesis of MoSi₂-SiC composites was done by Yandhyala [107].

2.15 Theoretical possibility to form SiC in-situ in Al-Si alloy

Figure 5 [42] shows a ternary Al-Si-C phase diagram. As seen from the figure Al-Si melt can be in equilibrium with silicon carbide. This fact means that if carbon is introduced into Al-Si melt, there is a theoretical possibility to form SiC in-situ in Al-Si alloy but surprisingly no trials have been made to produce a composite material in this way.

2.16 Conclusions

Literature review showed that incorporation of silicon carbide particles into

aluminum alloys allows to improve mechanical properties of this material comparing to unreinforced matrix alloy. Unfortunately during liquid stage production of aluminum matrix composites reinforced with silicon carbide aluminum carbide is formed and it is responsible for reactive degradation of mechanical properties of the composite. To avoid aluminum carbide formation high silicon concentrations should be employed. Also the composite is relatively expensive because of the high price of silicon carbide. The other possibility to produce thermodynamically stable and cheap composite is by in-situ reaction of aluminum-silicon melt with carbon. To make the composite successfully it is necessary to have complete thermodynamic analysis of the ternary Al-Si-C system and experimentally try different different carbon sources if they are suitable for silicon carbide production. On the base of these conclusions the following objectives were established for this work:

2.17 Research objectives:

1. Thermodynamic analysis of Al-Si-C system with the goal to find optimum conditions for in-situ formation of SiC.
2. Experimental study of the suitability of different carbon sources for in-situ formation of SiC.
3. Microstructure of the intermediate and final products and determination the mechanism and the rate of reaction.
4. Cheap and effective method of in-situ production of Al/SiC composite for industrial consideration.

3. THERMODYNAMIC CALCULATIONS

3.1 Introduction

The calculations of equilibrium species distribution were performed using the program "HSC Chemistry for Windows" developed by Outkumpu Research Oy, Pori, Finland and commercially available. The name of the program is based on the fact that it automatically utilizes extensive thermochemical data base which contains enthalpy (H), entropy (S) and heat capacity data for more than 5600 chemical compounds.

The program is based on the free energy minimization method. This means that the program finds the phase combination and composition where the Gibbs energy of the system reaches its minimum value at a fixed mass balance. The algorithm was first described by White et. al. [108]. Recently similar approach was successfully applied for development of a new process for the direct conversion of high grade nickel matte to nickel [109].

The following are two basic equations:

$$G = \sum n_i(G_i) = \min \quad (27)$$

$$b_j = \sum (n_i \times a_{ij}) \quad (28)$$

where G is the total Gibbs energy of the system, G_i is the Gibbs energy of species i, n_i is the number of moles of species i, a_{ij} is the number of atoms of j in species of i, b_j is the number of moles of element j.

The calculations were done for Ar atmosphere. The following assumptions were made during the calculations:

1. Si and Al form liquid solution and activity coefficient of Al is one

2. Al_4C_3 and SiC are solid species which can be present in the system as separate phases
3. No ternary phase can form.

Activity coefficient of Si in Al was described using quasi-regular solution model:

$$\ln(f_{Si}) = (h_1 + h_2/T)(1-X_{Si})^2 \quad (29)$$

where f_{Si} is activity coefficient of Si, h_1 and h_2 are constants, T is temperature, X_{Si} is mole fraction of Si.

Two composition limiting conditions were used to determine h_1 and h_2 . From the eutectic point on the Al-Si phase diagram [35] at $T=850K$ and $x_{Si} = 0.122$ activity coefficient of silicon was found to be

$$f_{Si} = 1 \cdot X_{Si} = 8.197 \quad (30)$$

with pure solid silicon as a standard state.

The following approach was used to determine the second condition. The results of preliminary calculations with the use of ideal solution model for Al-Si system coincided with the experimental data [41,45] at approximately 1423K. So it was assumed that solution becomes ideal at this temperature and for the temperature interval 1423-1573K f_{Si} was taken as one. For the temperature interval 973-1423K the activity coefficient was found to be:

$$\ln(f_{Si}) = (-4.048 + 5760/T)(1-X_{Si})^2 \quad (31)$$

Results of the calculations together with experimental data [42,43,45,46] and the calculated values of Lloyd [49] on the temperature dependance of silicon concentration in aluminum alloy (point A on the phase diagram, Figure 5) are given in Figure 9. As seen from the figure experimental results are satisfactorily described by the model

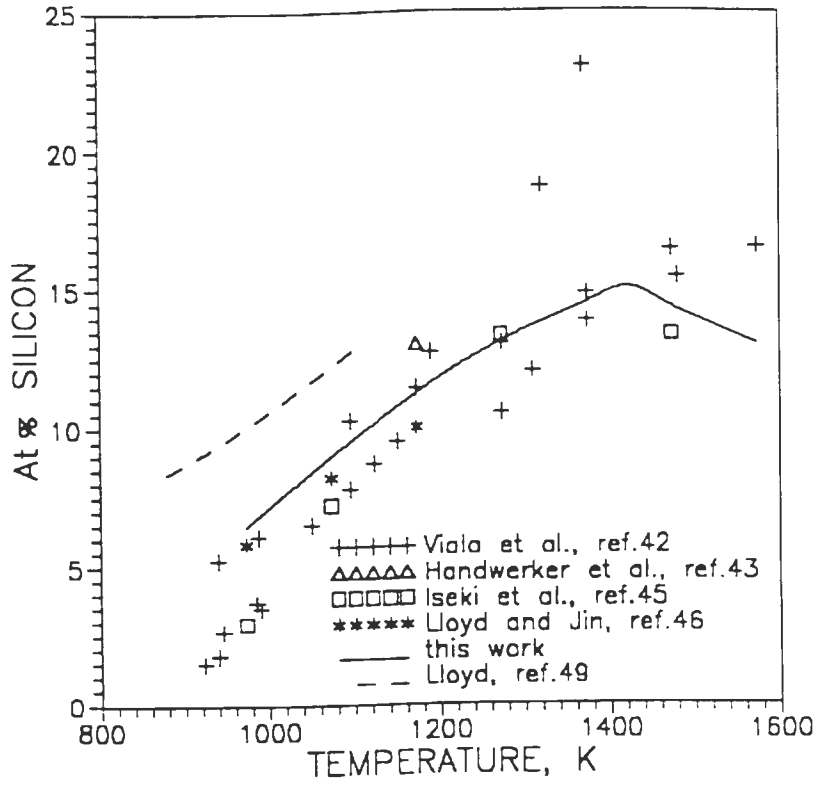


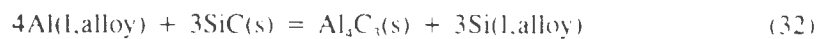
Figure 9 Effect of temperature on the silicon concentration in the melt (point A on the phase diagram, Figure 5).

developed in this work. So the model may be used for analysis of Al-SiC interactions.

A point of maximum in Figure 9 at 1423K is the point where liquid Al-Si solution becomes ideal. At lower temperatures the behavior of the system is determined by strong temperature dependence of the activity coefficient of silicon in the melt. It decreases from 8.197 to 1, when the temperature increases from 973 to 1423K. At higher temperatures the activity coefficient of silicon is one and the behavior of the system is determined by the Gibbs energy of the reaction between Al and SiC.

3.2 Pure Al with SiC.

The calculations were made to study the effect of initial composition and temperature on the equilibrium species distribution in the Al-Si-C system. Table 3 and Figure 10 show the effect of SiC addition to pure Al at $T=1073\text{K}$. As seen from the figure, when small quantity of SiC is added it reacts completely producing Al_4C_3 and Si in the melt:



$$\Delta G = -49,706 + 76.15T \text{ J/mol} \quad (33)$$

Equilibrium constant for the reaction (32) may be expressed by the following equation

$$K = (a_{\text{Al}_4\text{C}_3} a_{\text{Si}}^3) / (a_{\text{Al}}^4 a_{\text{SiC}}^3) \quad (34)$$

Taking into account that $a_{\text{Al}_4\text{C}_3} = 1$, $a_{\text{SiC}} = 1$, and $a_{\text{Al}} \approx 1$, equation (34) may be rewritten

in the following form:

$$K = a_{\text{Si}}^3 = f_{\text{Si}}^3 X_{\text{Si}}^3 \quad (35)$$

Table 3 Effect of SiC/Al ratio on the equilibrium species distribution

T, K	Initial composition of alloy, mol%		Addition, mol% of alloy	Equilibrium composition				
	Al	Si		Alloy mol%	Composition of alloy, mol %		SiC mol%	Al ₂ C ₃ mol%
					Al	Si		
1073	100	-	2.1% SiC	99.3	97.89	2.11	0	0.70
1073	100	-	5.1% SiC	98.3	94.81	5.19	0	1.70
1073	100	-	8.1% SiC	97.3	91.68	8.32	0	2.70
1073	100	-	10.1% SiC	95.78	91.01	8.99	1.5	2.87
1073	100	-	20.1% SiC	87.18	91.01	8.99	10.21	2.61
1073	100	-	40.1% SiC	73.89	91.01	8.99	23.88	2.21
1073	100	-	80.1% SiC	56.66	91.01	8.99	41.65	1.70
1073	100	-	140.1% SiC	41.96	91.01	8.99	56.78	1.26
1073	100	-	200.1% SiC	33.32	91.01	8.99	65.68	1.00

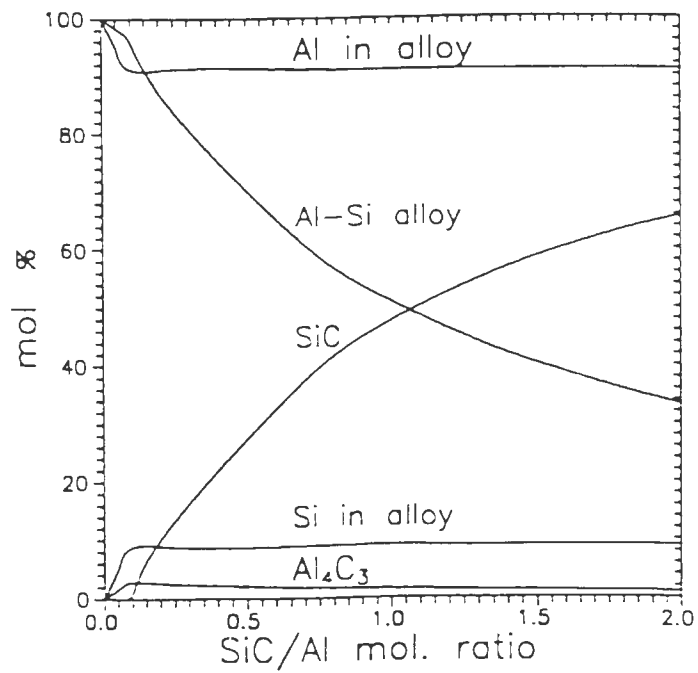


Figure 10 Effect of SiC/Al ratio on the equilibrium species distribution in the system at 1073K.

and hence

$$X_{Si} = K^{1/3} f_{Si} \quad (36)$$

As seen from equation (36) silicon concentration in the melt and accordingly extent of reaction (32) is determined not only by K value (or Gibbs energy of reaction) but also by solution properties of the melt (f_{Si}). Effect of temperature on f_{Si} is much more pronounced than on Gibbs energy and as a result the reaction (32) becomes more driven by solution properties of the melt than by Gibbs energy of reaction. The effect of temperature on the silicon concentration is given in Figure 9. The following equations were found to describe the silicon concentrations:

$$X_{Si} = -39.29 + 0.06601T - 1.955 \cdot 10^{-6}T^2 \quad (973-1423K) \quad (37)$$

$$X_{Si} = 50.02 - 0.03455T + 7.000 \cdot 10^{-6}T^2 \quad (1423-1573K) \quad (38)$$

As seen from Figure 10 SiC appears in the equilibrium composition after the SiC/Al mol. ratio accedes 0.1. This is also the point at which Al_4C_3 (2.9mol pct) and Si concentration in alloy (8.99mol pct) reach maximum, while Al in alloy (91.01mol pct) reaches minimum. With further additions of reinforcement, alloy and Al_4C_3 fractions decrease, SiC increases, while the concentrations of Si and Al in alloy do not change. As seen from the figure, aluminum carbide, which is detrimental for physical properties of the composite, is always present in the system. Therefore pure Al should not be used as matrix metal for silicon carbide.

The corresponding compositional path is shown in Figure 11. When small quantity of SiC is added the composition lies in the $L_1 + Al_4C_3$ binary phase triangle. Addition of SiC such that SiC/Al ratio reaches 0.1 is equal to reaching ternary phase $L_2 + SiC$

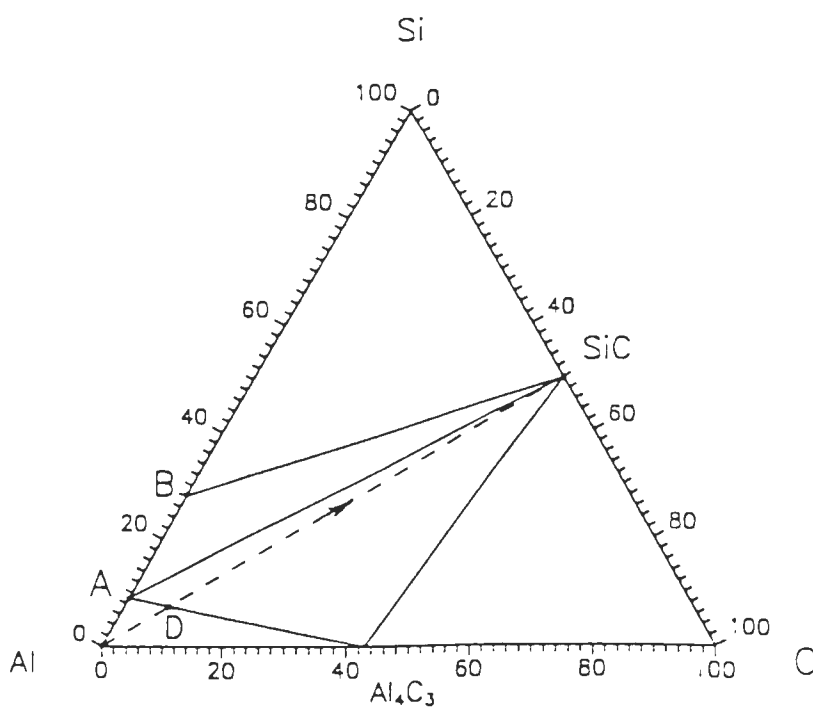


Figure 11 Al-Si-C phase diagram at 1073K with compositional path corresponding to addition of SiC to pure Al. Phase identification is given in Figure 5.

+ Al_4C_3 at point D. With further SiC additions the composition of Al-Si alloy does not change and corresponds to the point A on the diagram.

Figure 12 [42] shows the microstructure Al/SiC sample after reaction for 1h at 1270K. Aluminum carbide forms a reaction layer on silicon carbide. The Al_4C_3 /SiC mole ratio estimated from Figure 12 was found to be 0.057 which is close to 0.048 calculated from Table 4. Figure 13 [42] shows X-ray diffraction pattern of the sample after reaction between Al and SiC. As seen from the figure both products of reaction (29) - Si metal and Al_4C_3 are present in the system.

Table 4 and Figure 14 show the effect of temperature on the species distribution in the system for initial SiC/Al mole ratio equal to 1. As seen from the figure temperature increase from 973 to 1423K leads to the increase of Si concentration in alloy from 6.46 to 15.43 mol pct, Al_4C_3 fraction from 1.09 to 2.64 mol pct, and alloy fraction from 50.54 to 51.32 mol pct, while Al concentration in alloy and SiC decrease from 93.54 and 48.37 mol pct respectively to 84.57 and 46.04 mol pct. Further increase of temperature from 1423 to 1573K leads to decreasing silicon concentration in alloy to 13.74 mol pct, aluminum carbide to 2.34 mol pct, and alloy fraction to 51.17 mol pct, while the concentration of aluminum in alloy and the fraction of silicon carbide in the system increase to 86.26 and 46.49 mol pct respectively.

The corresponding effect of temperature on the phase diagram is shown in Figure 15. The increase of temperature from 973 to 1423K is equal to the movement of point A_1 toward point A_2 , and point B_1 toward point B_2 . As a result the ternary phase triangle $L_2 + \text{SiC} + \text{Al}_4\text{C}_3$ is now reached at point D_2 . Accordingly the corresponding

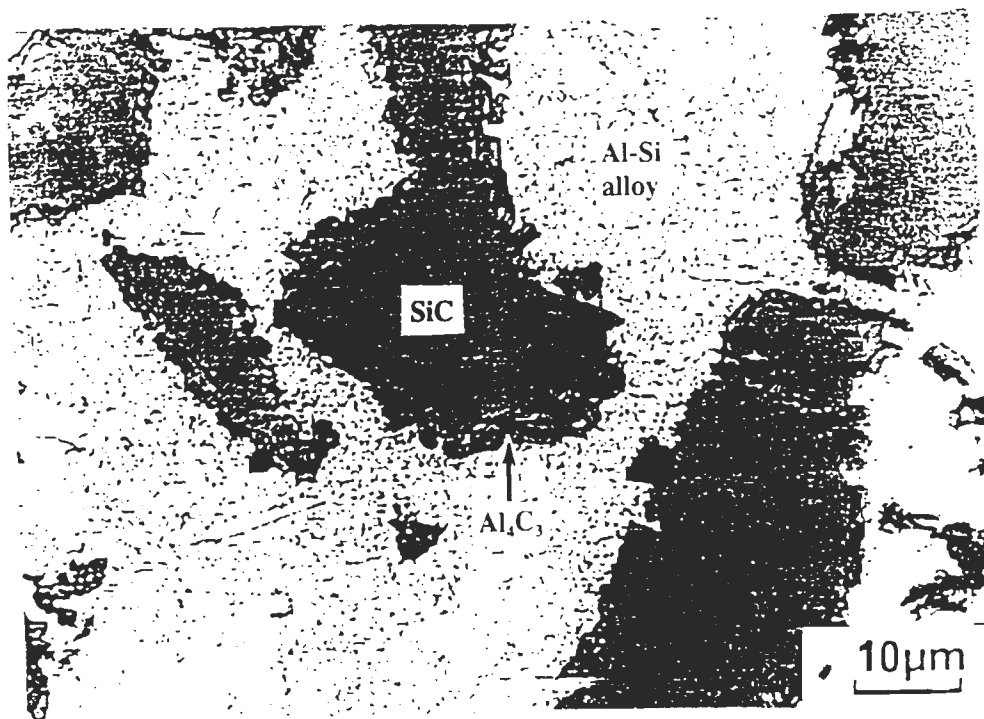


Figure 12 Optical micrograph of an Al-SiC sample after reaction for 1h at 1270K [42].

Table 4 Effect of temperature on the equilibrium species distribution

Temp K	Initial composition of alloy, mol%		Addition, mol% of alloy	Equilibrium composition				
	Al mol%	Si mol%		Alloy mol%	Composition of alloy, mol%		SiC mol%	Al ₄ C ₃ mol%
					Al	Si		
973	100	-	100% SiC	50.54	93.54	6.46	48.37	1.09
1073	100	-	100% SiC	50.76	91.01	8.99	47.72	1.52
1173	100	-	100% SiC	50.96	88.71	11.29	47.12	1.92
1273	100	-	100% SiC	51.13	86.78	13.22	46.62	2.25
1373	100	-	100% SiC	51.26	85.22	14.78	46.21	2.53
1423	100	-	100% SiC	51.32	84.57	15.43	46.04	2.64
1473	100	-	100% SiC	51.27	85.18	14.82	46.20	2.53
1573	100	-	100% SiC	51.17	86.26	13.74	46.49	2.34
1673	100	-	100% SiC	51.09	87.18	12.82	46.73	2.18

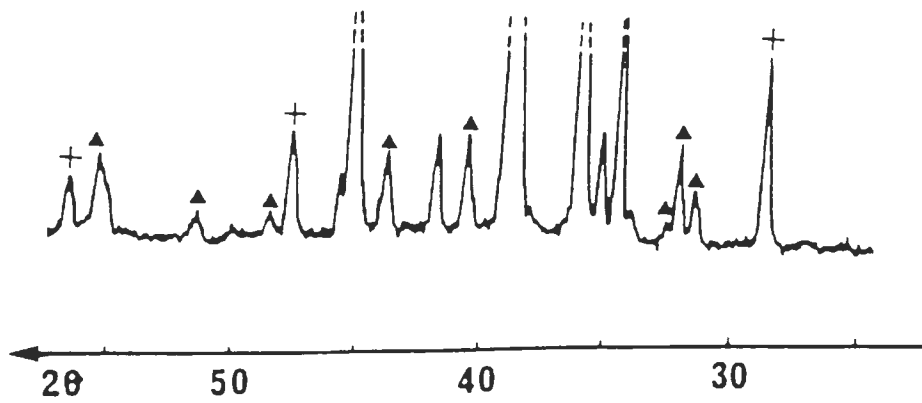


Figure 13 XRD specter of Al-SiC sample reacted at 1270K for 1h [42].

▲ - Al_4C_3 , + - Si.

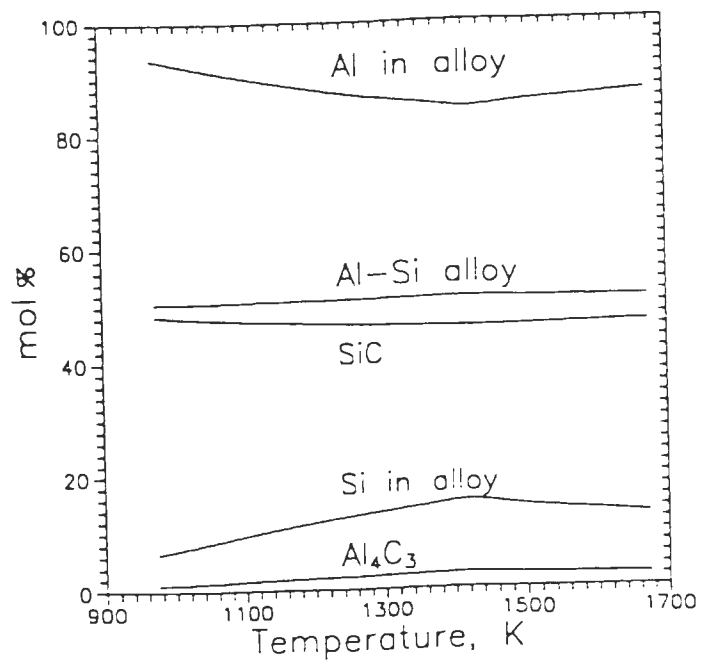


Figure 14 Effect of temperature on the equilibrium species distribution.
initial SiC/Al=1.

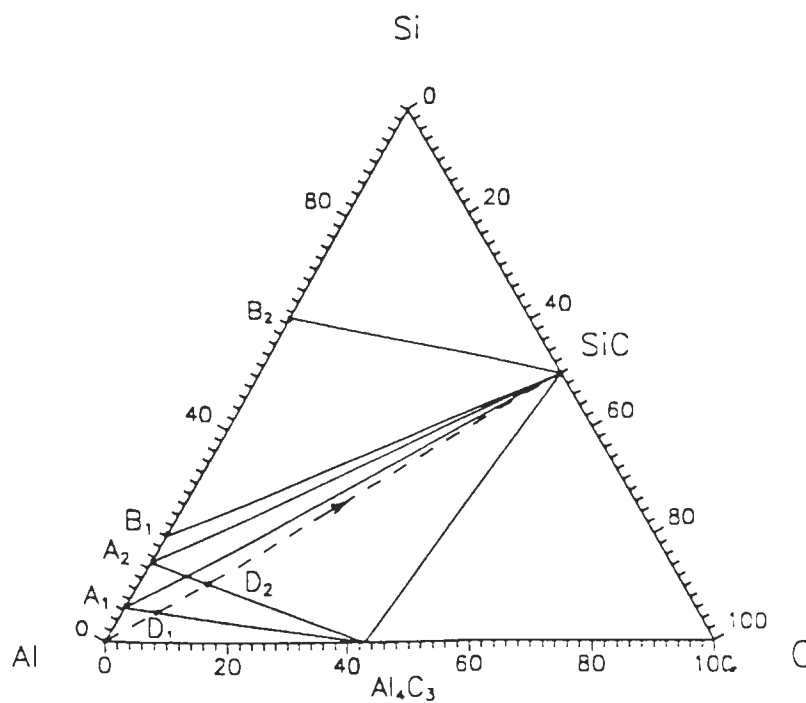


Figure 15 Effect of temperature on the Al-Si-C phase diagram and compositional path corresponding to addition of SiC to pure Al. For points A_1 and B_1 , $T=973\text{K}$, for points A_2 and B_2 , $T=1423\text{K}$. Phase identification is given in Figure 5.

values of Al_4C_3 and Si concentration in alloy increase. The further increase of temperature after 1423K was reached leads to the movement of point B_2 toward Si but now point A_2 moves back toward point A_1 . As a result the fraction of Al_4C_3 and Si concentration in alloy decrease.

Table 5 and Figure 16 show the effect of SiC/Al ratio and temperature on the formation of Al_4C_3 in more details. As seen from the figure the temperature decrease from 1273 K to 973K allows to decrease the quantity of Al_4C_3 approximately two times. Maximum of Al_4C_3 is reached for SiC/Al ratio in the range 0.1-0.2. The points of maximum correspond to the points D of crossing (at different temperatures) A- Al_4C_3 and Al-SiC lines (Figure 15).

3.3 Al-Si alloy with SiC.

When Si is present in initial Al alloy it may decrease or completely prevent the reaction between Al and SiC [45] and Table 6 and Figure 17 give the quantitative estimation of this effect. Minimum silicon concentrations enough to prevent Al_4C_3 formation for each temperature are determined by position of point A on the phase diagram and are the same silicon concentrations as given on Figure 9. As seen from Figure 17 this minimum concentration strongly depends on the temperature. For example, 7 mol pct Si is enough to prevent Al_4C_3 formation at 973 K, while at 1073 K 0.5 mol pct of Al_4C_3 may be formed.

These results were compared with experimental data of Lloyd [49]. According to [49] an alloy A356, containing 7 wt. pct Si (6.74 mol pct), reinforced with 15 vol pct

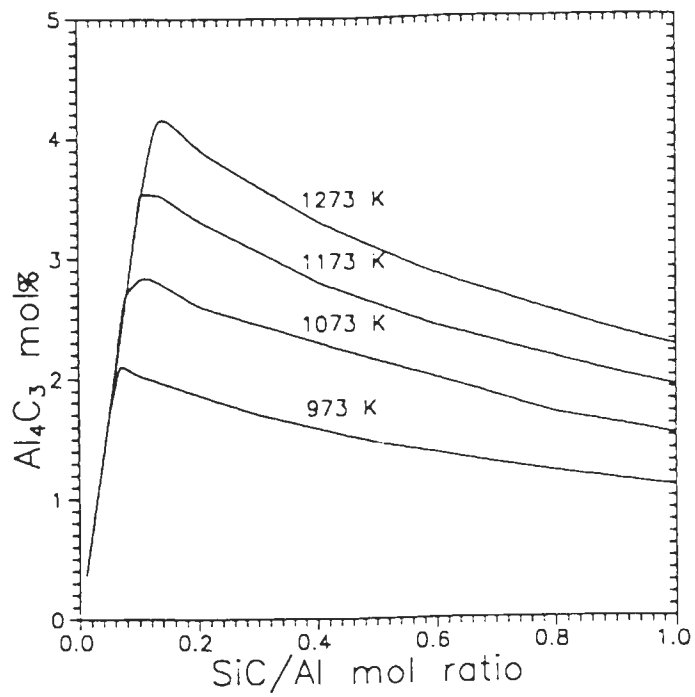


Figure 16 Effect of SiC/Al mol ratio and temperature on the equilibrium mol fraction of Al_4C_3 .

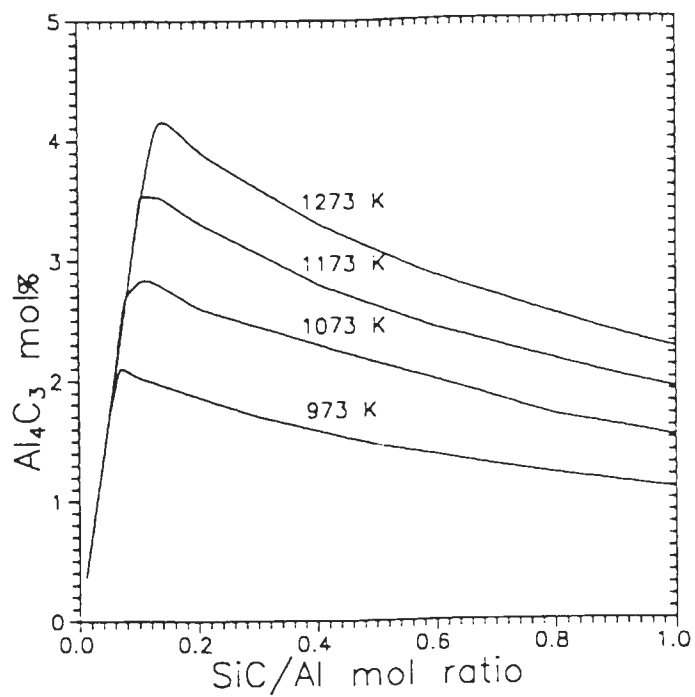


Figure 16 Effect of SiC/Al mol ratio and temperature on the equilibrium mol fraction of Al_4C_3 .

Table 6 Effect of Si concentration in Al alloy on the formation of Al_4C_3
(Al - 20mol% SiC)

Initial concentration of Si in alloy, mol%	Equilibrium concentration of Al_4C_3 , mol%			
	Temperature, K			
	973	1073	1173	1273
0.01	1.85	2.61	3.32	3.92
1.96	1.27			3.30
3.85	0.73	1.45	2.13	2.71
5.67	0.22			2.16
6.46	0			
7.42		0.44	1.09	
8.99		0		
9.10				1.15
10.72			0.16	
11.29			0	
12.29				0.25
13.22				0

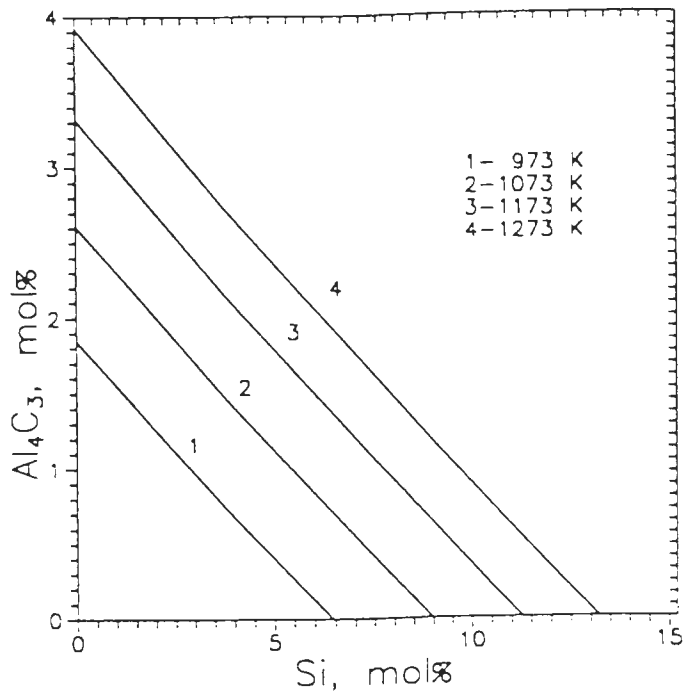


Figure 17 Effect of temperature and initial Si concentration in Al alloy on the equilibrium mol fraction of Al_4C_3 .

SiC was melted and held for 2 hours at 998 and 1073K. Aluminum carbide was detected after keeping the composite at 1073K but was not found after treatment at 998K. From the equation (37) at 998K the reaction (32) will be prevented if Si is higher than 7.12 mol pct, which is very close to the Si concentration in the A356 alloy. So there is a good agreement between calculated and experimental data.

The effect of silicon addition on the compositional path is shown in Figure 18. As seen from the figure effect of silicon addition up 20 mol pct is equal to sliding the first point of the compositional path from pure Al toward point F. As a result when point A is reached equilibrium composition will consist only of liquid alloy and SiC and no aluminum carbide can form.

Figure 19 [42] shows the micrograph of the SiC heated in the presence of Al-Si alloy containing 20 mol pct Si. Comparison of this Figure with Figure 12 shows that in accordance with thermodynamic calculations no aluminum carbide was formed.

3.4 Al-Si alloy with carbon.

For in-situ formation of silicon carbide, carbon may be added to liquid aluminum-silicon alloy. In this case the following reaction may take place:



$$\Delta G = -72.705 + 7.45T, \text{ J/mol} \quad (40)$$

Table 7 and Figure 20 show the equilibrium species distribution, when carbon is added to the liquid alloy, containing 30 mol pct Si. Silicon reacts with carbon, forming SiC until addition of 19 mol pct of carbon. This is the point when aluminum carbide

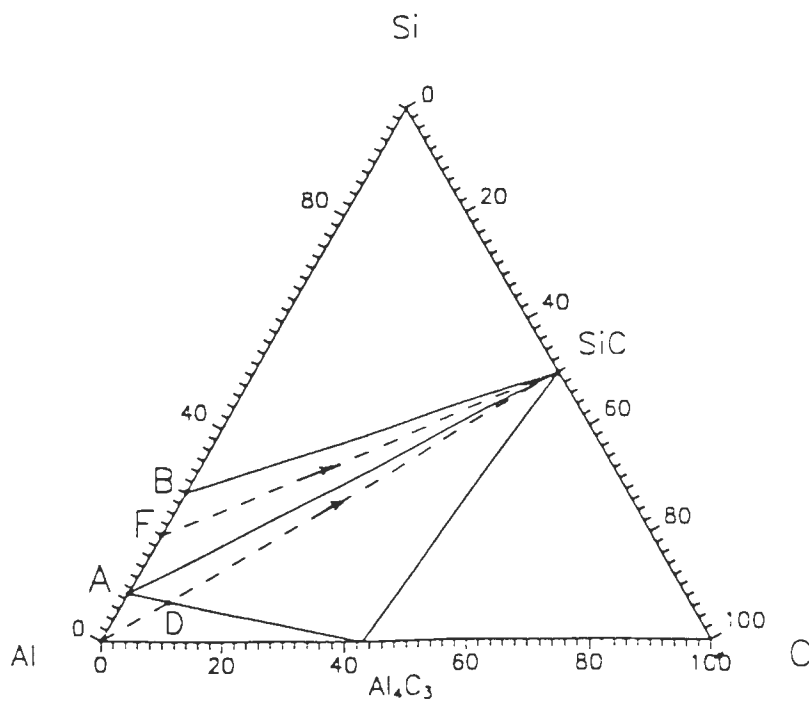


Figure 18 Effect of silicon alloying of aluminum on the compositional path corresponding to addition of SiC to alloy at 1073K.
Phase identification is given in Figure 5.

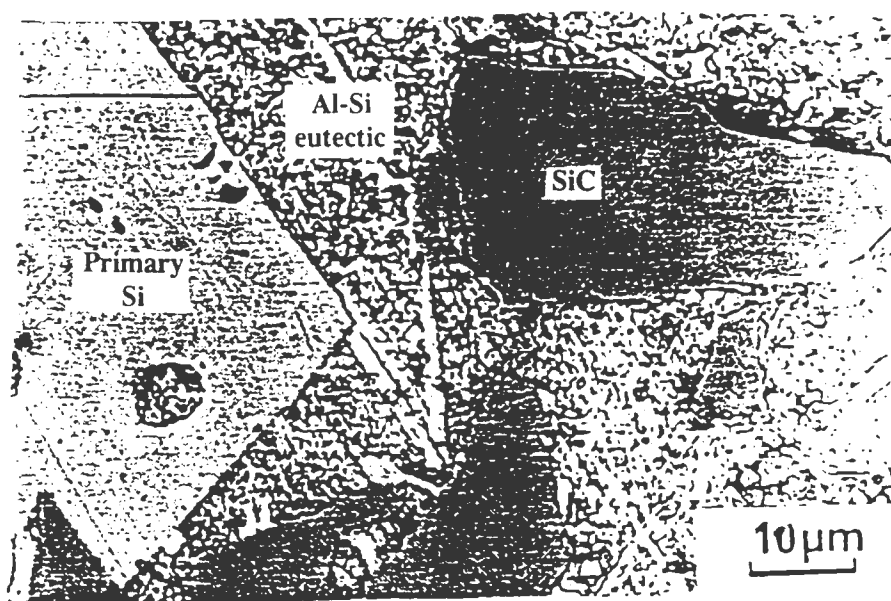


Figure 19 Optical micrograph of SiC particles heated for 1h at 1270K in the presence of Al-Si alloy containing 20 mol% Si [42].

Table 7 Effect of temperature and carbon addition to 30mol%Si-70mol%Al alloy on the formation of SiC and Al₄C₃

T. K	Initial composition of alloy, mol%		Addition of carbon mol% of alloy	Equilibrium composition				
	Al mol%	Si mol%		Alloy mol%	Composition of alloy, mol%		SiC mol%	Al ₄ C ₃ mol%
					Al	Si		
1273	70	30	16.01%C	83.99	83.34	16.66	16.01	0
1273	70	30	20.01%C	80.25	86.78	13.22	19.56	0.19
1273	70	30	24.01%C	77.71	86.78	13.22	20.94	1.35
1373	70	30	16.01%C	83.99	83.34	16.66	16.01	0
1373	70	30	20.01%C	80.82	85.22	14.78	18.59	0.59
1373	70	30	24.01%C	78.23	85.22	14.78	20.02	1.75
1473	70	30	16.01%C	83.99	83.34	16.66	16.01	0
1473	70	30	20.01%C	80.83	85.18	14.82	18.57	0.60
1473	70	30	24.01%C	78.24	85.18	14.82	19.99	1.76
1573	70	30	16.01%C	83.99	83.34	16.66	16.01	0
1573	70	30	20.01%C	80.44	86.26	13.74	19.24	0.32
1573	70	30	24.01%C	77.88	86.26	13.74	20.64	1.48

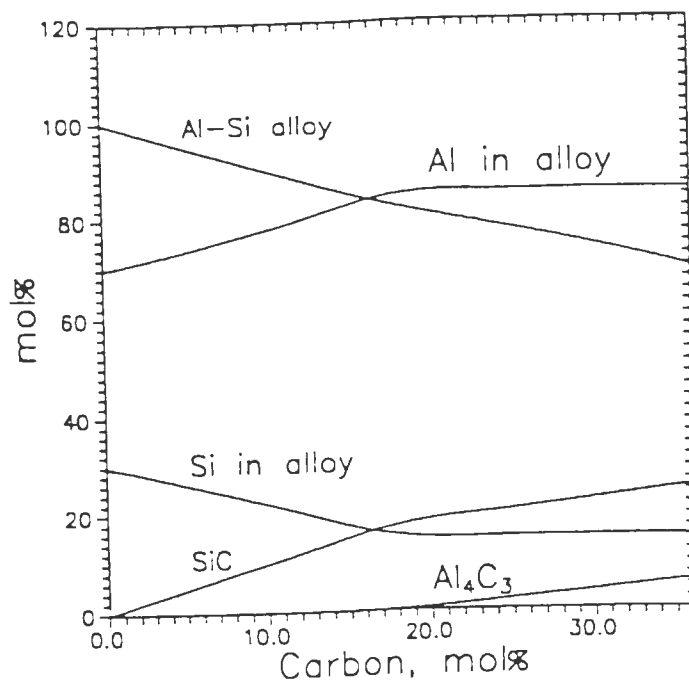
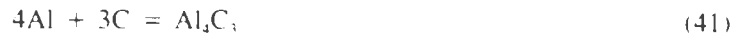


Figure 20 Effect of carbon addition to the 70mol%Al-30mol%Si alloy on the equilibrium species distribution in the system at 1473K.

appears in the equilibrium composition. Formation of aluminum carbide takes place according to reaction:



$$\Delta G = -268.185 + 98.59T, \text{ J/mol} \quad (42)$$

Reaction (39) is parallel to the reaction (41). After Al_4C_3 appears in the equilibrium composition the concentrations of Al and Si do not change, the fraction of alloy decreases, while the quantity of SiC grows simultaneously with Al_4C_3 . The alloy composition corresponds to point A on the phase diagram. To avoid aluminum carbide formation the addition of carbon should be limited.

According to Table 7 addition of less than 16 mol pct of C to alloy with 30 mol pct of Si allows to form only silicon carbide. During experiments described in more details in Chapter 5, 10.2 mol pct of carbon were added to the mentioned alloy at 1573K. As predicted by thermodynamic calculations only SiC was formed. The microstructure of the sample is given in Figure 40. Effect of Si concentration in initial alloy on the maximum concentration of SiC which can be reached without Al_4C_3 formation is shown in Tables 8 and 9 and Figure 21. At 1473 K alloy with 30 mol pct of Si allows to reach 18 mol pct of SiC, alloy with 40 mol pct of Si - 28 mol pct of SiC, while alloy with 50 mol pct of Si - 40 mol pct of SiC. As seen from Table 8 addition of less than 24 pct of C to alloy with 40 pct of Si allows to form only silicon carbide. During experiments described in more details in Chapter 5, 20 mol pct of carbon were added to the mentioned alloy at 1573K. As predicted by thermodynamic calculations only SiC was formed. The microstructure of the sample is given in Figures 66 and 67. The

Table 8 Effect of temperature and carbon addition to 40mol%Si-60mol%Al alloy on the formation of SiC and Al₄C₃

T, K	Initial composition		Addition of carbon mol% of alloy	Equilibrium composition				
	Al mol%	Si mol%		Alloy mol%	Composition of alloy, mol%		SiC mol%	Al ₄ C ₃ mol%
					Al	Si		
1373	60	40	16.01%C	83.99	71.44	28.56	16.01	0
1373	60	40	24.01%C	75.99	78.96	21.04	24.01	0
1373	60	40	32.01%C	68.68	85.22	14.78	30.65	0.67
1373	60	40	40.01%C	62.45	85.22	14.78	34.47	3.08
1473	60	40	16.01%C	83.99	71.44	28.56	16.01	0
1473	60	40	24.01%C	75.99	78.96	21.04	24.01	0
1473	60	40	32.01%C	68.69	85.18	14.82	30.63	0.68
1473	60	40	40.01%C	62.46	85.18	14.82	34.45	3.09
1573	60	40	16.01%C	83.99	71.44	28.56	16.01	0
1573	60	40	24.01%C	75.99	78.96	21.04	24.01	0
1573	60	40	32.01%C	68.44	86.26	13.74	31.12	0.44
1573	60	40	40.01%C	62.27	86.26	13.74	34.87	2.85

Table 9 Effect of temperature and carbon addition to 50mol%Si-50mol%Al alloy on the formation of SiC and Al_4C_3

T. K	Initial composition		Addition mol% of alloy	Equilibrium composition				
	Al mol%	Si mol%		Alloy mol%	Composition of alloy, mol%		SiC mol%	Al_4C_3 mol%
					Al	Si		
1373	50	50	32.01%C	67.99	73.54	26.46	32.01	0
1373	50	50	40.01%C	59.99	83.35	16.65	40.01	0
1373	50	50	48.01%C	53.06	85.22	14.78	45.03	1.91
1373	50	50	56.01%C	45.43	85.22	14.78	50.05	4.51
1473	50	50	32.01%C	67.99	73.54	26.46	32.01	0
1473	50	50	40.01%C	59.99	83.35	16.65	40.01	0
1473	50	50	48.01%C	53.06	85.18	14.82	45.02	1.92
1473	50	50	56.01%C	45.43	85.18	14.82	50.05	4.52
1573	50	50	32.01%C	67.99	73.54	26.46	32.01	0
1573	50	50	40.01%C	59.99	83.35	16.65	40.01	0
1573	50	50	48.01%C	52.95	86.26	13.74	45.32	1.73
1573	50	50	56.01%C	45.37	86.26	13.74	50.28	4.34

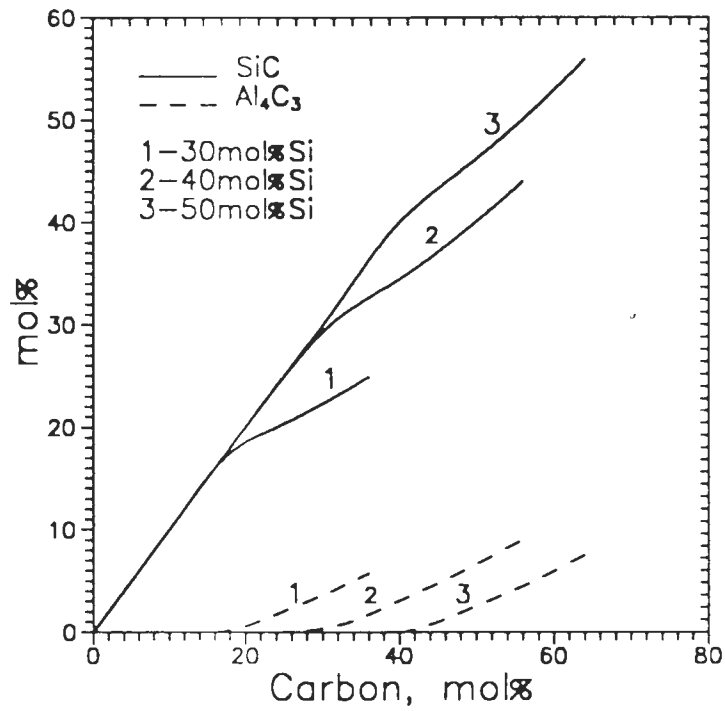


Figure 21 Effect of initial Al-Si alloy composition and carbon addition to the alloy on the formation of SiC and Al₄C₃ at 1473K.

final composition of this sample is approximately the same as of the one produced by addition of SiC to Al-Si alloy with 20 mol pct Si and presented in Figure 19. Comparison of Figures 66 and 19 shows that the difference between them lies in the shape of SiC. In-situ formed SiC from Figure 66 retains the round shape of precursor carbon particles, while SiC from Figure 19 has irregular jagged surface.

Effect of Si concentration on the compositional path is shown in Figure 22. Carbon addition to alloy with 30 mol pct of Si is equal to movement from point G_1 toward carbon. When small amount of carbon is added the composition lies in the $L_3 + \text{SiC}$ phase triangle. With further additions of carbon the compositional path crosses the boundary line of ternary phase at point H_1 . At this point aluminum carbide appears in the equilibrium composition. Increase of Si concentration in initial alloy from 30 to 50 mol pct is equal to the sliding the first point of compositional path from point G_1 toward point G_2 and as a result the maximum SiC concentration, which may be achieved without Al_4C_3 formation increases.

Also as seen from Figure 23 the increase of temperature from 1173 K to 1423 K leads to the decrease of maximum of SiC achievable without Al_4C_3 from 20 to 17 mol pct. At 1423K according to Figure 23 the behavior of the system changes to reverse. At temperatures higher than 1423K raising the temperature leads to slight increase in SiC and decrease in Al_4C_3 .

The effect of temperature on the phase diagram is shown in Figure 24. Temperature increase from 1173 to 1423 K is equal to sliding of point A_1 toward A_2 and point B_1 toward point B_2 . At the same time the point where Al_4C_3 appears in the

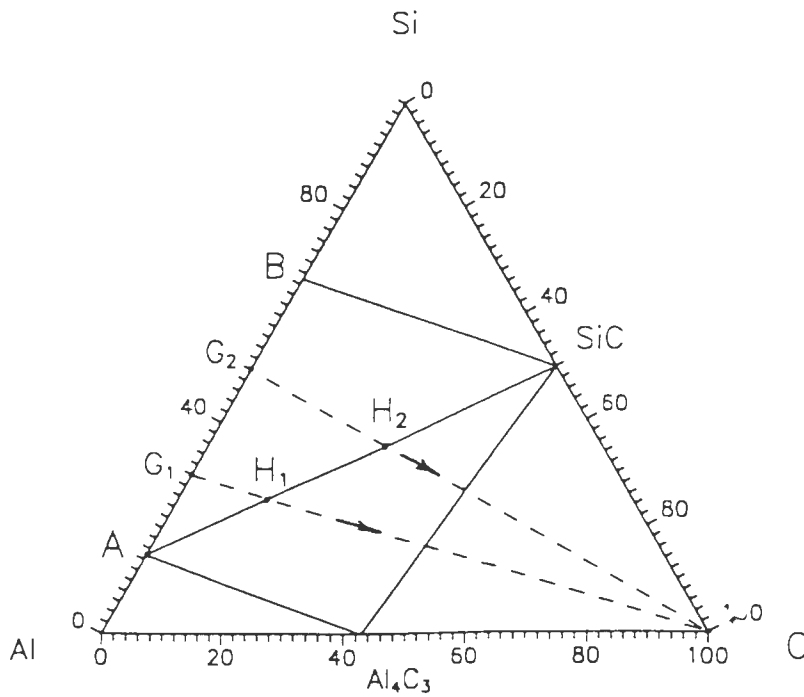


Figure 22 Effect of Si concentration in Al alloy on the compositional path corresponding to in-situ formation of SiC at 1473K.

Phase identification is given in Figure 5.

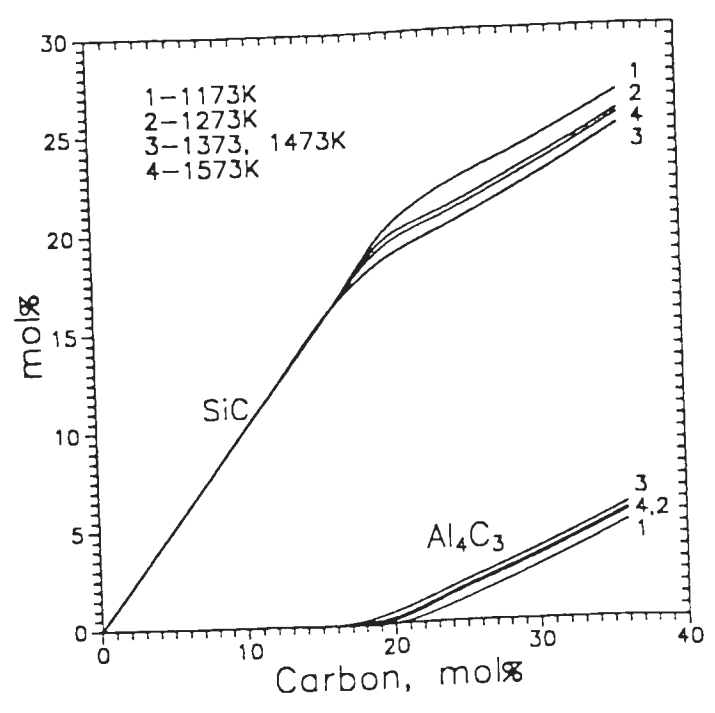


Figure 23 Effect of temperature and carbon addition to the 70%mol Al - 30%mol Si alloy on the formation of SiC and Al₄C₃.

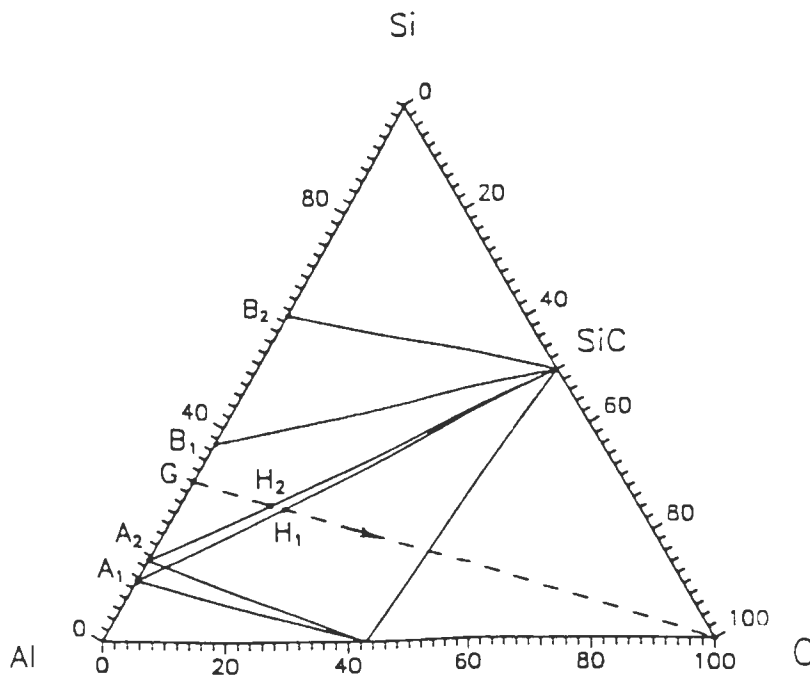


Figure 24 Effect of temperature on the Al-Si-C phase diagram and compositional path corresponding to addition of carbon to 70mol%Al-30mol%Si alloy. Phase identification is given in Figure 5.

equilibrium composition moves from H_1 to H_2 and the quantity of SiC achievable without Al_4C_3 formation decreases slightly. At temperatures higher than 1423K the movement direction of points A_2 and H_2 changes to reverse.

4. EXPERIMENTAL PROCEDURE

4.1 Chemicals and materials

Al, granular, 2-5 mesh, 99.9% pure was purchased from Aldrich Chemical Company, Inc. Si, powder, -325 mesh, 99% pure was purchased from Aldrich Chemical Company, Inc. Activated carbon, designated Norit RO 3515 was purchased from Norit N.V., Netherlands. Natural gas was of industrial supply. Ar gas was purchased from Sierra Welding Supply, Sparks, NV. Alumina crucibles and tubes were purchased from Coors Ceramics Company, Golden, Colorado.

4.2 High temperature furnace set-up

Lindberg, single zone, vertical tube furnace, type 54433 with working temperature range 773-1773 K was used in all experiments. The furnace consists of a working chamber, heating elements, insulation, platinum-platinum-13% rhodium thermocouple, and a control console. Double-end silicon carbide heating elements are mounted above and below furnace chamber. The positioning of elements compensates for heat loss from the ends of the process tube and improves the system performance. The chamber is constructed of high-temperature graded insulation, assuring excellent chamber temperature uniformity and thermal efficiency. Control console model 59545 is a specially designed instrument for use with silicon carbide heating element furnace and calibrated for platinum thermocouple. This instrument system consists of a Lindberg solid state temperature controller with a 4-digit thumbwheel setpoint switch and phase-angle fired output pulses, a Lindberg power output module, and an on/off power input circuit

breaker. The controller with adjustable proportional band and fixed reset and rate functions also features an adjustable maximum power control that varies the load voltage from 0 to 100%. This power control is used to reduce output voltage to compensate for lower heating element resistance during heat up and to increase output voltage to compensate for higher heating element resistance due to aging. Temperature profile of the furnace is given in Figure 25. About 6 cm length of constant temperature zone with ± 2 K was obtained.

4.3 Preparation of alloy

Aluminum-silicon alloy was prepared by mixing Al and Si. The mixture was placed into alumina crucible of 30 mm diameter and 100 mm height. The crucible was introduced into the furnace under Ar atmosphere. The furnace was heated to 1773K and kept at this temperature for one hour to ensure complete melting of the alloy. Experimental setup is given in Figure 26. It included the resistance furnace with alumina tube inside it, thermocouple, gas inlet and gas outlet. Crucible was placed on ceramic support. Alloys containing 30, 40 or 50 mol pct of Si were used in further experiments.

4.4 Reaction with natural gas

After melting of the alloy the furnace was cooled to desired temperature and after 30 min. of exposure kinetic experiments were started. Gas mixture of Ar and 10, 20 or 40% of CH_4 was bubbled through the melt. Gas flow was 2 l/min. In a certain time intervals 2-3 g alloy samples were sucked using 5 mm diameter quartz tube from the bottom of the crucible. When the melt was becoming viscous the process was stopped.

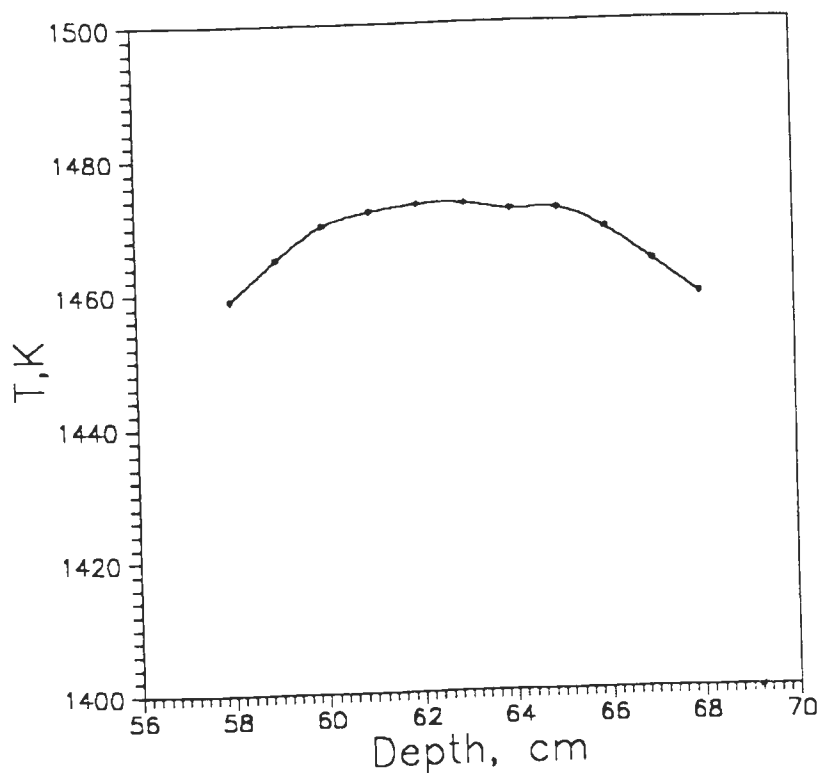


Figure 25 Temperature profile of the furnace.

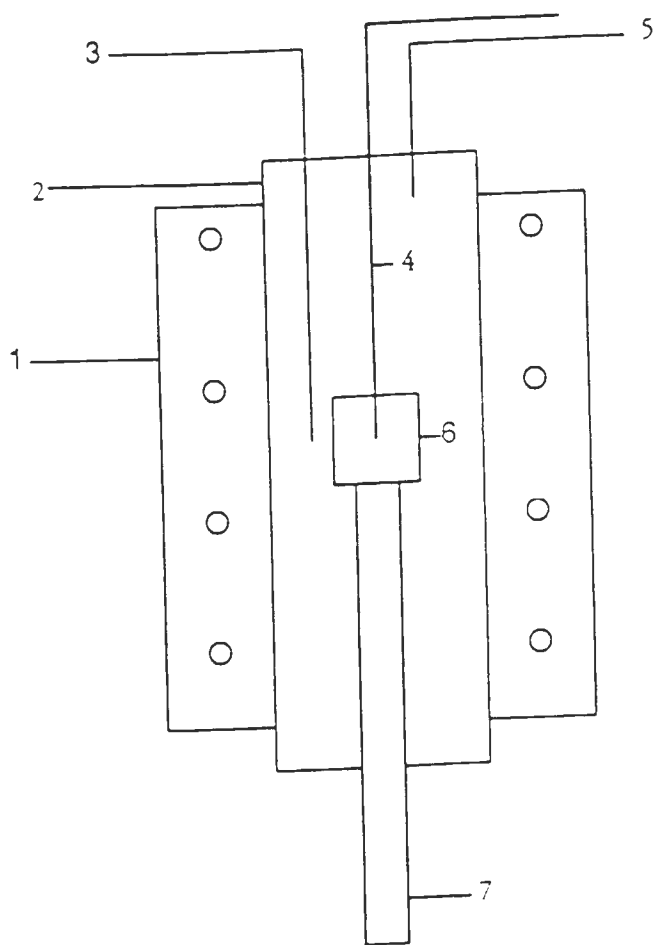


Figure 26 Experimental setup
1- furnace
2 - alumina tube
3 - thermocouple
4 - gas inlet
5 - gas outlet
6 - crucible
7 - ceramic support

the crucible was removed from the furnace and quenched in air. Each sample was analyzed on carbon using LECO carbon and sulfur analyzer and some of the samples were subjected to X-ray diffraction and microscopic evaluation.

4.5 Reaction with graphite rod

After melting of alloy graphite rod 500 mm long and 15 mm in diameter was introduced into the crucible. Ar was bubbled through the melt to provide mixing and reaction was carried for 4 hours. Then the rod was removed from the melt and quenched in air. The part of the rod which reacted with the melt was cut into pieces and subjected to ESM-EDAX analysis.

4.6 Reaction with activated carbon particles

Activated carbon in the form of small rods 1mm in diameter and 3 to 5 mm long was added to the melt. After 15 min of exposure argon gas was bubbled through the melt. This provided mixing and carbon incorporation into the liquid alloy. Gas flow rate was 2 l/min. After certain reaction time the crucible was removed from the furnace and quenched in air. An extent of reaction was calculated using the following equation.

$$X = S_{SiC} / S_C$$

where X is fraction transformed, S_{SiC} is area of SiC formed, S_C is area of nonreacted carbon.

4.7 SEM-EDAX analysis

The samples were fractured, polished and the microstructure was analyzed using

SEM-EDAX system. SEM analysis was done using JSM-840 Scanning Electron Microscope. Energy dispersive spectrometry was done using KEVEX software.

4.8 X-ray powder diffraction

The phase content of the samples was determined by the X-ray powder diffraction method. The X-ray source was Cu-K α radiation with a monochromator. The scanning 2θ angle was from 10° to 90° at a scanning rate of $2^\circ/\text{min}$ and a chart speed of $2.5 \text{ cm}/\text{min}$. For the X-ray diffraction pattern analysis, Braggs Law was applied in the form

$$\lambda = 2d \sin \theta$$

Knowing λ , the wavelength of Cu-K α (1.542 Å) radiation and the 2θ angle of reflection, the d-spacings were calculated for diffraction peaks. By comparing the calculated d spacings with the standard JCPDS data file, the phases in each specimen were determined.

4.9 Chemical analysis

Carbon analysis was done using LECO CS-46 System. The system consists of a Model 770-200 Determinator and a Model 763-600 Induction Furnace. Principally, the sample is combusted with oxygen in a LECO Induction Furnace using LECOCEL accelerator. Approximately 97% of the carbon is oxidized to CO_2 and about 3% combusts to CO (except on low carbon samples where very little CO is formed), sulfur oxidizes to SO_2 . During combustion the concentration of gases in the closed loop rapidly becomes homogenous. All three gases are detected separately in the same chamber.

The solid state detectors are energy detectors. Filters are used to pass the appropriate IR wavelengths to each detector. In the absence of CO, CO₂, and SO₂ the energy recieved by each detector is maximum. During combustion the IR adsorption properties of CO, CO₂ and SO₂ gases in the chamber cause a loss of energy; therefore a loss in signal results which is proportional to the concentration of each gas. Accuracy of analysis is 5%.

5. EXPERIMENTAL RESULTS

5.1 Experimental trials

5.1.1 Reaction with natural gas

The effect of time (4 to 120 minutes), temperature (1273 and 1473K) and gas composition (10, 20, and 40 pct of CH₄ with Ar) on in-situ formation of SiC in 30 mol pct Si - 70 mol pct Al melt was investigated. The X-ray analysis of the samples (Figure 27) showed that SiC was formed but its quantity was extremely low. As can be seen from Figure 27, along with SiC, Al₂O₃ was also formed. The natural gas used was of commercial grade. The formation of alumina in the melt may be due to the reaction of aluminum with impurities present in the natural gas such as CO, CO₂ and H₂O. The results of experiments are summarized in Tables 10 and 11.

5.1.2 Effect of time, temperature and gas composition.

As can be seen from Figure 28 there is no significant effect of time and gas composition on the SiC formation in the melt at 1273K. The carbon content of the melt remained in the range of 0.15 to 0.30 wt. pct. If generated silicon carbide particles were randomly distributed in alloy the carbon content would increase with time. But after 0.15-0.30 wt pct carbon in the melt was reached at the very beginning of the process there were only small variations of carbon concentration. The reason for that is flotation of silicon carbide particles to the surface. After the crucibles were cooled some kind of

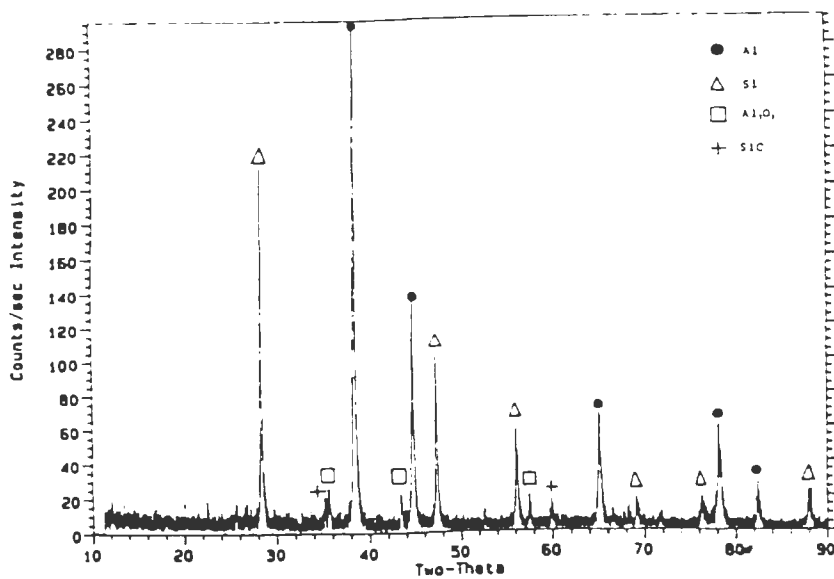


Figure 27 X-ray diffraction pattern of the sample with 0.3wt% carbon after 1 hour of reaction of natural gas with 70wt%Al-30wt%Si alloy.

Table 10 Results of Al-Si alloy analysis on carbon after reaction of 70 wt% Al - 30 wt% Si alloy with natural gas at 1473K.

Time, min	Concentration of natural gas		
	10%	20%	40%
	Carbon, wt% .		
0	0	0	0
1	0.1	0.05	0.06
2	0.2	0.10	0.12
3			0.18
4	0.28	0.15	
6			0.20
10		0.21	0.21
10.5	0.25		
14			0.16
15.5	0.24		
16.5		0.25	
22			0.18
23		0.18	
23.5	0.19		
27			0.15
30		0.18	
31	0.19		
33.5			0.16
38		0.20	
38.5	0.19		
40.5			0.19
46.5	0.20	0.20	
56.5	0.31		
62			0.24
71	0.23		
76			0.21
90	0.23		
110	0.23		

Table 11 Results of Al-Si alloy analysis on carbon after reaction of 70wt% Al-30wt% Si alloy with natural gas (Ar-10%CH₄) at 1473K.

Time, min	Carbon concentration, wt%
0	0
17	0.74
33	0.37
48	0.30

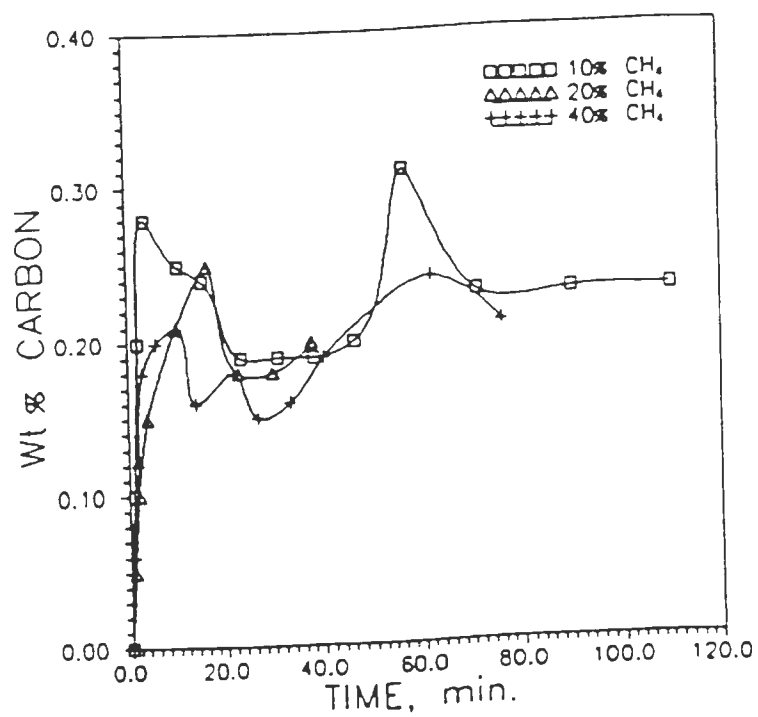


Figure 28 Effect of reaction time and partial pressure of natural gas on carbon content in the melt at 1273K.

"metal foam" was detected on the walls of the crucibles. The concentration of carbon in the "foam" was 0.52 to 0.88 wt pct, which was 2 to 4 times higher than the average concentration of carbon in the bulk alloy. Overall efficiency of natural gas was very low: 3 pct for 10 pct of CH_4 , 2 pct for 20 pct of CH_4 and 0.6 pct for 40 pct of CH_4 . Maximum silicon carbide concentration reached in the "metal foam" was 3 wt pct. Figure 29 shows typical microstructure of the samples taken from the bulk alloy and from the "foam". The "foam" was much more porous but XRD pattern showed that the composition of it was practically the same as of the bulk alloy. The possible silicon carbide particles were too small and were not identified by energy dispersive spectrometry during scanning electron microscopic analysis.

Figure 30 shows the effect of temperature and time on the carbon concentration in the bulk alloy. As can be seen from Figure 30 temperature does not have significant effect on SiC formation in the alloy. For example, after one hour of reaction time carbon content in the alloy at 1273K was 0.3 wt pct. The same concentration was achieved at 1473K.

To understand the reasons of low natural gas efficiency the calculations were made to study the effect of temperature on the species distribution in C-H system. Figure 31 shows the results of such calculations. As seen from the figure at temperatures higher than 1073K natural gas is not stable. So when the mixture of natural gas and argon was introduced into melt, natural gas decomposed into carbon powder and hydrogen. But most of the carbon formed was removed from the melt by Ar, which served as a carrier gas. As a result the efficiency of natural gas was extremely low [110].

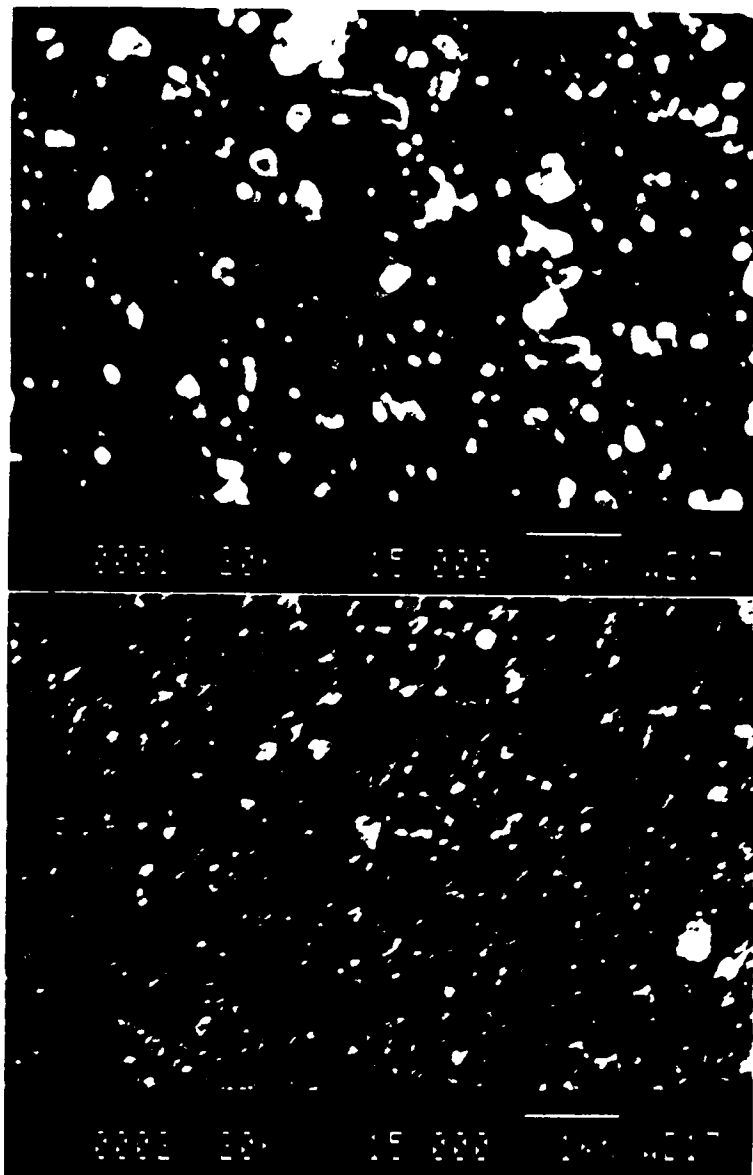


Figure 29 Typical SEM images of the sample after the reaction of natural gas with (70wt% Al-30wt% Si) alloy, (0001) - metal "foam" from the top of the crucible, (0002) - bulk alloy.

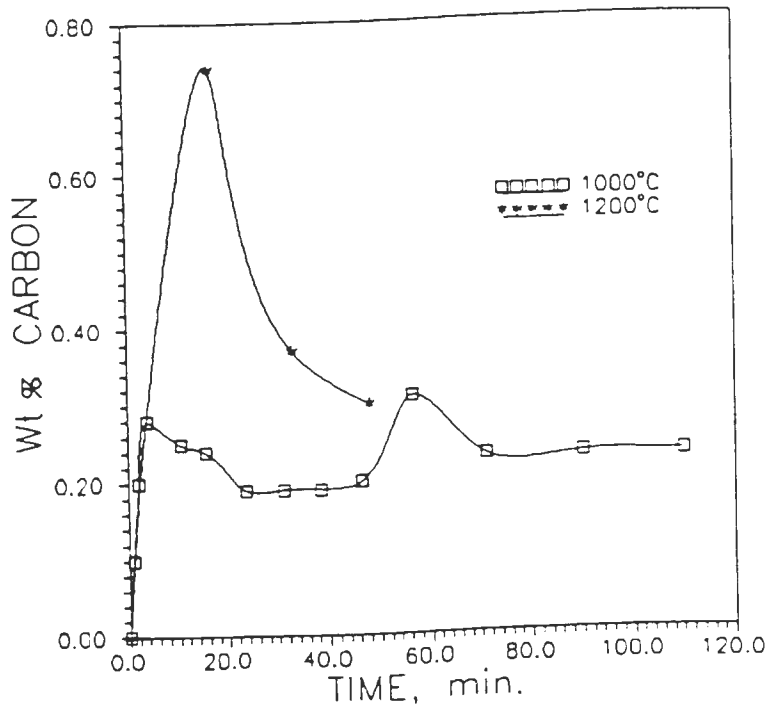


Figure 30 Effect of reaction time and temperature on carbon content in the melt for 90%Ar - 10%CH₄ gas mixture.

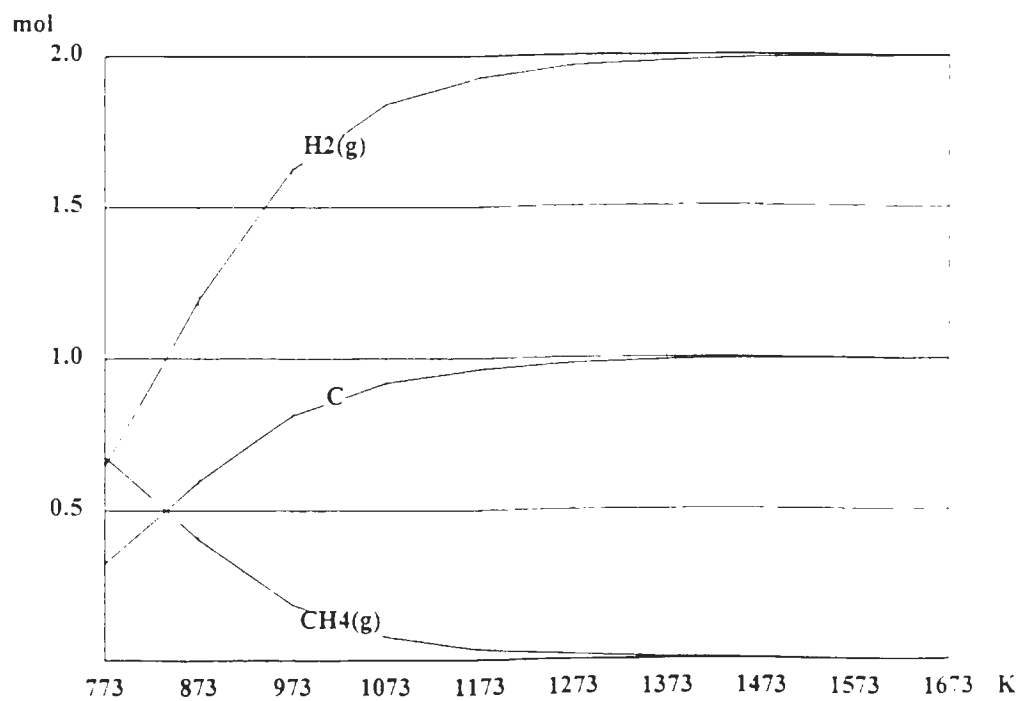


Figure 31 Effect of temperature on the species distribution in the C-H system for 100% CH₄ gas.

5.1.3 Conclusions on the experiments with natural gas

The study of natural gas as a carbon source was done at 1273 to 1473K. concentration of CH_4 was 10 to 40 pct and reaction time 4 to 120 min. Maximum SiC concentration formed was only 0.88 wt pct. Hence due to very low efficiency (less than 3 pct) natural gas is not suitable as a carbon source for silicon carbide formation.

5.1.4 Reaction with graphite rod

Reaction with graphite rod was carried out at 1773K for 6 hours. The liquid alloy reacted with the rod and the reaction zone was formed. Figures 32 to 34 show SEM images in backscattered electrons of the reaction zone with different magnification. As seen from Figure 32 reaction zone has the form of a ring around the graphite rod. The thickness of the zone was estimated to be $300 \pm 100 \mu\text{m}$. Figures 35 to 37 show EDS spectra of the sample at points 1 and 2 (Figure 34) and average analysis of the zone. Close to the inside surface of a zone aluminum carbide prevailed, while close to the outer surface silicon carbide prevailed. But practically everywhere both were present close to each other. Figures 33 and 34 show that darker areas representing mostly aluminum carbide are mutually penetrating with lighter areas representing mostly silicon carbide. Average EDS analysis of the sample (Figure 35) shows that the quantity of silicon carbide was a little higher. Because only a small portion of carbon reacted, according to the phase diagram there should be no aluminum carbide. But actual presence of aluminum carbide may be explained using the following mechanism: the melt penetrated small pores and cavities in the carbon rod. So at the contact between the melt and



Figure 32 SEM image in backscattered electrons of the reaction zone on the graphite rod with magnification 15X.

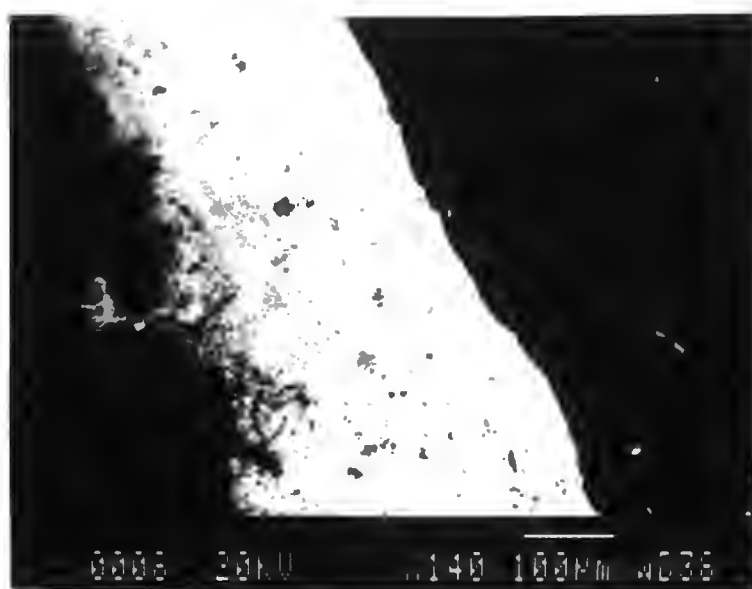


Figure 33 SEM image in backscattered electrons of the reaction zone on the graphite rod with magnification 140X.

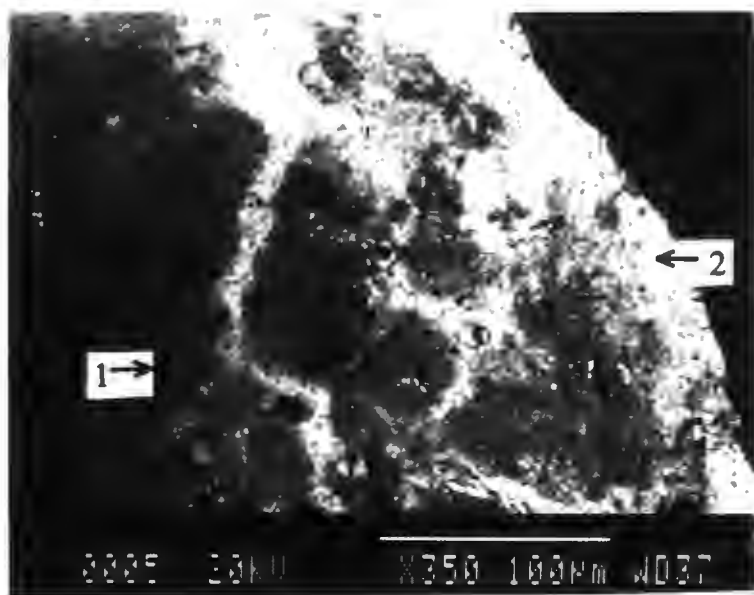


Figure 34 SEM image in backscattered electrons of the reaction zone on the graphite rod with magnification 350X, 1 - Al_4C_3 , 2 - SiC .

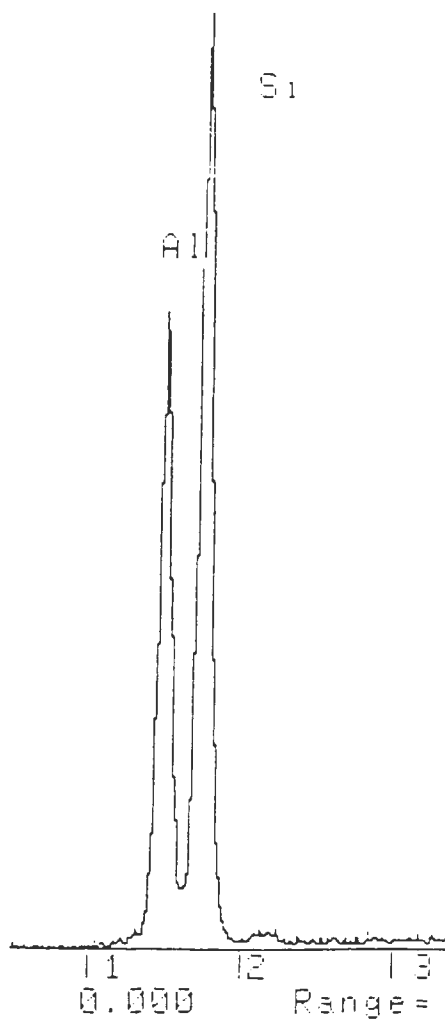


Figure 35 EDS spectra corresponding to the average concentration of the reaction zone (Fig. 34) on the graphite rod.

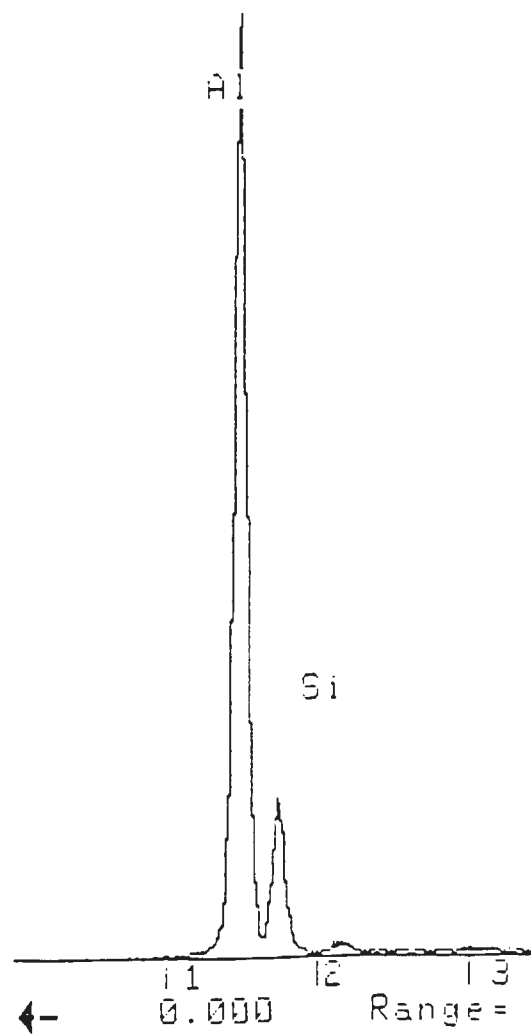


Figure 36 EDS spectra of the reaction zone (Fig. 34) on the graphite rod at point 1.

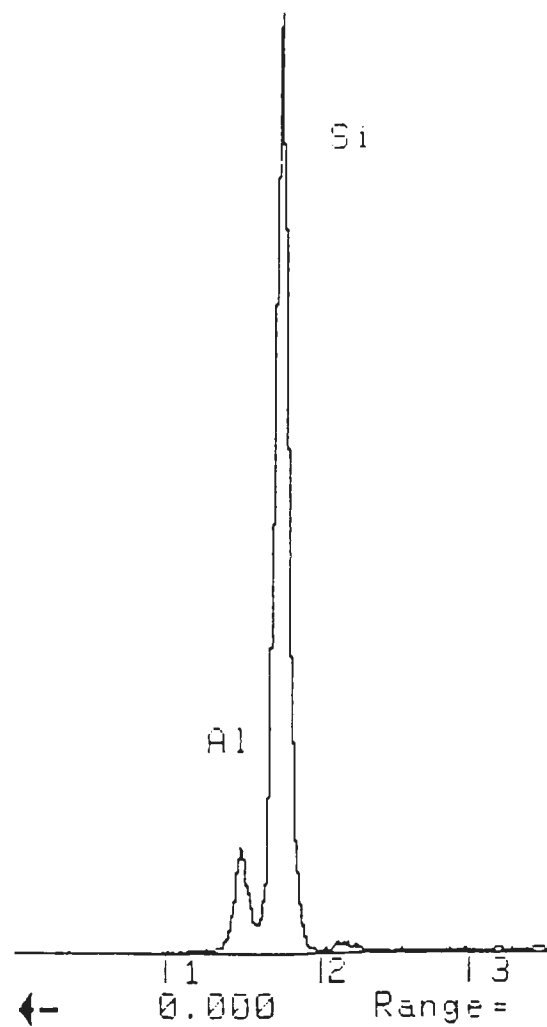


Figure 37 EDS spectra of the reaction zone (Fig. 34) on the graphite rod at point 2.

graphite there was an excess of carbon and as a result of local equilibrium both SiC and Al_4C_3 formed. So the deeper the melt penetrated, the more excess carbon was at the contact and the more aluminum carbide formed. Because of that close to the inside surface aluminum carbide prevailed. At the outer surface the melt was stirred, there was no excess carbon and mostly silicon carbide was produced [111]. The results of experiments with graphite rod is presented in Table 12. The piece of rod with reaction zone was left in air and its outer surface decomposed into powder in a few days. This is well known behavior of composite degradation when aluminum carbide is present in the material.

5.1.5 Conclusions on the experiments with graphite rod

Reaction with graphite rod was carried out for 6 hours. Reaction zone of $300\ \mu\text{m}$ was formed consisting of the mixture of SiC and Al_4C_3 . Due to the Al_4C_3 formation, graphite is not suitable as a carbon source for SiC formation.

5.1.6 Reaction with activated carbon

One experiment was performed to see if *activated carbon* is a suitable source of carbon for SiC formation. Initial alloy composition was 70 mol pct Al - 30 mol pct Si and 10.2 mol pct of carbon was added. Reaction time was 20 hours and temperature 1373K. The final sample was cut, polished and analyzed using SEM-EDAX system. Microphotographs of different areas of the sample are given in Figures 38, 40 and 41. Most of the carbon added completely reacted to form silicon carbide and Figure 38

Table 12 Results of experiments on reaction between 70 wt% Al - 30 wt% Si alloy and graphite rod at 1773K.

Time, hours	Reaction zone length, μm	Characterization of reaction products
6	300 ± 100	mixture of SiC and Al_4C_3

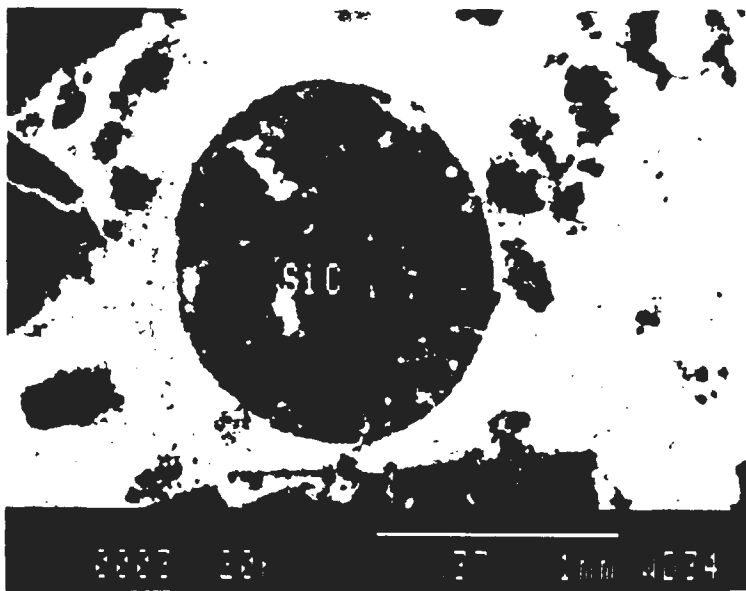


Figure 38 SEM image in backscattered electrons of a SiC particle after reaction at 1573 K for 20 hours. Initial alloy 70wt% Al-30wt% Si.

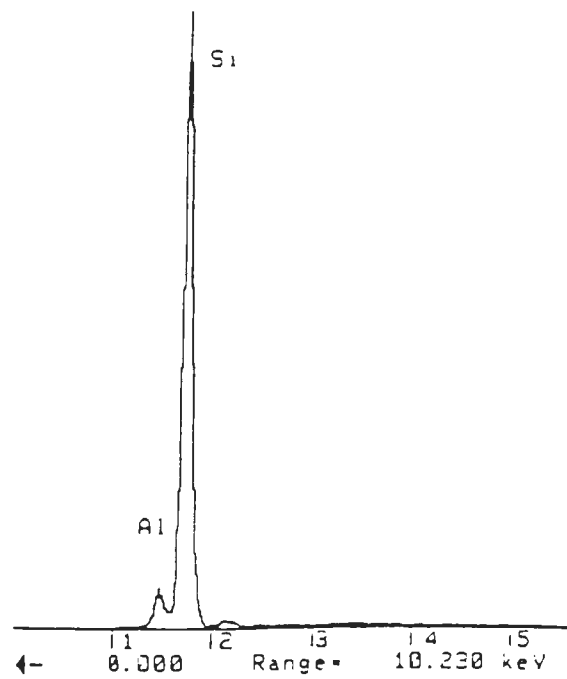


Figure 39 Energy spectra of the SiC particle from Figure 38.

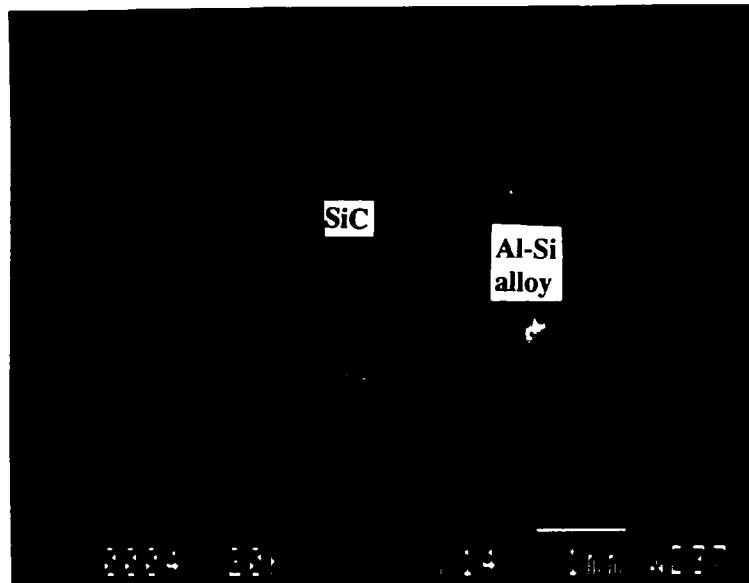


Figure 40 SEM image in backscattered electrons of several SiC particles after reaction at 1573 K for 20 hours. Initial alloy 70wt% Al-30wt% Si.

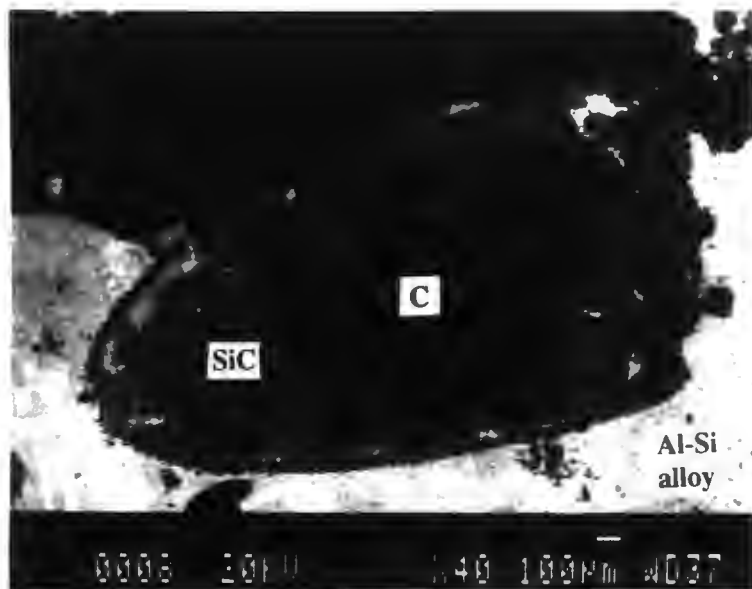


Figure 41 SEM image in backscattered electrons of a non-completely reacted particle with a carbon core after reaction at 1573 K for 20 hours. Initial alloy 70wt% Al-30wt% Si.

shows one of the SiC particles. No residual carbon is seen. EDS analysis (Figure 39) shows high Si peak proving the particle to be SiC (carbon is not detectable by this method). Because of the small carbon addition and the chosen form of mixing the distribution of SiC was not random and the particles concentrated in certain areas. Figure 40 shows one of such areas with several SiC particles. As seen from Figures 38 and 40, the SiC particles mostly retained the round shape and the size of initial carbon rods. No aluminum carbide was detected in any sample. Figure 41 shows the particle which still has a carbon core. This particle did not react completely. Its microstructure shows that the SiC layer grew from the surface to the center of the particle.

As predicted by thermodynamic calculations with addition of 10.2 mol pct of activated carbon to the liquid aluminum-silicon alloy only silicon carbide was formed. The microstructure of incompletely reacted particle allows to conclude that silicon carbide formation was taking place through the movement of the reaction front from the surface to the center of the particle. Most probable mechanism of this process was diffusion of silicon to the SiC/C interface, where it reacted with carbon to form silicon carbide. The fact that all particles had approximately the same size as initial carbon means that no SiC was formed by nucleation and growth mechanism [112].

The result of experiment with activated carbon is presented in Table 13.

5.1.7 Conclusions on the experiments with activated carbon

Reaction between 70 mol pct Al - 30 mol pct Si alloy and 10.2 mol pct carbon was carried out at 1373K for 20 hours. Only silicon carbide was formed. Hence *activated*

Table 13 Result of experiment on reaction between 70 wt% Al - 30 wt% Si alloy and activated carbon at 1573K.

Time, hours	Extent of reaction, %	Characterization of reaction products
20	99	SiC and unreacted carbon

carbon is an excellent source of carbon for SiC formation and detailed study of the mechanism of reaction of SiC formation was undertaken.

5.2 MECHANISM OF SiC FORMATION

5.2.1 Characterization of activated carbon

Figure 42 shows a photograph of as received activated carbon particles. As seen from the figure they have a rod-like shape 1mm in diameter and 3 to 7 mm long. Figures 43 to 45 show the microstructure of activated carbon at different magnifications. The penetration of black and white colors means that the material is highly porous and its porosity provides high surface area for reaction.

Figures 44 and 45 show that depending on the particular spot there is a significant difference in density and porosity level. Figure 44 shows the microstructure of the pore, while Figure 45 shows more dense part of the carbon particle.

Figure 46 shows EDS spectra of activated carbon. Because carbon is not detectable by this method the fact that the main peak was identified as potassium means that this is the main impurity, while other impurities are Al, Si, and Ca. These are typical ash constituents and usually they are present in the form of different oxides. Gold peak comes from the coating.

The term *activated or active carbon* in its broadest sense includes a wide range of amorphous carbon based materials prepared to exhibit a high degree of porosity and interparticulate surface area. These are obtained by combustion, partial combustion, and thermal decomposition of various carbonaceous substances. These materials may be in granular or in powdered form. The granular form is characterized by a large internal surface and small pores, whereas the finely divided powdered form is associated with larger pore diameters but a smaller internal surface area [113].

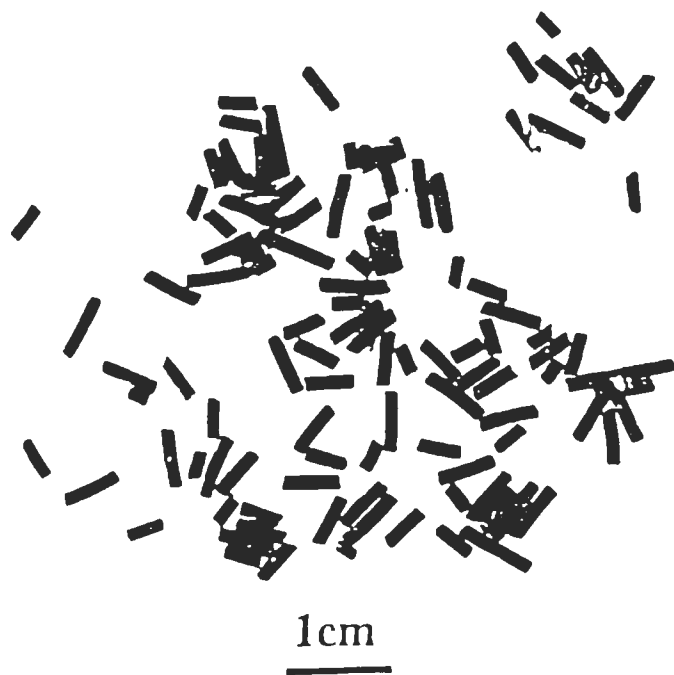


Figure 42 A photograph of as received activated carbon particles.

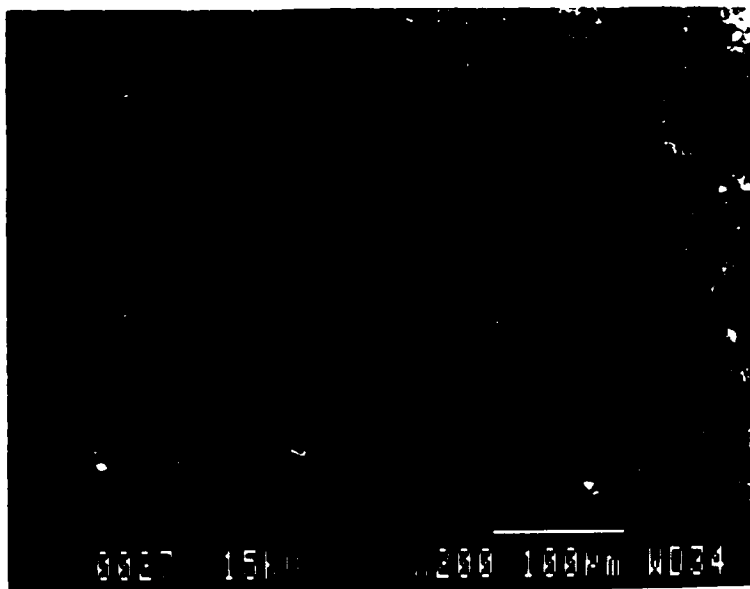


Figure 43 SEM image in backscattered electrons of an activated carbon particle, magnification 200X.

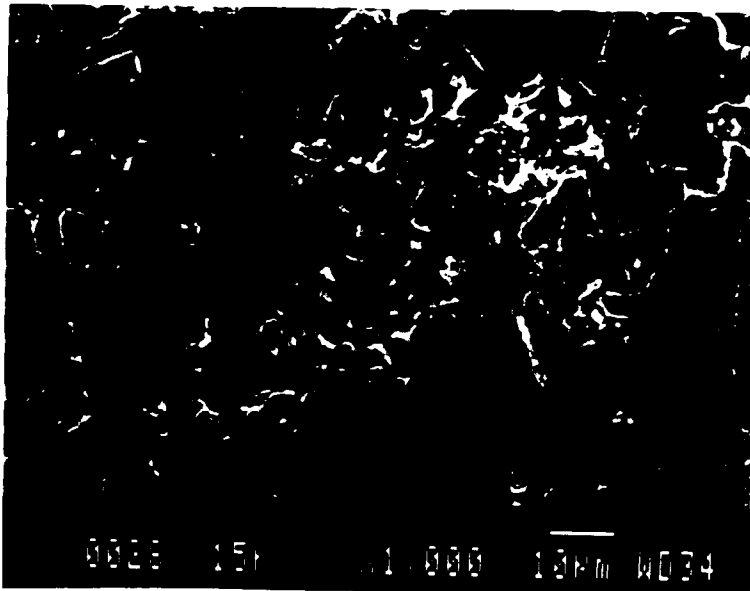


Figure 44 SEM image in backscattered electrons of a pore in the activated carbon particle, magnification 1000X.



Figure 45 SEM image in backscattered electrons of a dense part of the activated carbon particle, magnification 1000X.

Activated carbons are excellent adsorbents and thus are used to purify, decolorize, deodorize, dechlorinate, detoxicate, filter, or remove or modify the salts, separate, and concentrate in order to permit recovery; they are also used as catalysts and catalyst supports.

The adsorbent properties of activated carbons are essentially attributed to their large surface area, a high degree of surface reactivity, universal adsorption effect, and favorable pore size, which makes the internal surface accessible, enhances the adsorption rate, and enhances mechanical strength. The most widely used commercial activated carbons have a specific surface area in the order of 800 to 1500 m²/g. This surface area is contained predominantly within micropores, which have effective diameters smaller than 2 nm. In fact, a particle of activated carbon is made up of a complex network of pores which have been classified into micropores (diameters < 2 nm), mesopores (diameter between 2 and 50 nm), and macropores (diameters > 50 nm). The macropores do not contribute much toward surface area but act as conduits for the passage of the adsorbate into the interior mesopore and the micropore surface where most of the adsorption takes place. The pore size distribution in a given carbon depends on the type of the raw material and the method of manufacture of the carbon.

The large surface area of the activated carbon is the result of the activation process in which a carbonaceous char with little internal surface is oxidized in an atmosphere of air, carbon dioxide, or steam at a temperature between 1073 and 1173K. This causes the oxidation of some of the regions within the char in preference to others so that as combustion proceeds a preferential etching occurs, resulting in the development

of a large internal surface area, which in some cases may be as high as 2500 m² g.

Transmission electron microscopy of carbonaceous materials has shown that the activated carbon structure can be visualized as stacks of flat aromatic sheets crosslinked in a random manner (Figure 47) [113]. Activation by carbon dioxide or steam in the range 1073 to 1173K reduces the number of these aromatic sheets in the original stacks, leaving in some cases single and in general nonplanar layers.

Electron spin resonance studies have revealed that the aromatic sheets in activated carbons contain free radical structures or structures with unpaired electrons. These unpaired electrons are resonance stabilized and are trapped during the carbonization process as a result of the breaking up bonds at the edges of the aromatic sheets thus creating edge carbon atoms. These edge carbon atoms have unsatisfied valences and can thus interact with heteroatoms such as oxygen, hydrogen, nitrogen, and sulfur, giving rise to different types of surface functional groups. The elemental composition of a typical activated carbon was found to be 88% C, 0.5% H, 0.5% N, 1% S, and 6 to 7% O, the balance representing inorganic ash constituents. The oxygen content of an activated carbon can, however vary between 1 and 25 wt %, depending on the type of raw material and the conditions of the activation process. One of the possible activation processes includes the following steps: 1. impregnation of raw materials such as coke or coal with potassium hydroxide, carbonate, or sulfate, 2. heating to 973-1173K, 3. cooling and washing with water to remove the impregnant. As a result of such treatment and although because of the presence of ash constituents EDS specter of activated carbon particle showed high potassium peak.

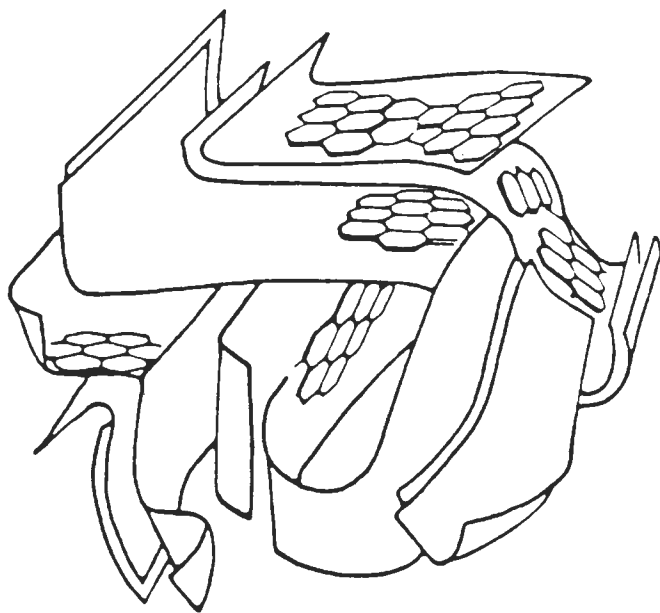


Figure 47 Schematic representation of the microstructure of activated carbon [113].

5.2.2 Initial stage of carbon reaction with the melt

To study the mechanism of reaction between activated carbon and Al-Si alloy carbon particles were introduced into the melt. The melt was kept at 1373 to 1573K for 1 to 6 hours. Reaction products were studied using SEM-EDAX system.

Figures 48 and 49 show several carbon particles after they were incorporated into the melt. As seen from the figure at 1473 K after 1 hour of reaction time the particles keep their round shape. Also some of the particles form agglomerates. Figures 50 and 51 show one of the particles with higher magnification. As seen from this figure no reaction zone has been formed on the interface between the carbon and the matrix alloy. Figures 52 and 53 show the interface at higher magnification. Because carbon is highly porous material the matrix alloy occupies the surface pores but there is no signs of melt penetration into the carbon at this stage.

Figure 54 shows the microstructure of the matrix alloy on the boundary with carbon. It consists of primary silicon crystals (EDS spectra is given in Figure 55) and Al-Si eutectic mixture (Average spectra of the eutectic mixture is given in Figure 56). There is no solid solubility of Si in Al or Al in Si and therefore an eutectic composition represents a mechanical mixture of pure metals [36]. It has the composition of 12.2 mol pct Si and 87.8 mol pct Al and it is presented by Si laminates in Al matrix. Corresponding EDS spectra are given in Figures 57 and 58.

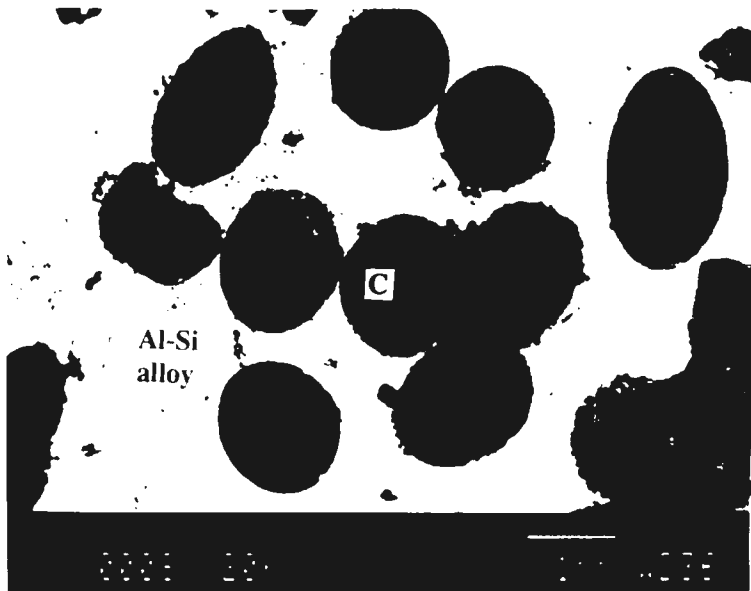


Figure 48 Microstructure of the alloy after incorporation of carbon at 1473K for 1 hour. SEM image in backscattered electrons.

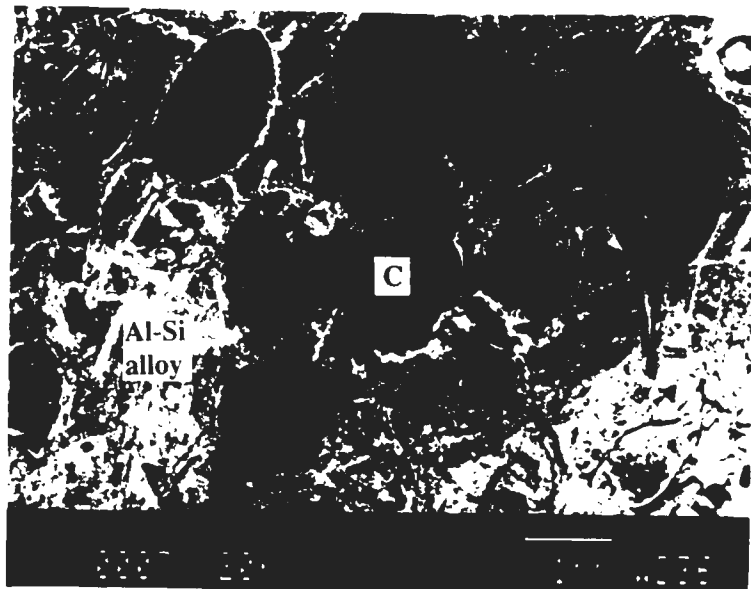


Figure 49 Microstructure of the alloy after incorporation of carbon at 1473K for 1 hour. SEM image in secondary electrons.

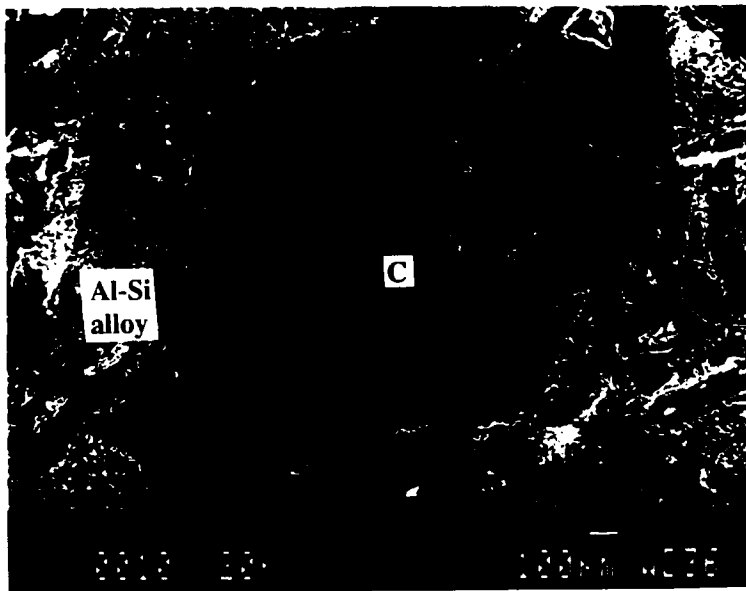


Figure 50 SEM image in secondary electrons of one carbon particle after reaction at 1473K for 1 hour.

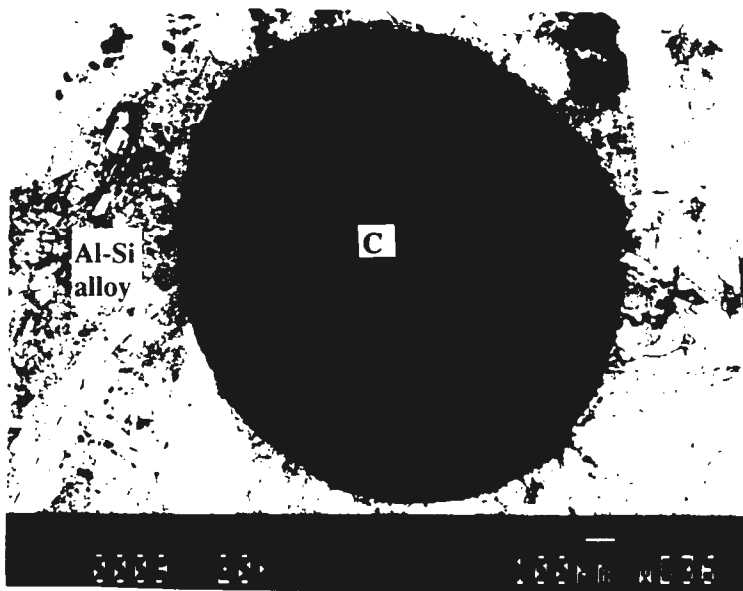


Figure 51 SEM image in backscattered electrons of one carbon particle after reaction at 1473K for 1 hour.

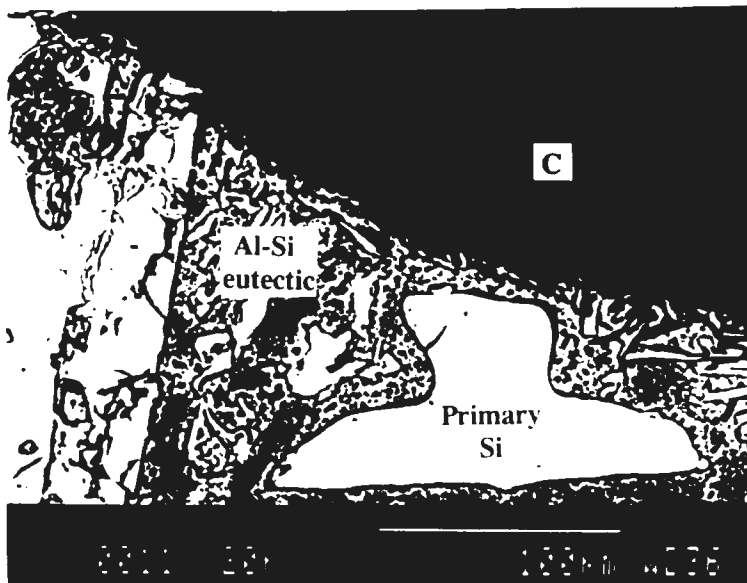


Figure 52 The microstructure of the interface between the carbon and matrix alloy after reaction at 1473K for 1 hour. SEM image in backscattered electrons.

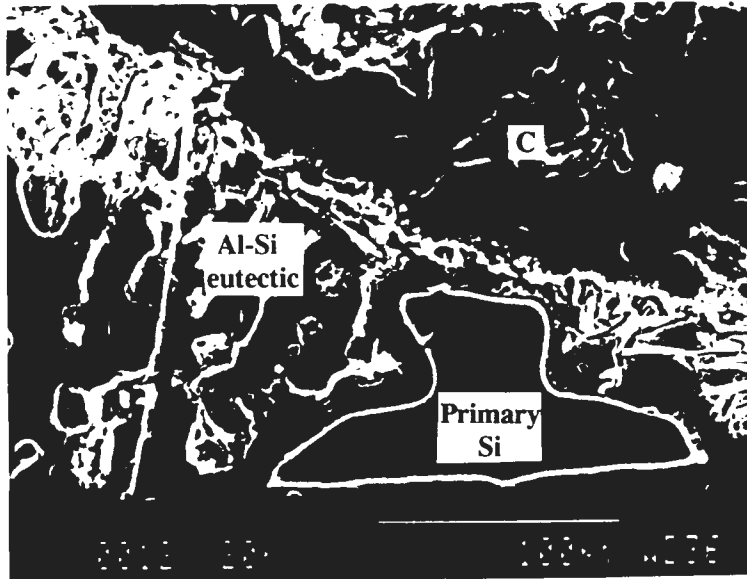


Figure 53 The microstructure of the interface between the carbon and matrix alloy after reaction at 1473K for 1 hour. SEM image in secondary electrons

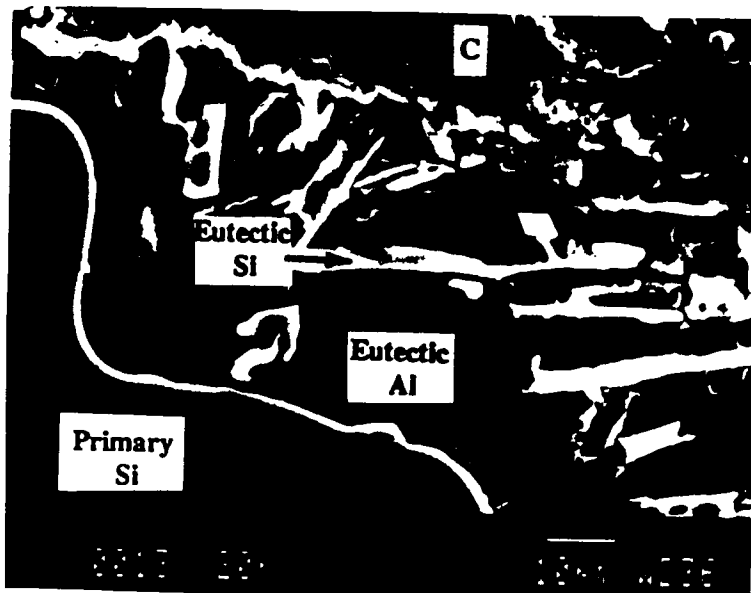


Figure 54 The microstructure of Al-Si eutectic in the matrix alloy after reaction at 1473K for 1 hour, SEM image in secondary electrons.

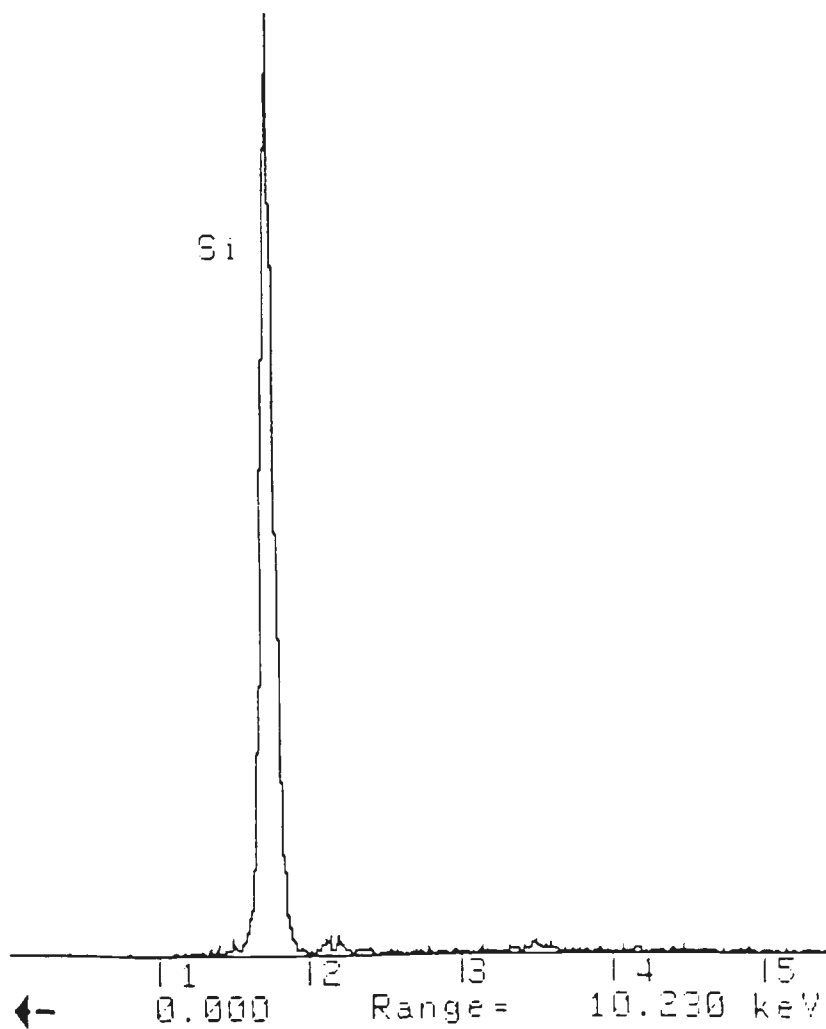


Figure 55 EDS spectra of primary Si crystals from Figure 54.

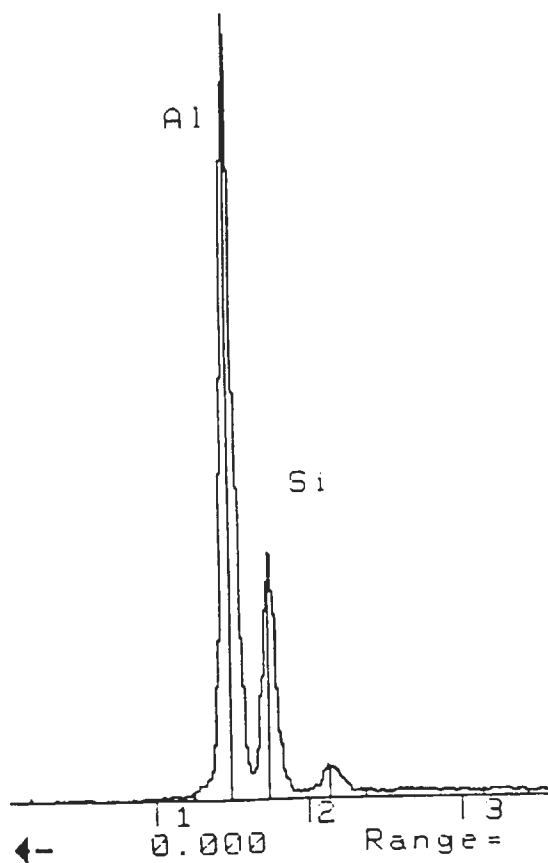


Figure 56 EDS spectra of Al-Si eutectic mixture from Figure 54.

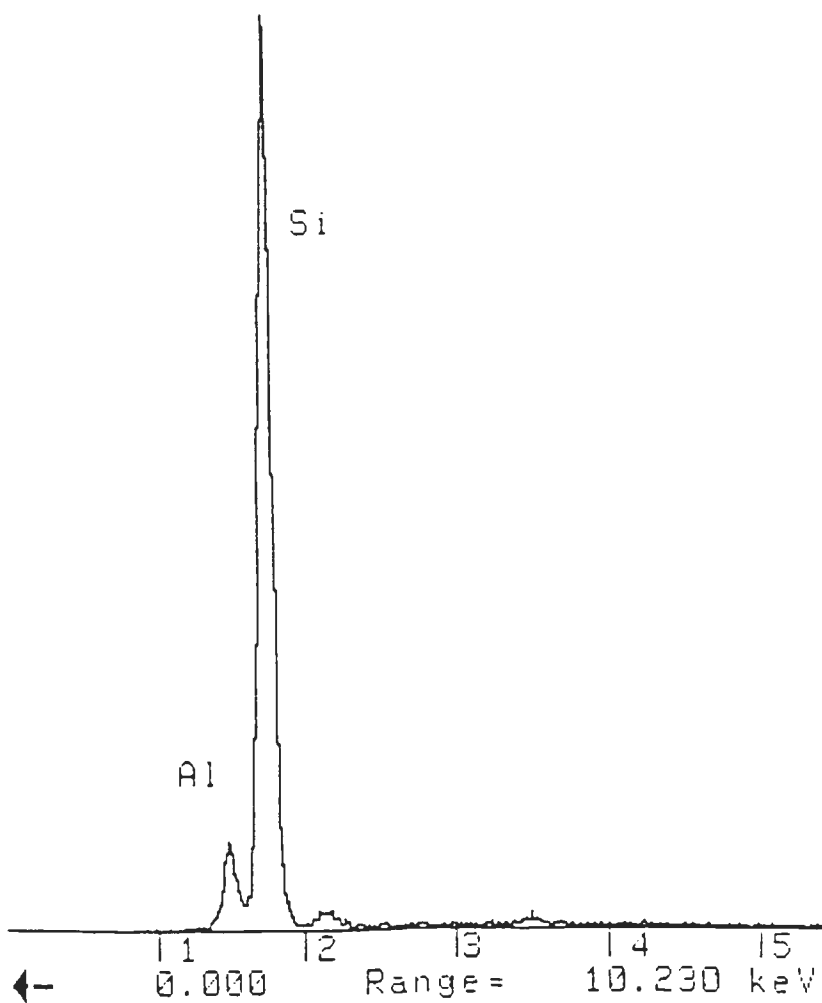


Figure 57 EDS spectra of Si crystals in eutectic mixture from Figure 54.

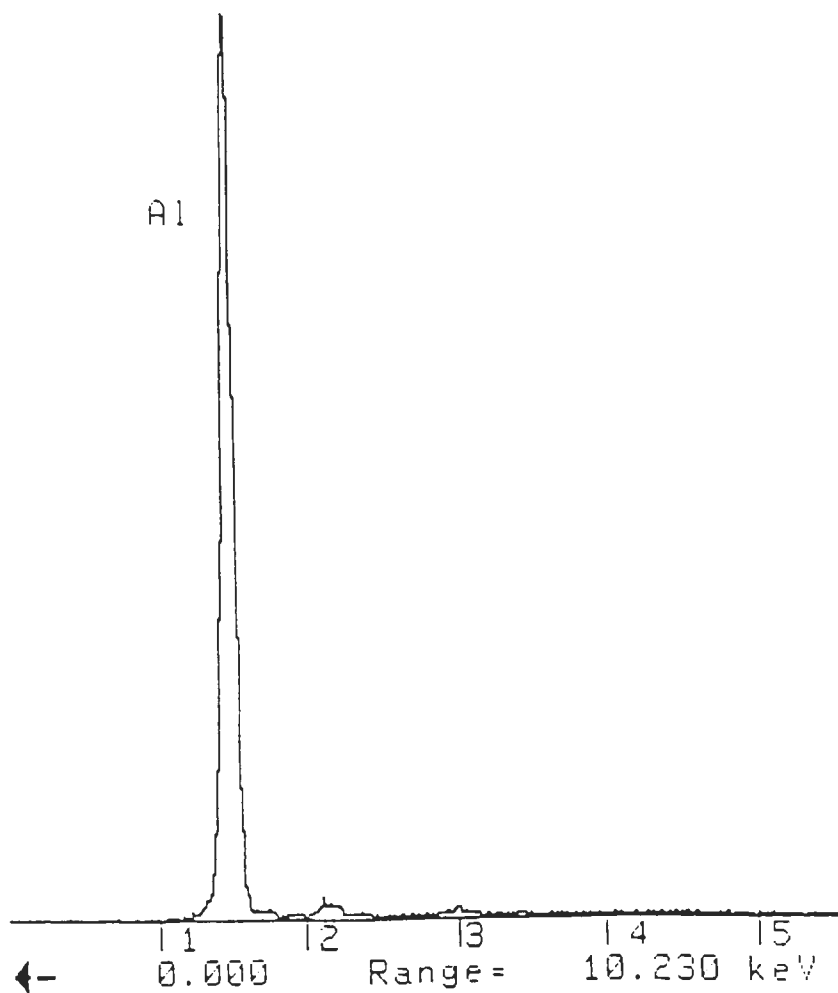


Figure 58 EDS spectra of aluminum crystals in eutectic mixture from Figure 54.

5.2.3 Intermediate stage of reaction

Figures 59 and 60 show several partly reacted SiC particles after reaction at 1373K. Figure 61 shows one of the particles with high magnification. As seen from these figures reaction proceeds from the surface to the center of the particles. Variation of reaction zone thickness on different particles was estimated to be from 0 to 0.5 mm (half of the particle diameter). Figures 62 and 63 show the reaction zone at high magnification. EDS spectra of the reaction zone (Figure 64) showed high Si peak proving it to be SiC (carbon is not detectable by this method). As seen from Figure 63 freshly formed SiC is presented in the form of individual grains, meaning that each carbon grain reacted separately forming a grain of SiC.

Figure 65 shows typical microstructure at higher temperatures (1473 to 1573K). One particle completely reacted, while the others did not react at all. So the extent of reaction was either 0 or 1 and each particle has its own activation time, which was a probability function.

Comparison of Figures 59 and 65 shows that initial stages of reaction are activation and movement of the reaction front. At lower temperatures (1373K) the limiting stage is the movement of the reaction zone. At higher temperatures (1473 to 1573K) the reaction is limited by an activation time and as soon as the reaction starts for each individual particle it quickly proceeds to complete transformation of carbon to silicon carbide.

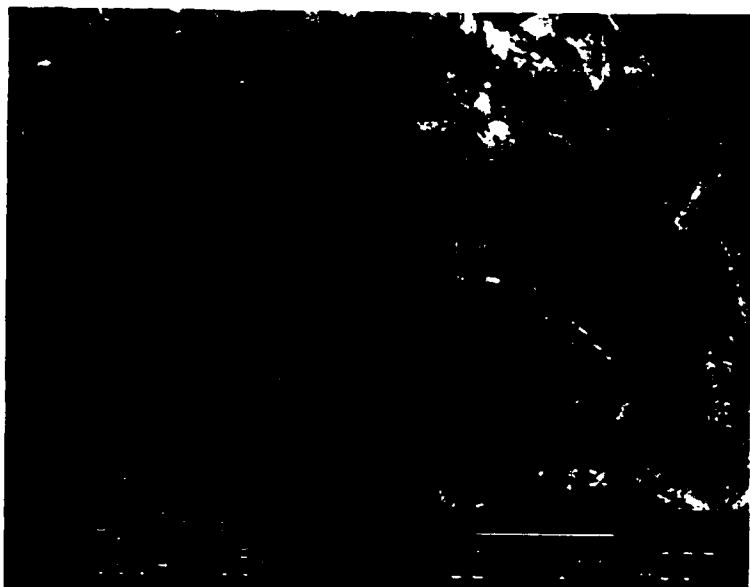


Figure 59 A micrograph of several partly reacted carbon particles after reaction at 1373K for 6 hours. SEM image in backscattered electrons .



Figure 60 A micrograph of several partly reacted carbon particles after reaction at 1373K for 6 hours. SEM image in secondary electrons.

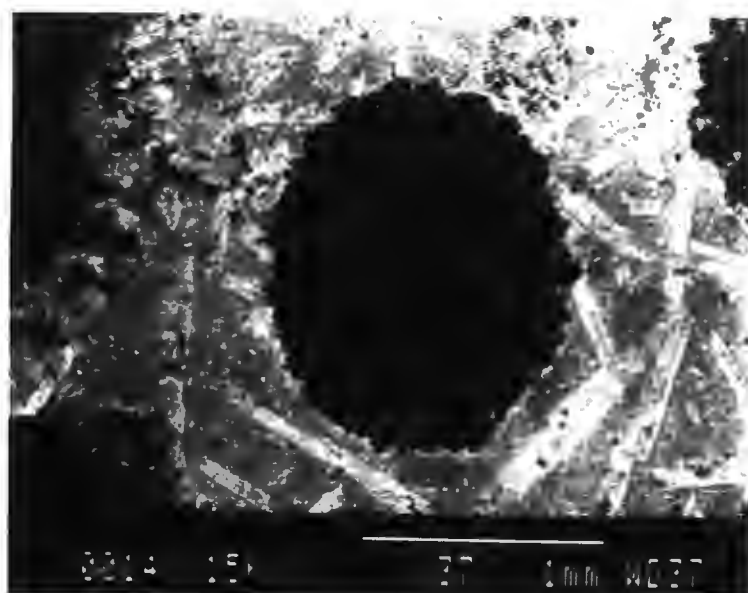


Figure 61 Partly reacted carbon particle after reaction at 1373K for 6 hours,
SEM image in backscattered electrons.

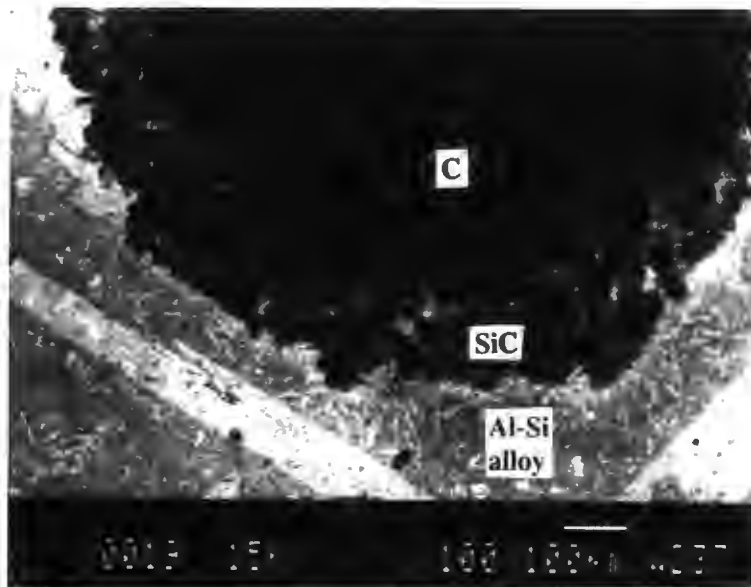


Figure 62 Reaction zone on the partly reacted carbon particle after reaction at 1373K for 6 hours. SEM image in backscattered electrons.

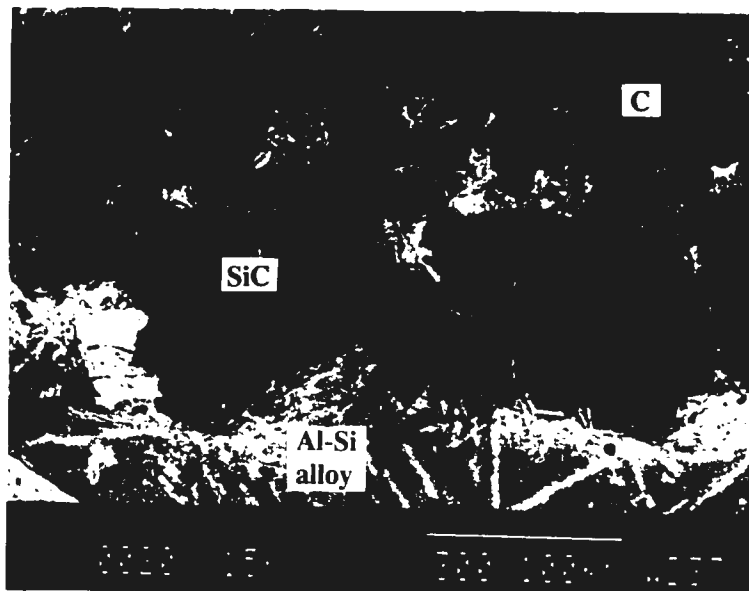


Figure 63 A micrograph of the interface between the carbon and matrix alloy with high magnification after reaction at 1373K for 6 hours.

SEM image in backscattered electrons.

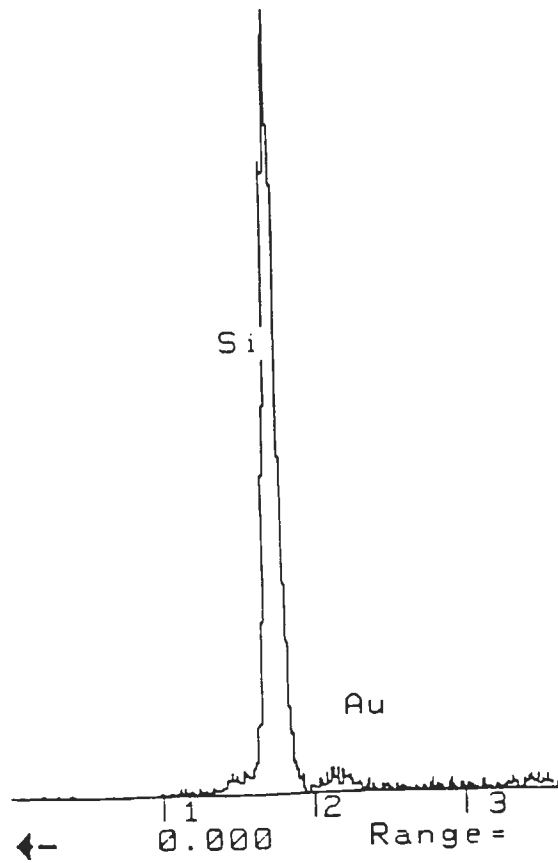


Figure 64 EDS spectra of the reaction formed SiC from Figure 63.

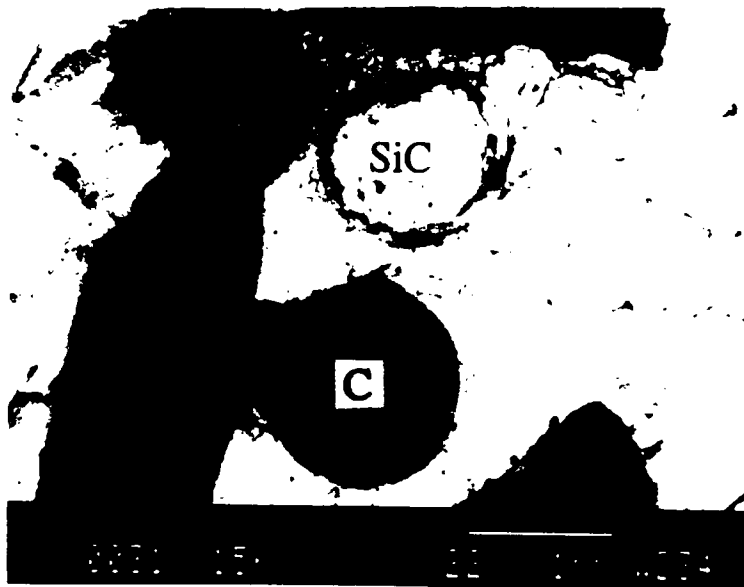


Figure 65 A micrograph of several C and SiC particles after reaction at 1473K for 2 hours. One particle completely reacted and formed SiC. Other particles did not react at all.

5.2.4 Final stage of reaction. Characterization of in-situ formed Al/SiC composite

Figures 66 and 67 show the microstructure of the in-situ formed Al/SiC composite. As seen from the figures all the particles have appearance of SiC and well distributed in the space. Hence the main goal of this work - to form SiC in-situ was achieved. The particles retain the size and the shape of initial carbon. From the Figures 61 to 63 one can conclude that the reaction proceeded from the surface to the center of the carbon particles.

Figures 68 to 70 show two different individual SiC particles. As seen from the figures there is high concentration of white matter on the interface different in appearance from SiC or matrix alloy. Figures 71 and 72 show the interface of SiC particles with high magnification. EDS spectra taken at different spots (Figures 73 to 75) allowed to identify several oxides (Al-Si-O, Si-Al-Ca-O) of different compositions. The high oxygen concentration in the system may originate from three different sources:

1. oxygen present as ash constituent,
2. oxygen introduced with carbon particles,
3. oxygen coming from the leak in the system.

But the absence of substantial oxide amounts in non-reacted or partly reacted samples means that the most important source of oxygen was ash constituents. The presence of Ca in oxides indicates that calcium and oxygen were pushed out of SiC and formed oxides of different composition. These oxides concentrated on the boundary between SiC and matrix alloy.

Figure 76 shows the microstructure of SiC with high magnification. As seen from the figure some porosity still exists but it is very low comparing with initial carbon. Also



Figure 66 Microstructure of in-situ formed Al/SiC composite after reaction at 1573K for 6 hours. SEM image backscattered electrons.

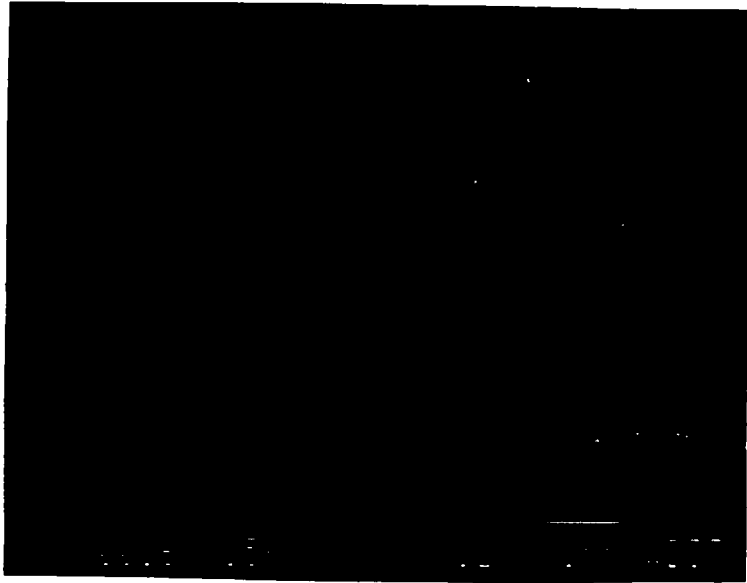


Figure 67 Microstructure of in-situ formed AlSiC composite after reaction at 1573K for 6 hours. SEM image in secondary electrons.

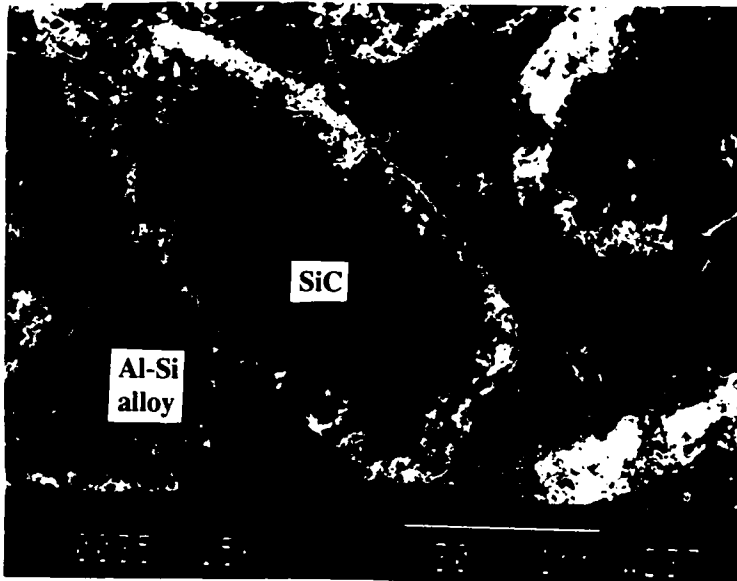


Figure 68 Microstructure of one SiC particle after reaction at 1573K for 6 hours. SEM image in backscattered electrons.

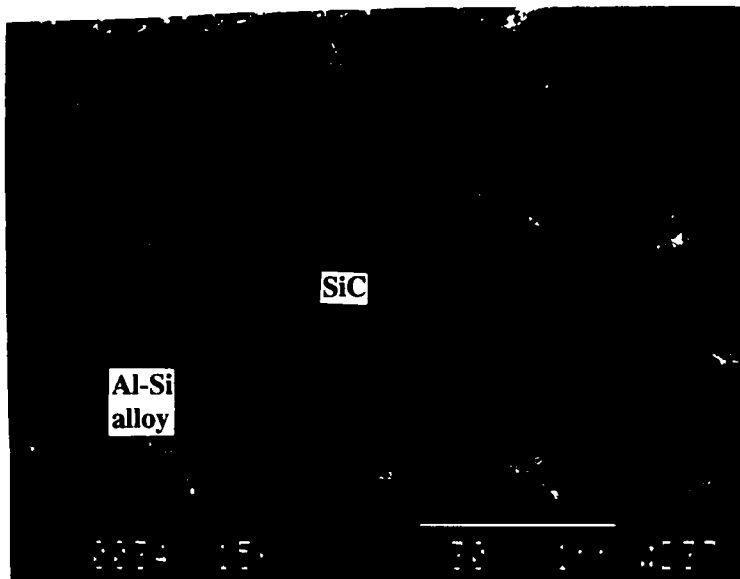


Figure 69 Microstructure of one SiC particle after reaction at 1573K for 6 hours, SEM image in secondary electrons.

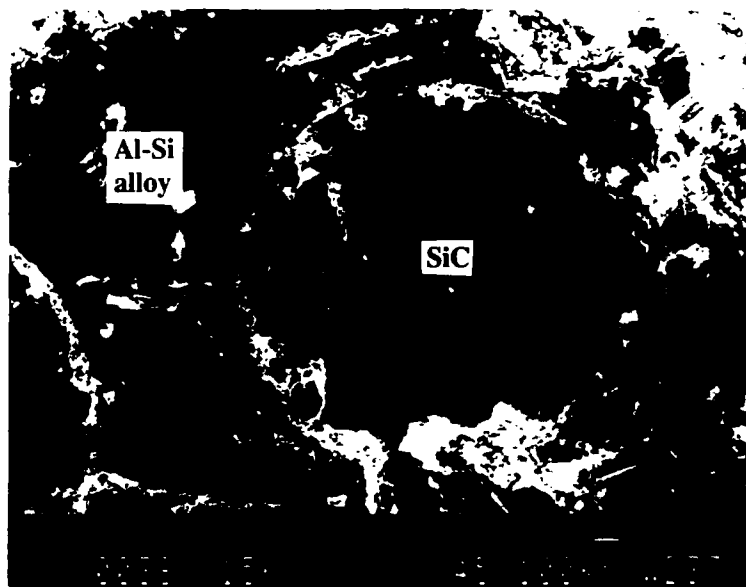


Figure 70 Microstructure of a SiC particle with round shape after reaction at 1573K for 6 hours. SEM image in backscattered electrons.



Figure 71 Microstructure of the interface between SiC and matrix alloy with high concentration of oxides after reaction at 1573K for 6 hours. SEM image in backscattered electrons.

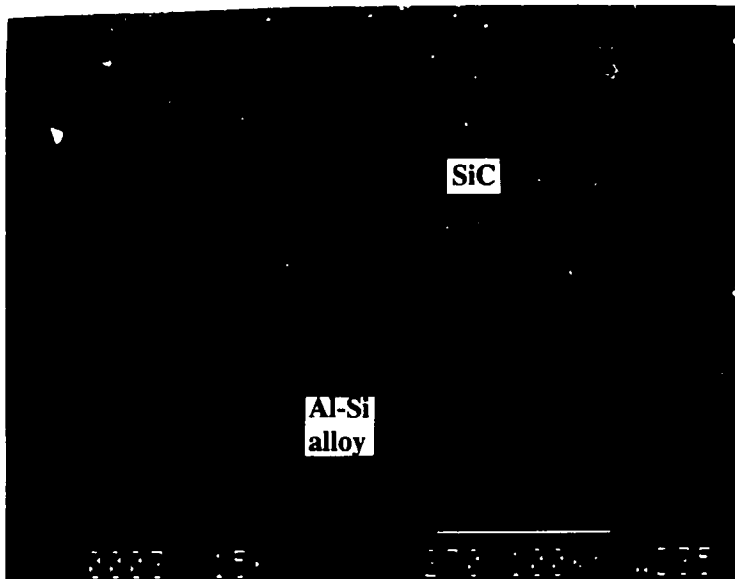


Figure 72 Microstructure of the interface between SiC and matrix alloy with high concentration of oxides after reaction at 1573K for 6 hours. SEM image in secondary electrons.

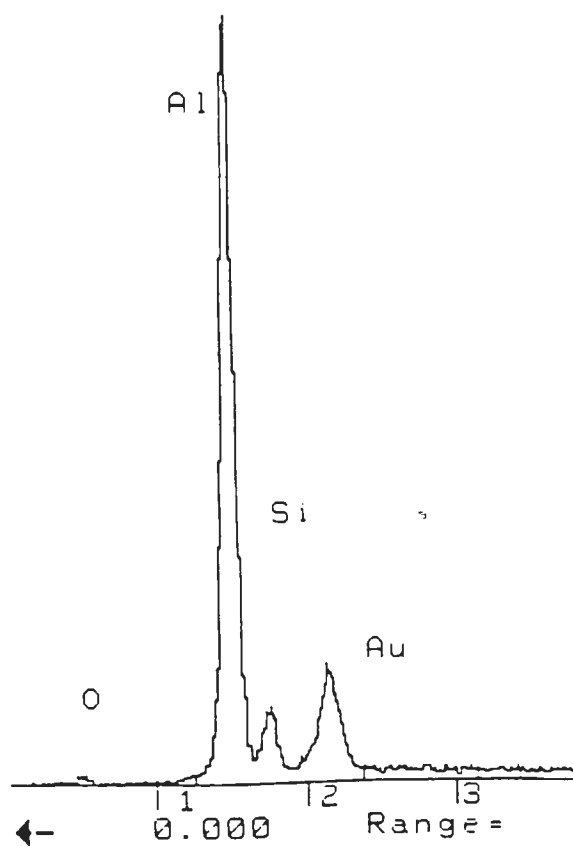


Figure 73 EDS spectra at point 1 of Figure 71.

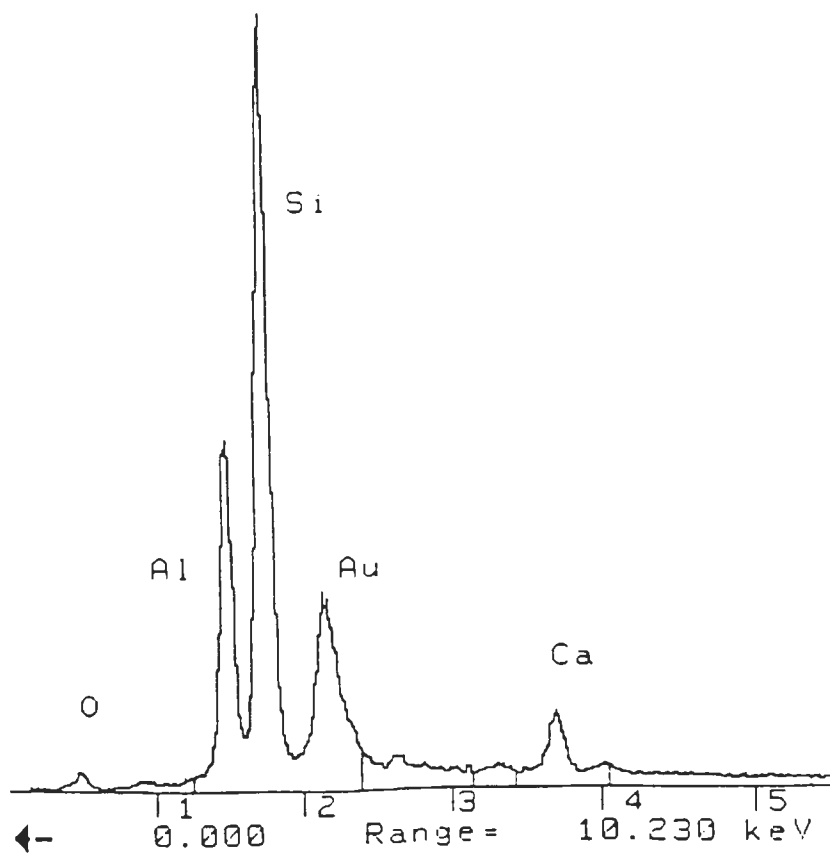


Figure 74 EDS spectra at point 2 of Figure 71.

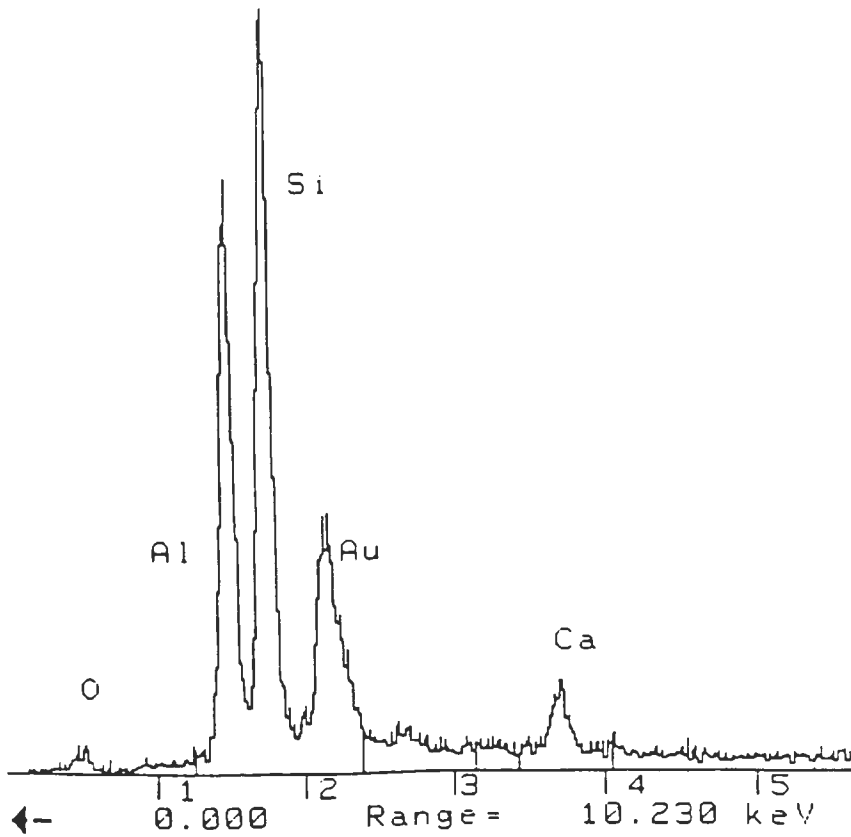


Figure 75 EDS spectra at point 3 of Figure 71.

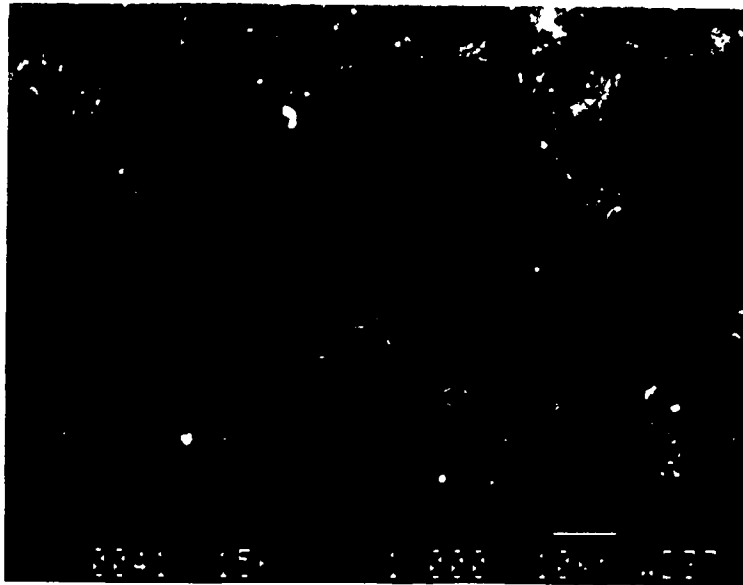


Figure 76 Microstructure of SiC, SEM image in secondary electrons.

comparison with freshly formed SiC (Figure 63) shows that if in the latter case SiC was present in the form of individual grains in the latter case grain boundaries are no longer seen. Hence SiC went through sintering process.

Figure 77 shows the interface between the matrix alloy and SiC with low concentration of oxides. The SiC has a perfect round shape also meaning that there was a sintering effect.

On the base of available data the mechanism of reaction may be broken into 3 stages:

1. Activation (no changes in carbon or matrix alloy are seen). Activation time is a probability function.
2. Reaction proceeds from the surface to the center of carbon particles. SiC is produced in the form of individual grains.
3. Sintering of SiC.

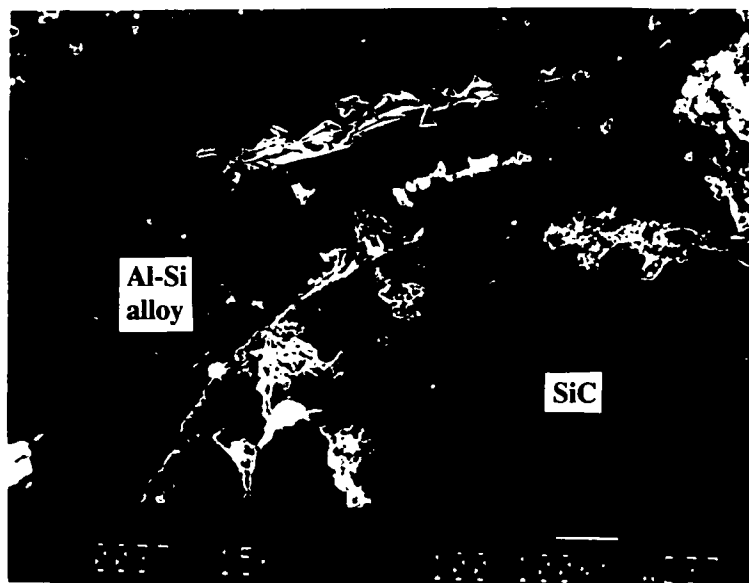


Figure 77 Microstructure of the interface between SiC and matrix alloy with low concentration of oxides after reaction at 1573K for 6 hours. SEM image in backscattered electrons.

5.2.5 Reaction rate

To determine the rate of reaction the experiments were performed at temperatures 1373 to 1573K for 0.5 to 6 hours. The results of experiments are presented in Table 14.

Microstructural analysis of the reaction products has shown that the characteristic features of the mechanism of reaction are activation, movement of the reaction zone and sintering. According to Sohn [114] these are typical features of the nucleation growth kinetics. In such case a fluid-solid reaction starts by forming nuclei at the surface of the solid. As the reaction progresses, these nuclei grow in size and new ones are formed. Eventually they overlap one another and cover the whole surface, thus forming what is called the reaction interface in a shrinking - core system. Usually such type of nucleation growth kinetics gives sigmoidal curve for conversion as a function of time and may be treated using Avrami equation [115].

The relationship between volume transformed and time may be expressed using the following equation:

$$\alpha = 1 - \exp(-kt^n) \quad (38)$$

where α is the volume fraction transformed, K is the rate constant and t is the time.

The experimental data were fitted to the above model through a linear transformation of equation (38):

$$\ln [\ln (1 - \alpha)^{-1}] = n \ln t + \ln K \quad (39)$$

Plots of $\ln [\ln (1 - \alpha)^{-1}]$ vs $\ln t$ were constructed for temperatures 1473 and 1573K (Figure 78). From these plots values of n and K were determined and are given in Table 15.

Table 14 Results of experiments on reaction between 60 mol% Al - 40 mol% Si alloy and activated carbon

Temperature, K	Time, hours				
	0.5	1	2	4	6
	Extent of reaction, %				
1373					7
1473	0	0	11	25	72
1573			18	36	90

Table 15 K and n values in Avrami equation

T, K	n	K
1473	2.082	0.02381
1573	2.117	0.03835

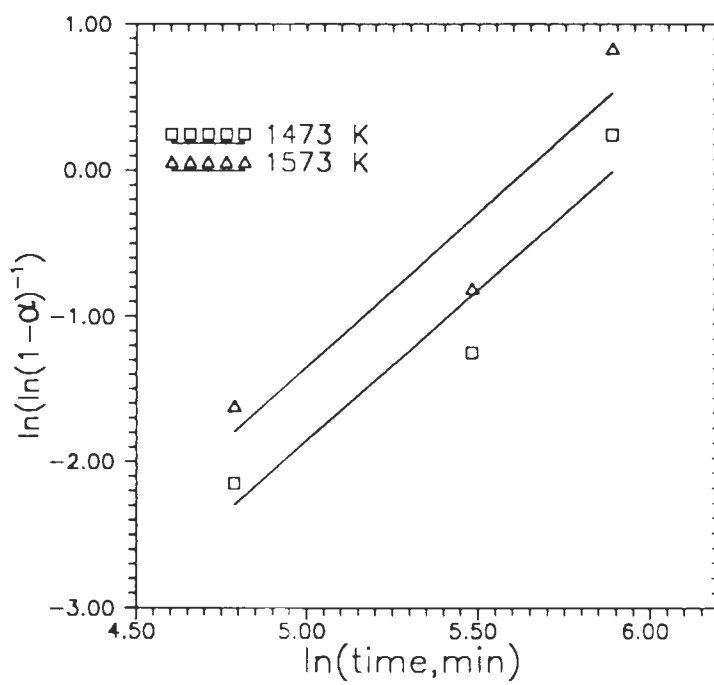


Figure 78 Transformation kinetics of carbon into silicon carbide

$$\text{At temperature 1473K} \quad \ln [\ln (1 - \alpha)^{-1}] = 2.082 \ln t - 3.738 \quad (40)$$

$$\text{At temperature 1573K} \quad \ln [\ln (1 - \alpha)^{-1}] = 2.1165 \ln t - 3.261 \quad (41)$$

Figure 79 shows the values calculated using Avrami equation and experimental results. The discrepancy between the model and experimental values is connected with low precision in measurements of extent of reaction. The average error in measurements was around $\pm 20\%$.

Activation energy of reaction was determined using Arrhenius relationship:

$$K = A \exp(-E_a/RT) \quad (42)$$

where A is a constant, E_a is activation energy, R is gas constant, and T is temperature

From equation (42) we obtain:

$$\ln K = \ln A - E_a/RT \quad (43)$$

The $\ln K$ vs $1/T$ is presented in figure 80. It was found that

$$\ln K = 3.758 - 11042/T \quad (44)$$

and E_a was found to be 92 kJ/mol.

According to Christiansen [115] $n=2$, is characteristic of transformation, controlled by grain edge nucleation, while $n=2.5$, is characteristic of diffusion controlled growth. The fact that in this study n was found to be 2.08 to 2.12 points out to mixed regime where the rate of reaction is controlled by both: nucleation at the interface and diffusion. At 1373K most of the particles slowly grew from the surface to the center, which is characteristic of diffusion controlled growth. At 1573K some of the particles quickly transformed into SiC, while others remained unreacted. This is characteristic of the process controlled by nucleation at the interface.

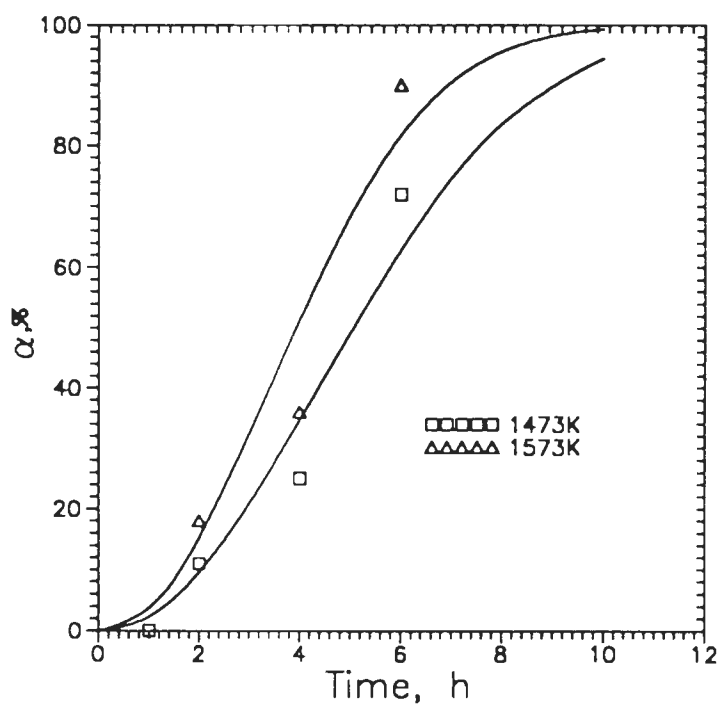


Figure 79 Effect of time and temperature on the transformation of carbon into silicon carbide.

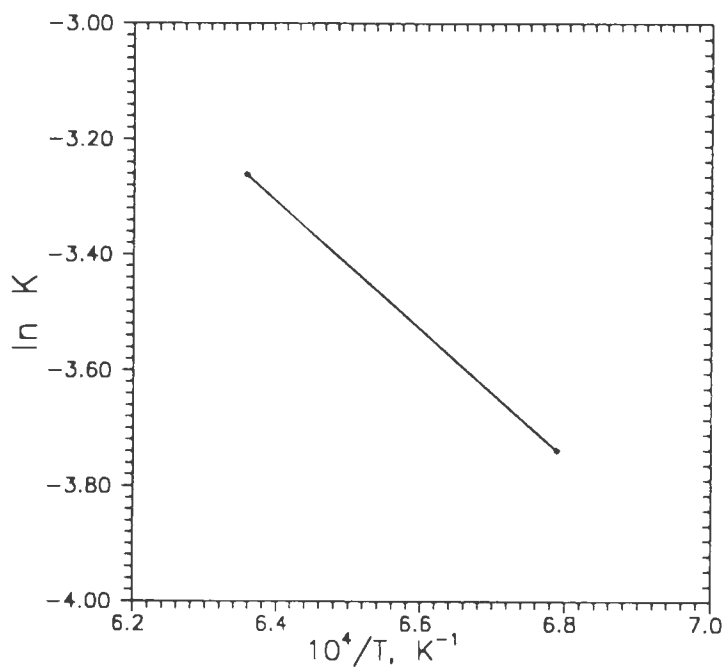


Figure 80 Correlation between $\ln K$ and $1/T$

6. SUMMARY AND CONCLUSIONS

1. A new process of in-situ formation of Al/SiC composite has been developed. Comparing to the conventional method of SiC production from SiO₂ and carbon, the temperature of SiC formation was decreased from 3000K to 1573K and the operation time from 48 to 10 hours.
2. The binary Al-Si solution was described using quasi-regular solution model and activity coefficient of Si was found to be:

$$\ln(f_{Si}) = (-4.048 + 5760/T) \times (1-x_{Si})^2 \quad (973-1423K)$$

$$f_{Si} = 1 \quad (1423-1573K)$$

3. Thermodynamic analysis of Al-SiC system which corresponds to conventional processing of Al/SiC composite showed that Al₄C₃ (which is detrimental for physical properties of the composite) forms at all studied temperatures and SiC concentrations and therefore pure aluminum should be avoided as a matrix metal with SiC as reinforcement.
4. To decrease or even prevent the formation of aluminum carbide silicon may be added to aluminum alloy. The silicon concentration enough to completely prevent aluminum carbide formation may be calculated using the following equations.

$$[Si] = -39.29 + 0.06601T - 1.955 \times 10^{-6}T^2 \quad (973-1423K)$$

$$[Si] = 50.02 - 0.03455T + 7.000 \times 10^{-6}T^2 \quad (1423-1573K)$$

5. It was shown that if carbon is added to aluminum alloys containing 30, 40, or 50 mol pct of Si than 16, 24, or 40 mol pct of SiC can be formed respectively without any aluminum carbide formation.

6. The results of thermodynamic analysis found excellent agreement with experimental data obtained in this work and given in the literature.
7. Three different carbon sources were tried for in-situ formation of SiC. Natural gas was found unsuitable because of very low efficiency. During reaction it decomposed into carbon and hydrogen but most of the carbon powder was removed from the melt by argon which served as a carrier gas.
Graphite was also found unsuitable because of aluminum carbide formation. The melt penetrated cavities in graphite and because of local carbon excess aluminum carbide formed together with SiC.
Activated carbon was found to be an excellent source for SiC formation. During experiments only SiC was formed at all temperatures, silicon and carbon concentrations.
8. The study of reaction mechanism between Al-Si alloy and activated carbon showed that reaction proceeds through three distinct stages:
 - activation (no changes in carbon or matrix alloy are seen)
 - reaction (reaction front moves from the surface to the center of carbon particles)
 - sintering of SiC.Reaction formed SiC retains the size and the shape of initial carbon.
9. After complete transformation oxides present in activated carbon as ash constituents precipitated on the interface between the matrix alloy and SiC.
10. Kinetic study showed that the reaction proceeds in the mixed regime with control of both nucleation at the interface and diffusion. The rate of the process was

described using Avrami equation and activation energy was found to be 92 kJ/mol.

7. RECOMMENDATION

Extensive study of mechanical properties of in-situ formed Al/SiC composite is recommended. After that the developed process may be tried on industrial scale.

8. REFERENCES

1. C. Zweben, "Metal Matrix Composites," *Advanced Materials & Processes*, vol.145, 1994, p.28-30.
2. W. H. Hunt, Jr., "Redefining the Limits of Aluminum-Based Materials", *Journal of Metals*, vol.45, 1993, p.18.
3. M. G. McKimpton, E. L. Pohlenz, and S. R. Thompson, "Evaluating the Mechanical Properties of Commercial DRA", *Journal of Metals*, vol.45, 1993, p.26-29.
4. J. E. Allison and G. S. Cole, "Metal-Matrix Composites in the Automotive Industry: Opportunities and Challenges", *Journal of Metals*, vol.45, 1993, p.19-24.
5. S. Ray, "Synthesis of Cast Metal Matrix Particulate Composites," *Journal of Materials Science*, vol.28, 1993, p. 5397-5413.
6. R. Y. Lin "Composite Interfacial Reactions", *Journal of Metals*, vol.45, 1993, p.20.
7. J. A. DeKock and Y. A. Chang, "The Stability of Interfaces in High-Temperature Metal-Matrix Composites", *Journal of Metals*, vol. 45, 1993, p.21-23.
8. M. J. Koczak and M. K. Premkumar, "Emerging Technologies for the In-Situ Production of MMCs", *Journal of Metals*, vol.45, 1993, p.44-48.
9. H. Lagace and D. J. Lloyd "Microstructural Analysis of Al-SiC Composites," *Canadian Metallurgical Quarterly*, vol.28, 1989, p.145-152.
10. J. O. Carlsson, "Silicon Carbide," *Encyclopedia of Materials Science and*

- Engineering, ed.-in-chief M. B. Bever, Pergamon Press, vol.6, 1986, p.4403-4408.
11. A. J. Moulson and J. M. Herbert, "Electroceramics: Materials, Properties, Applications," Chapman and Hall, 1990, p.465.
 12. A. R. Verma and P. Krishna, "Polymorphism and Polytypism in Crystals," John Wiley & Sons, Inc., 1966, p.341
 13. D. E. Cagliostro and S. R. Riccitiello, "Model for the Formation of Silicon Carbide from the Pyrolysis of Dichlorodimethylsilane in Hydrogen: 1. Silicon Formation from Chlorosilanes," *Journal of American Ceramic Society*, vol.76, 1993, p.39-48.
 14. D. E. Cagliostro and S. R. Riccitiello, "Model for the Formation of Silicon Carbide from the Pyrolysis of Dichlorodimethylsilane in Hydrogen: 2. Silicon Carbide Formation from Silicon and Methane," *Journal of American Ceramic Society*, vol.76, 1993, p.49-53.
 15. T. Darroudi, R. Tressler, and M. Kasprzyk, "Low-Cost Melt-Formed Siliconized Silicon Carbide Radiant Tube Materials," *Journal of American Ceramic Society*, vol.76, 1993, p.173-179.
 16. V. D. Krstic, "Production of Fine, High-Purity Beta Silicon Carbide Powders," *Journal of American Ceramic Society*, vol.75, 1992, p.170-174.
 17. M. J. Ledoux, S. Hantzer, C. P. Huu, J. Guille, and M. P. Desaneaux, "New Synthesis and Uses of High-Specific-Surface SiC as a Catalytic Support that is Chemically Inert and Has High Thermal Resistance," *Journal of Catalysis*,

- vol.114, 1988, p.176-185.
18. M. Benaissa, J. Wercmann, G. Ehret, E. Peschiera, J. Guille, and M. J. Ledoux, "Structural Studies of Active Carbon used in the growth of Silicon Carbide Catalyst Support," *Journal of Materials Science*, vol.29, 1994, p.4700-4707.
 19. K. Okada, H. Kato, and K. Nakajima, "Preparation of Silicon Carbide Fiber from Activated Fiber and Gaseous Silicon Monoxide," *Journal of American Ceramic Society*, vol.77, 1994, p.1691-1693.
 20. N. S. Jacobson and E. J. Opila, "Thermodynamics of Si-C-O System," *Metallurgical Transactions*, vol.24A, 1993, p.1212-1214.
 21. A. Jha "Phase Equilibria in the Si-C-N-O System and the Kinetic Analysis of Silicon Carbide Whisker Growth," *Journal of Materials Science*, vol.28, 1993, p.3069-3079.
 22. M. Nagamori, I. Malinsky, and A. Claveau, "Thermodynamics of the Si-C-O System for the Production of Silicon Carbide and Metallic Silicon," *Metallurgical Transactions*, vol.17B, 1986, p.503-514.
 23. T. Rosenqvist and J. Kr. Tuset, "Discussion of "Thermodynamics of the Si-C-O System for the Production of Silicon Carbide and Metallic Silicon," *Metallurgical Transactions*, vol.18B, 1987, p.471-472.
 24. M. Nagamori, I. Malinsky, and A. Claveau, "The Role of SiO(l) in the Production of Metallic Silicon," *Metallurgical Transactions*, vol.18B, 1987, p.472-475.
 25. N. S. Jacobson, K. N. Lee, and D. S. Fox, "Reactions of Silicon Carbide and

- Silicon Oxide at Elevated Temperatures," *Journal of American Ceramic Society*, vol.75, 1992, p.1603-1611.
26. J. J. Biernacki and G. P. Wozak, "Stoichiometry of the C + SiO₂ Reaction," *Journal of American Ceramic Society*, vol.72, 1989, p.122-129.
27. D. H. Filsinger and D. B. Bourrie, "Silica to Silicon: Key Carbothermic Reactions and Kinetics," *Journal of American Ceramic Society*, vol.73, 1990, p.1726-1732.
28. M. H. Hon and R. F. Davis, "Self-Diffusion of ¹⁴C in Polycrystalline β-SiC," *Journal of Materials Science*, vol.14, 1979, p.2411-2421.
29. M. H. Hon and R. F. Davis, "Self-Diffusion of ³⁰Si in Polycrystalline β-SiC," *Journal of Materials Science*, vol.15, 1980, p.2073-2080.
30. I. S. T. Tsong, "Atomic-Level Characterization of Cubic Silicon Carbide Surfaces - A Review," *Journal of American Ceramic Society*, vol.76, 1993, p.269-272.
31. H. Du, Z. Yang, M. Libera, D. C. Jacobson, Y. C. Wang, and R. F. Davis, "Chemistry and Structure of Beta Silicon Carbide Implanted with High-Dose Aluminum," *Journal of American Ceramic Society*, vol.76, 1993, p.330-335.
32. N. S. Jacobson, "Corrosion of Silicon-Based Ceramics in Combustion Environments," *Journal of American Ceramic Society*, vol.76, 1993, p.13-28.
33. W. F. Smith, "Structure and Properties of Engineering Alloys," McGraw-Hill, Inc., 1993, p.630.
34. Aluminum. Properties, Physical Metallurgy and Phase Diagrams, ed. K. R. Van

- Horn, ASM, Metals Park, Ohio, vol.1, 1967, p.425
35. Binary Alloy Phase Diagrams, T.B. Massalski, ed. in chief, 2nd ed., ASM International, vol. 1, 1990, p.130, 212, 883.
36. H. Yokokawa, M. Fujishige, S. Ujiie, and M. Dokiya, "Phase Relations Associated with the Aluminum Blast Furnace: Aluminum Oxycarbide Melts and Al-C-X (X=Fe,Si) Liquid Alloys," *Metallurgical Transactions*, vol. 18B, 1987, p.433-444.
37. L. L. Oden and R.A. McCune, "Phase Equilibria in the Al-Si-C System," *Metallurgical Transactions*, vol.18A, 1987, p.2005-2014.
38. L. L. Oden and N. A. Gokcen, "Cu-C and Al-Cu-C Phase Diagrams and Thermodynamic properties of C in the Alloys from 1550°C to 2300°C," *Metallurgical Transactions*, vol.23B, 1992, p.453-458.
39. Ajay K. Misra, "Thermochemical Analysis of the Silicon Carbide - Alumina Reaction with Reference to Liquid - Phase Sintering of Silicon Carbide," *Journal of American Ceramic Society*, vol.74, 1991, p.345-351.
40. Ternary Alloys: a comprehensive compendium of evaluated constitutional data and phase diagrams, ed. G. Petzow and G. Effenberg, VCH, vol.3,1990, p.382.
41. J. C. Viala, P. Fortier, C. Bernard, and J. Bouix, "Interaction Chimique Matrice Renfort Dans Les Composites Al-SiC," Developments in the Science and Technology of Composite Materials, ed. A. R. Bunsell, P. Lamicq, and A. Massiah, ECCM, Bordeaux, France, 1985, p.583-588.
42. J. C. Viala, P. Fortier and J. Bouix, "Stable and Metastable Phase Equilibria in

- the chemical Interaction between Aluminum and Silicon Carbide," *Journal of Materials Science*, vol. 25, 1990, p. 1842-1850
43. C. A. Handwerker, M. D. Vaudin, U. R. Kattner, and D. J. Lee, "Interface Reactions and Phase Stability in the Al-SiC system," *Metal-Ceramic Interfaces*, M. Ruhle, A. G. Evans, M. F. Ashby, and J. P. Hirth, eds., Pergamon Press, 1989, p.129-137.
 44. K. K. Chawla, *Composite Materials. Science and Engineering*, Springer-Verlag, New-York Inc., 1987, p.285.
 45. T. Iseki, T. Kameda, and T. Maruyama, "Interfacial Reactions between SiC and Aluminum during Joining", *Journal of Materials Science*, vol.19, 1984, p.1692-1698.
 46. D. J. Lloyd and I. Jin, "A method of Assessing the Reactivity between SiC and Molten Al", *Metallurgical Transactions*, vol.19A, 1988, p.3107-3109.
 47. A. E. Hughes, M. M. Hedges, and B. A. Sexton, "Reactions at the Al SiO₂ SiC layered interface", *Journal of Materials Science*, vol.25, 1990, p.4856-4865.
 48. J. C. Viala, F. Bosselet, V. Laurent, and Y. Lepetitcorps, "Mechanism and Kinetics of the Chemical Interaction between Liquid Aluminum and Silicon Carbide Single Crystals," *Journal of Materials Science*, vol.28, 1993, p.5301-5312.
 49. D. J. Lloyd, "The Solidification Microstructure of Particulate Reinforced Aluminum/SiC Composites," *Composites Science and Technology*, vol.35, 1989, p.159-179.

50. D. J. Lloyd, H. Lagace, A. McLeod, and P. L. Morris, "Microstructural Aspects of Aluminum-Silicon Carbide Particulate Composites Produced by a Casting Method " *Materials Science and Engineering*, vol. A107, 1989, p.73-80.
51. G. Carotenuto, A. Gallo, and L. Nicolais, "Degradation of SiC Particles in aluminum-based composites," *Journal of Materials Science*, vol.29, 1994, p.4967-4974.
52. N. Wang, Z. Wang, and G. C. Weatherly, "Formation of Magnesium Aluminate (Spinel) in Cast SiC Particulate-Reinforced Al(A356) Metal Matrix Composites," *Metallurgical Transactions*, vol.23A, 1992, p.1423-1430.
53. P. L. Ratnaparkhi and J. M. Howe "Characterization of a Diffusion-Bonded Al-Mg Alloy/SiC Interface by High Resolution and Analytical Electron Microscopy," *Metallurgical and Materials Transactions*, vol.25A, 1994, p.617-627.
54. T. A. Chernyshova, and L. I. Kobeleva, "Products of Interaction in the Al-Si Alloy-Carbon Fibre System," *Journal of Materials Science*, vol. 20, 1985, p.3524-3528.
55. M. Suery, G. L'Esperance, B. D. Hong, L. N. Thanh, and F. Bordeaux, "Development of Particulate Treatments and Coatings to Reduce SiC Degradation by Liquid Aluminum," *Journal of Materials Engineering and Performance*, vol. 2, 1993, p.365-372.
56. V. Laurent, D. Chatain, and N. Eustathopoulos, "Wettability of SiC by aluminum and Al-Si alloys," *Journal of Materials Science*, vol.22, 1987, p.244-250.
57. S.-Y. Oh, J. A. Cornie, and K. C. Russell, "Wetting of Ceramic Particulates

- with Liquid Aluminum Alloys: Part 1. Experimental Techniques," *Metallurgical Transactions*, vol. 20A, 1989, p.527-532.
58. S.-Y. Oh, J. A. Cornie, and K. C. Russell, "Wetting of Ceramic Particulates with Liquid Aluminum Alloys: Part 2. Study of Wettability," *Metallurgical Transactions*," vol.20A, 1989, p.533-541.
59. M. Kobashi, T. Mohri, and T. Choh, "Role of Mg and Ti on a SiC_p , ZrC_p /Al Composite at Elevated Temperatures," *Journal of Materials Science*, vol.28, 1993, p.5707-5712.
60. M. Kobashi and T. Choh, "The Wettability and the Reaction for SiC Particle Al Alloy System," *Journal of Materials Science*, vol.28, 1993, p.684-690.
61. D. M. Stefanescu, A. Moitra, A. S. Kacar, and B. K. Dhinaw, "The Influence of Buoyant Forces and Volume Fraction of Particles on the Particle Pushing/Entrapment Transition during Directional Solidification of Al-SiC and Al/Graphite Composites," *Metallurgical Transactions*, vol.21A, 1990, p.231-239.
62. P. K. Rohatgi, K. Pasciak, C. S. Narendranath, S. Ray, and A. Sachdev, "Evolution of Microstructure and Local Thermal Conditions during Directional Solidification of A356-SiC Particle Composites," *Journal of Materials Science*, vol.29, 1994, p.5357-5366.
63. P. K. Rohatgi, "Low-Cost, Fly-Ash-Containing Aluminum-Matrix Composites," *Journal of Metals*, vol.46, 1994, p.55-59.
64. A. M. Samuel, H. Liu, and F. H. Samuel, "Effect of Melt, Solidification and Heat Treatment Processing Parameters on the properties of Al-Si-Mg- SiC_p

- composites," *Journal of Materials Science*, v.28 (1993), 6785-6798
65. F. H. Samuel, H. Liu, and A. M. Samuel, "Effect of Melt Cleanliness on the Properties of an Al-10 Wt Pct Si-10 Vol Pct SiC_{10p} Composite," *Metallurgical Transactions*, vol.24A, 1993, p.1631-1645.
66. F. H. Samuel and A. M. Samuel, "Effect of Heat Treatment on the Microstructure, Tensile Properties, and Fracture Behavior of Permanent Mold al-10 wt pct Si-0.6wt pct Mg-SiC_{10p} Composite Castings," *Metallurgical Transactions*, vol.25A, 1994, p.2247-2262.
67. H. Ribes, M. Suery, G. L'Esperance, and J. G. Legoux, "Microscopic Examination of the Interface Region in 6061-Al/SiC Composites Reinforced with as-Received and Oxidized SiC Particulates," *Metallurgical Transactions*, vol.21A, 1990, p.2489-2496.
68. J. Yan, L. Chunzhi, M. Jiawei, and Y. Mingguo, "Microstructure of SiC_p-reinforced A356 Cast Al Metal-Matrix Composites," *Journal of Materials Science*, vol.28, 1993, p.6000-6006.
69. J. M. Chiou and D. D. L. Chang "Characterization of Metal-Matrix Composites Fabricated by Vacuum Infiltration of a Liquid Metal under an Inert Gas pressure," *Metal & Ceramic Matrix Composites: Processing, Modeling & Mechanical Behavior*, R.B. Bhagat, A.H. Clauer, P. Kumar, and A.M. Ritter, eds., TMS, Warrendale, PA, 1990, p.107-115.
70. Z. Wang and R. Zhang, "Mechanical Behavior of Cast Particulate SiC-Al (A356) Metal Matrix Composites," *Metallurgical Transactions*, vol.22A, 1991, p.1585-

- 1593.
71. Y.-H. Kim, S. Lee, and N. J. Kim, "Fracture Mechanisms of a 2124 Aluminum Matrix Composite Reinforced with SiC Whiskers," *Metallurgical Transactions*, v.23A (1992), 2589-2596.
 72. S. Lee, T. H. Kim, and D. Kwon, "Microstructural Analysis of Fracture Toughness Variation in 2XXX-Series Aluminum Alloy Composites Reinforced with SiC Whiskers," *Metallurgical Transactions*, vol.25A, 1994, p.2213-2223.
 73. Y. Sugimura and S. Suresh, "Effects of SiC Content on Fatigue Crack Growth in Aluminum Alloys Reinforced with SiC Particles," *Metallurgical Transactions*, vol.23A, 1992, p.2231-2242.
 74. K. Xia and T. G. Langdon, "Review: The Toughening and Strengthening of Ceramic Materials through Discontinuous Reinforcement," *Journal of Materials Science*, vol.29, 1994, p.5219-5231.
 75. H. J. Ning and P. Pirouz, "The Microstructure of SCS-6 SiC fiber," *Journal of Materials Research*, vol.6, 1991, p.2234-2248.
 76. K. T. V. Rao, S. C. Siu, and R. O. Ritchie, "Failure Mechanisms in SiC-Fiber Reinforced 6061 Aluminum Alloy Composites under Monotonic and Cyclic Loading," *Metallurgical Transactions*, vol.24A, 1993, p.721-734.
 77. J.-M. Yang, W. H. Kao, and C. T. Liu, "Interface Characterization of Fiber-Reinforced Ni₃Al Matrix Composites," *Metallurgical Transactions*, vol.20A, 1989, p.1989-2459.
 78. C. Badini, M. Ferraris, and F. Marchetti, "Thermal Stability of Interfaces in Ti-

- 6Al-4V Reinforced by SiC Sigma Fibers," *Journal of Materials Science*, vol.29, 1994, p.4840-4846.
79. P. Krishnan and M. J. Kaufman, "Development and Characterization of Interface Coatings in Molybdenum-Reinforced NiAl Matrix Composites," *Metallurgical and Materials Transactions*, vol.25A, 1994, p.2111-2116.
80. S. Nourbakhsh, H. Margolin, and F. L. Liang, "Microstructural Observations of Pressure Cast Ni₃Al/Al₂O₃ and Ni/Al₂O₃ Composites," *Metallurgical Transactions*, vol.20A, 1989, p.2159.
81. S. G. Fishman, "In-situ Processing of Metal-Ceramic Composites," *In Situ Composites: Science and Technology*, M. Singh and D. Lewis, eds., TMS, Warrendale, PA, 1994, p.1-19.
82. S. Antolin, A. S. Nagelberg, D K. Creber, Formation of Al₂O₃/Metal Composites by the directed oxidation of Molten Aluminum-Magnesium-Silicon Alloys: Part 1, Microstructural Development," *Journal of American Ceramic Society*, vol.75, 1992, p.447-454.
83. A. S. Nagelberg, S. Antolin, and A. W. Urquhart, "Formation of Al₂O₃/Metal Composites by the Directed Oxidation of Molten Aluminum-Magnesium-Silicon Alloys: Part 2, Growth Kinetics," *Journal of American Ceramic Society*, vol.75, 1992, p. 455-62.
84. E. Manor, H. Ni, C. G. Levy, R. Mehrabian, "Microstructure Evolution of SiC/Al₂O₃ Composites Produced by Melt Oxidation," *Journal of American Ceramic Society*, vol.76, 1993, p.1777-1787.

85. D. Lewis and M. Singh, "Recent Developments and Future Prospects For XD™ and Lanxide™ *In situ* composite materials." In Situ Composites: Science and Technology, M. Singh and D. Lewis, eds., TMS, Warrendale, PA, 1994, p.21-36.
86. M. Koczak and K. Kumar, US Patent 4,808,372 "In-Situ Process for Producing a Composite Containing Refractory Material," Feb. 28, 1989.
87. P. Sahoo and M. J. Koczak, "A Microstructural Characterization of In-situ TiC Nucleation and Growth in Aluminum Matrix Composites," Metal & Ceramic Matrix Composites: Processing, Modeling & Mechanical Behavior, R. B. Bhagat, A. H. Clauer, P. Kumar, and A.M. Ritter, eds., TMS, Warrendale, PA, 1990, p.617-627.
88. M. J. Koczak and M. K. Premkumar, "Emerging Technologies for the In-Situ Production of MMCs," *Journal of Metals*, vol.45, 1993, p.44-48.
89. M. G. Chu and M. K. Premkumar, "Mechanism of TiC Formation in Al TiC In Situ Metal-Matrix Composites," *Metallurgical Transactions*, vol. 24A, 1993, p.2803-2805.
90. M. K. Premkumar and M. G. Chu, "Synthesis of TiC Particulates and Their Segregation during Solidification in In-Situ Processed Al-TiC composites," *Metallurgical Transactions*, vol.24A, 1993, p.2358-2362.
91. V. Shtessel, S. Sampath, and M. Koczak, "Processing and Analysis of In-situ Composites," In Situ Composites: Science and Technology, M. Singh and D. Lewis, eds., TMS, Warrendale, PA, 1994, p.37-60.

92. S. Khatri, V. Shtessel, M. Koczak, A. P. Divecha, and J. Kerr, "Net Shaped Manufacturing of Aluminum Matrix Composites via Reactive Infiltration," In Situ Composites: Science and Technology, M. Singh and D. Lewis, eds., TMS, Warrendale, PA, 1994, p.115-134.
93. A. E. W. Jarfors, L. Svendsen, M. Wallinder, and H. Fredriksson, "Reactions during Infiltration of Graphite Fibers by Molten Al-Ti Alloy," Metallurgical Transactions, v.24A, 1993, p.2577-2583.
94. L. Svendsen and A. Jarfors, "Al-Ti-C Phase Diagram," Materials Science and Technology, vol.9, 1993, p.948-952.
95. A. Banerji and W. Reif, "Development of Al-Ti-C Grain Refiners Containing TiC," Metallurgical Transactions, vol.17A, 1986, p.2127-2137.
96. M. E. Fine and J. G. Conley, "Discussion of "On the Free Energy of Formation of TiC and Al_4C_3 ," Metallurgical Transactions, vol.21A, 1990, p.2609-2610
97. R. A. Rapp and X. Zheng, "Thermodynamic Consideration of Grain Refinement of Aluminum Alloys by Titanium and Carbon," Metallurgical Transactions, vol.22A, 1991, p.3071-3075.
98. H. Yokokawa, N. Sakai, T. Kawada, and M. Dokiya, "Chemical Potential Diagram of Al-Ti-C System: Al_4C_3 Formation on TiC Formed in Al-Ti Liquids Containing Carbon," Metallurgical Transactions, vol.22A, 1991, p.3075-3076.
99. U. R. Kattner, J.-C. Lin, and Y. A. Chang, "Thermodynamic Assessment and Calculation of the Ti-Al System," Metallurgical Transactions, vol.23A, 1992, p.2081-2090.

100. F. J. J. van Loo and G. F. Bastin, "On the Diffusion of Carbon in Titanium Carbide," *Metallurgical Transactions*, vol.20A, 1989, p.403-411.
101. H. Klemm, K. Tanihata, and Y. Miyamoto, "Gas Pressure Combustion Sintering and Hot Isostatic Pressing in the Ti-Si-C System," *Journal of Materials Science*, vol.28, 1993, p.1557-1562.
102. M. Touanen, F. Teyssandier, M. Ducarroir, M. Maline, R. Hillel, and J. L. Derep, "Microcomposite and Nanocomposite Structures from Chemical Vapor Deposition in the Silicon-Titanium-Carbon System," *Journal of American Ceramic Society*, vol.76, 1993, p.1473-1481.
103. C. Racault, F. Langlais, and C. Bernard, "On the Chemical Vapor Deposition of Ti_3SiC_2 from $TiCl_4$ - $SiCl_4$ - CH_4 - H_2 Gas Mixtures. Part 1. A Thermodynamic Approach," *Journal of Materials Science*, vol.29, 1994, p.5023-5040.
104. A. Chrysanthou, G. Erbaccio, and J. V. Wood, "In situ Preparation of Copper-Matrix Composites," *Journal of Materials Science Letters*, vol.12, 1993, p.1635-1636.
105. J-M. Yang and S. M. Jeng, "Interface and Mechanical Behavior of $MoSi_2$ -based Composites," *Journal of Materials Research*, vol.6, 1991, p.505-513.
106. C. H. Henager, Jr. and J. L. Brimhall, "Structure and Properties of Composites Synthesized In-Situ Using Solid State Displacement Reactions," *In-Situ Composites: Science and Technology*, M. Singh and D. Lewis, eds., TMS, Warrendale, PA, 1994, p.61-80.
107. S. Jandhyala, "Thermochemical Evaluation of Combustion Synthesis of $MoSi_2$ -SiC

- Composites," *Journal of American Ceramic Society*, vol.76, 1993, p.226-228
108. W. B. White, S. M. Johnson, and G. B. Dantzig, "Chemical Equilibrium in Complex Mixtures," *Journal of Chemical Physics*, vol.28, 1958, p.751-755
109. D. M. Kocherginsky, R. G. Reddy, I. M. Soifer, V. V. Mechev, Metallurgical Processes for the Early Twenty-First Century, H. Y. Sohn, ed., TMS, Warrendale, PA, vol.1, 1994, p.373-381.
110. D. M. Kocherginsky and R. G. Reddy, Control of Interfaces in Metal and Ceramic Composites, R.Y. Lin and S.G. Fishman, eds., TMS, Warrendale, PA, 1994, p.71-79.
111. D. M. Kocherginsky and R. G. Reddy, "Reactions between Al-Si Melt and Carbon," presented at the ASM-TMS Symposium, Diffusion and Reaction in Composites, October 2-6, Rosemont, IL, 1994.
112. D. M. Kocherginsky and R. G. Reddy, In-Situ Reactions for Synthesis of Composites, Ceramics, and Intermetallics, E.V. Barrera, F. D. S. Marquis, W. E. Frazier, S. G. Fishman, N. N. Thadhani, and Z. A. Munir, eds., TMS, Warrendale, PA, 1995, p.159-167.
113. R. C. Bansal, J-B. Donnet, F. Stoeckli, "Active Carbon," Marcel Dekker, Inc., New York, 1988, p.482.
114. H. Y. Sohn, "The Law of Additive Reaction Times in Fluid-Solid Reactions," *Metallurgical Transactions*, vol.9B, 1978, p.89-96.
115. J. W. Christian, "The Theory of Transformations in Metals and Alloys," Pergamon Press, Oxford, 1965, p.975.

APPENDIX 1

Input data saved as: a:\alsic.IGI

Effect of SiC/Al ratio

Temperature: 700.000 C, Step = 0.000 C
 Pressure: 1.000 bar, Step = 0.000 bar
 Number of Steps: 10

Phase	Species	Temp C	Input mol	Step mol	Activity coefficient
1	Al(g)	25.000	0.000	0.000	1.000
2	Al2(g)	25.000	0.000	0.000	1.000
3	AlC(g)	25.000	0.000	0.000	1.000
4	Ar(g)	25.000	1.000	0.000	1.000
5	N2(g)	25.000	1.0000E-10	0.000	1.000
6	Si(g)	25.000	0.000	0.000	1.000
7	SiC(g)	25.000	0.000	0.000	1.000
8	Al	25.000	1.000	0.000	1.000
9	Si	25.000	0.000	0.000	f
10	SiC	25.000	0.001	0.100	1.000
11	Si3N4	25.000	0.000	0.000	1.000
12	Al4C3	25.000	0.000	0.000	1.000
13	AlN	25.000	0.000	0.000	1.000

$$9 \quad (-4.048+5760/T) \cdot (1-x(9))^{-2}$$

X	Y 1	Y 2	Y 3	Y 4
SiC	Al	SiC	Si	Al4C3
1.00000E-03	9.98670E-01	1.00000E-36	1.00000E-03	3.33330E-04
1.01000E-01	9.15690E-01	3.77700E-02	6.32300E-02	2.10770E-02
2.01000E-01	9.15690E-01	1.37770E-01	6.32300E-02	2.10770E-02
3.01000E-01	9.15690E-01	2.37770E-01	6.32300E-02	2.10770E-02
4.01000E-01	9.15690E-01	3.37770E-01	6.32300E-02	2.10770E-02
5.01000E-01	9.15690E-01	4.37770E-01	6.32300E-02	2.10770E-02
6.01000E-01	9.15690E-01	5.37770E-01	6.32300E-02	2.10770E-02
7.01000E-01	9.15690E-01	6.37770E-01	6.32300E-02	2.10770E-02
8.01000E-01	9.15690E-01	7.37770E-01	6.32300E-02	2.10770E-02
9.01000E-01	9.15690E-01	8.37770E-01	6.32300E-02	2.10770E-02

Input data saved as: a:\alsic.IGI

Effect of SiC/Al ratio

Temperature: 700.000 C, Step = 0.000 C
 Pressure: 1.000 bar, Step = 0.000 bar
 Number of Steps: 10

	Phase	Specie	Temp C	Input mol	Step mol	Activity coefficient
1	1	Al(g)	25.000	0.000	0.000	1.000
2	1	Al2(g)	25.000	0.000	0.000	1.000
3	1	AlC(g)	25.000	0.000	0.000	1.000
4	1	Ar(g)	25.000	1.000	0.000	1.000
5	1	N2(g)	25.000	1.0000E-10	0.000	1.000
6	1	Si(g)	25.000	0.000	0.000	1.000
7	1	SiC(g)	25.000	0.000	0.000	1.000
8	2	Al	25.000	1.000	0.000	1.000
9	2	Si	25.000	0.000	0.000	f
10	3	SiC	25.000	0.001	0.010	1.000
11	3	Si3N4	25.000	0.000	0.000	1.000
12	4	Al4C3	25.000	0.000	0.000	1.000
13	4	AlN	25.000	0.000	0.000	1.000

$$9 \quad (-4.048+5760/T) \cdot (1-x(9)) \cdot 2$$

X	Y 1	Y 2	Y 3	Y 4
SiC	Al	Si	SiC	Al4C3
1.00000E-03	9.98670E-01	1.00000E-03	1.00000E-36	3.33330E-04
1.10000E-02	9.85330E-01	1.10000E-02	1.00000E-36	3.66670E-03
2.10000E-02	9.72000E-01	2.10000E-02	1.00000E-36	7.00000E-03
3.10000E-02	9.58670E-01	3.10000E-02	1.00000E-36	1.03330E-02
4.10000E-02	9.45330E-01	4.10000E-02	1.00000E-36	1.36670E-02
5.10000E-02	9.32000E-01	5.10000E-02	1.00000E-36	1.70000E-02
6.10000E-02	9.18670E-01	6.10000E-02	1.00000E-36	2.03330E-02
7.10000E-02	9.15690E-01	6.32300E-02	7.76980E-03	2.10770E-02
8.10000E-02	9.15690E-01	6.32300E-02	1.77700E-02	2.10770E-02
9.10000E-02	9.15690E-01	6.32300E-02	2.77700E-02	2.10770E-02

Effect of SiC/Al ratio

Temperature: 800.000 C, Step = 0.000 C
 Pressure: 1.000 bar, Step = 0.000 bar
 Number of Steps: 12

Phase	Specie	Temp C	Input mol	Step mol	Activity coefficient
1	Al (g)	25.000	0.000	0.000	1.000
2	Al2 (g)	25.000	0.000	0.000	1.000
3	AlC (g)	25.000	0.000	0.000	1.000
4	Ar (g)	25.000	1.000	0.000	1.000
5	N2 (g)	25.000	1.0000E-10	0.000	1.000
6	Si (g)	25.000	0.000	0.000	1.000
7	SiC (g)	25.000	0.000	0.000	1.000
8	Al	25.000	1.000	0.000	1.000
9	Si	25.000	0.000	0.000	f
10	SiC	25.000	0.001	0.010	1.000
11	Si3N4	25.000	0.000	0.000	1.000
12	Al4C3	25.000	0.000	0.000	1.000
13	AlN	25.000	0.000	0.000	1.000

9 $(-4.048+5760/T) * (1-x(9))^{*2}$

X SiC	Y 1 Al	Y 2 Si	Y 3 Al4C3	Y 4 SiC
1.0000E-03	9.98670E-01	1.00000E-03	3.33330E-04	1.00000E-36
1.10000E-02	9.85330E-01	1.10000E-02	3.66670E-03	1.00000E-36
2.10000E-02	9.72000E-01	2.10000E-02	7.00000E-03	1.00000E-36
3.10000E-02	9.58670E-01	3.10000E-02	1.03330E-02	1.00000E-36
4.10000E-02	9.45330E-01	4.10000E-02	1.36670E-02	1.00000E-36
5.10000E-02	9.32000E-01	5.10000E-02	1.70000E-02	1.00000E-36
6.10000E-02	9.18670E-01	6.10000E-02	2.03330E-02	1.00000E-36
7.10000E-02	9.05330E-01	7.10000E-02	2.36670E-02	1.00000E-36
8.10000E-02	8.92000E-01	8.10000E-02	2.70000E-02	1.00000E-36
9.10000E-02	8.83630E-01	8.72770E-02	2.90920E-02	3.72280E-03
1.01000E-01	8.83630E-01	8.72770E-02	2.90920E-02	1.37230E-02
1.11000E-01	8.83630E-01	8.72770E-02	2.90920E-02	2.37230E-02

X SiC	Y 1 Al	Y 2 Si
1.00000E-03	9.99000E+01	1.00000E-01
1.10000E-02	9.89000E+01	1.10400E+00
2.10000E-02	9.78900E+01	2.11500E+00
3.10000E-02	9.68700E+01	3.13200E+00
4.10000E-02	9.58400E+01	4.15700E+00
5.10000E-02	9.48100E+01	5.18800E+00
6.10000E-02	9.37700E+01	6.22700E+00
7.10000E-02	9.27300E+01	7.27200E+00
8.10000E-02	9.16800E+01	8.32500E+00
9.10000E-02	9.10100E+01	8.98900E+00
1.01000E-01	9.10100E+01	8.98900E+00
1.11000E-01	9.10100E+01	8.98900E+00

Temperature: 800.000 C, Step = 0.000 C
 Pressure: 1.000 bar, Step = 0.000 bar
 Number of Steps: 12

Phase	Species	Temp C	Input mol	Step mol	Activity coefficient
1	Al (g)	25.000	0.000	0.000	1.000
2	Al2 (g)	25.000	0.000	0.000	1.000
3	AlC (g)	25.000	0.000	0.000	1.000
4	Ar (g)	25.000	1.000	0.000	1.000
5	N2 (g)	25.000	1.0000E-10	0.000	1.000
6	Si (g)	25.000	0.000	0.000	1.000
7	SiC (g)	25.000	0.000	0.000	1.000
8	Al	25.000	1.000	0.000	1.000
9	Si	25.000	0.000	0.000	1.000
10	SiC	25.000	0.001	0.200	f
11	Si3N4	25.000	0.000	0.000	1.000
12	Al4C3	25.000	0.000	0.000	1.000
13	AlN	25.000	0.000	0.000	1.000

$$9 \quad (-4.048 + 5760/T) \cdot (1 - x(9))^{-2}$$

X	Y 1	Y 2	Y 3	Y 4
SiC	Al	Al	Si	Al4C3
1.00000E-03	1.00000E-36	9.98670E-01	1.00000E-03	3.33330E-04
2.01000E-01	1.13720E-01	8.83630E-01	8.72770E-02	2.90920E-02
4.01000E-01	3.13720E-01	8.83630E-01	8.72770E-02	2.90920E-02
6.01000E-01	5.13720E-01	8.83630E-01	8.72770E-02	2.90920E-02
8.01000E-01	7.13720E-01	8.83630E-01	8.72770E-02	2.90920E-02
1.00100E+00	9.13720E-01	8.83630E-01	8.72770E-02	2.90920E-02
1.20100E+00	1.11370E+00	8.83630E-01	8.72770E-02	2.90920E-02
1.40100E+00	1.31370E+00	8.83630E-01	8.72770E-02	2.90920E-02
1.60100E+00	1.51370E+00	8.83630E-01	8.72770E-02	2.90920E-02
1.80100E+00	1.71370E+00	8.83630E-01	8.72770E-02	2.90920E-02
2.00100E+00	1.91370E+00	8.83630E-01	8.72770E-02	2.90920E-02
2.20100E+00	2.11370E+00	8.83630E-01	8.72770E-02	2.90920E-02

X	Y 1	Y 2
SiC	Al	Si
1.00000E-03	9.99000E+01	1.00000E-01
2.01000E-01	9.10100E+01	8.98900E+00
4.01000E-01	9.10100E+01	8.98900E+00
6.01000E-01	9.10100E+01	8.98900E+00
8.01000E-01	9.10100E+01	8.98900E+00
1.00100E+00	9.10100E+01	8.98900E+00
1.20100E+00	9.10100E+01	8.98900E+00
1.40100E+00	9.10100E+01	8.98900E+00
1.60100E+00	9.10100E+01	8.98900E+00
1.80100E+00	9.10100E+01	8.98900E+00
2.00100E+00	9.10100E+01	8.98900E+00
2.20100E+00	9.10100E+01	8.98900E+00

Input data saved as: a:\alsic.IGI

Effect of SiC/Al ratio

Temperature: 900.000 C, Step = 0.000 C
 Pressure: 1.000 bar, Step = 0.000 bar
 Number of Steps: 10

Phase	Specie	Temp C	Input mol	Step mol	Activity coefficient	
1	1	Al (g)	25.000	0.000	0.000	1.000
2	1	Al2 (g)	25.000	0.000	0.000	1.000
3	1	AlC (g)	25.000	0.000	0.000	1.000
4	1	Ar (g)	25.000	1.000	0.000	1.000
5	1	N2 (g)	25.000	1.0000E-10	0.000	1.000
6	1	Si (g)	25.000	0.000	0.000	1.000
7	1	SiC (g)	25.000	0.000	0.000	1.000
8	2	Al	25.000	1.000	0.000	1.000
9	2	Si	25.000	0.000	0.000	1.000
10	3	SiC	25.000	0.001	0.100	1.000
11	3	Si3N4	25.000	0.000	0.000	1.000
12	4	Al4C3	25.000	0.000	0.000	1.000
13	4	AlN	25.000	0.000	0.000	1.000

$$9 \quad (-4.048 + 5760/T) * (1 - x(9)) ^ 2$$

X	Y 1	Y 2	Y 3	Y 4
SiC	Al	SiC	Si	Al4C3
1.00000E-03	9.98670E-01	1.00000E-36	1.00000E-03	3.33330E-04
1.01000E-01	8.65330E-01	1.00000E-36	1.01000E-01	3.36670E-02
2.01000E-01	8.54890E-01	9.21690E-02	1.08830E-01	3.62770E-02
3.01000E-01	8.54890E-01	1.92170E-01	1.08830E-01	3.62770E-02
4.01000E-01	8.54890E-01	2.92170E-01	1.08830E-01	3.62770E-02
5.01000E-01	8.54890E-01	3.92170E-01	1.08830E-01	3.62770E-02
6.01000E-01	8.54890E-01	4.92170E-01	1.08830E-01	3.62770E-02
7.01000E-01	8.54890E-01	5.92170E-01	1.08830E-01	3.62770E-02
8.01000E-01	8.54890E-01	6.92170E-01	1.08830E-01	3.62770E-02
9.01000E-01	8.54890E-01	7.92170E-01	1.08830E-01	3.62770E-02

Input data saved as: a:\alsic.IGI

Effect of SiC/Al ratio

Temperature: 900.000 C, Step = 0.000 C
 Pressure: 1.000 bar, Step = 0.000 bar
 Number of Steps: 10

Phase	Specie	Temp C	Input mol	Step mol	Activity coefficient
1	Al (g)	25.000	0.000	0.000	1.000
2	Al2 (g)	25.000	0.000	0.000	1.000
3	AlC (g)	25.000	0.000	0.000	1.000
4	Ar (g)	25.000	1.000	0.000	1.000
5	N2 (g)	25.000	1.00000E-10	0.000	1.000
6	Si (g)	25.000	0.000	0.000	1.000
7	SiC (g)	25.000	0.000	0.000	1.000
8	Al	25.000	1.000	0.000	1.000
9	Si	25.000	0.000	0.000	1.000
10	SiC	25.000	0.001	0.015	f
11	Si3N4	25.000	0.000	0.000	1.000
12	Al4C3	25.000	0.000	0.000	1.000
13	AlN	25.000	0.000	0.000	1.000

$$9 \quad (-4.048+5760/T) \cdot (1-x(9))^2$$

X	Y 1	Y 2	Y 3	Y 4
SiC	Al	Si	Al4C3	SiC
1.00000E-03	9.98670E-01	1.00000E-03	3.33330E-04	1.00000E-36
1.60000E-02	9.78670E-01	1.60000E-02	5.33330E-03	1.00000E-36
3.10000E-02	9.58670E-01	3.10000E-02	1.03330E-02	1.00000E-36
4.60000E-02	9.38670E-01	4.60000E-02	1.53330E-02	1.00000E-36
6.10000E-02	9.18670E-01	6.10000E-02	2.03330E-02	1.00000E-36
7.60000E-02	8.98670E-01	7.60000E-02	2.53330E-02	1.00000E-36
9.10000E-02	8.78670E-01	9.10000E-02	3.03330E-02	1.00000E-36
1.06000E-01	8.58670E-01	1.06000E-01	3.53330E-02	1.00000E-36
1.21000E-01	8.38670E-01	1.08830E-01	3.62770E-02	1.21690E-02
1.36000E-01	8.18670E-01	1.08830E-01	3.62770E-02	2.71690E-02

Input data saved as: a:\alsic.IGI

Effect of SiC/Al ratio

Temperature: 1000 C, Step = 0.000 C
 Pressure: 1.000 bar, Step = 0.000 bar
 Number of Steps: 10

Phase	Species	Temp C	Input mol	Step mol	Activity coefficient
1	1	Al (g)	25.000	0.000	1.000
2	1	Al2 (g)	25.000	0.000	1.000
3	1	AlC (g)	25.000	0.000	1.000
4	1	Ar (g)	25.000	1.000	1.000
5	1	N2 (g)	25.000	1.0000E-10	1.000
6	1	Si (g)	25.000	0.000	1.000
7	1	SiC (g)	25.000	0.000	1.000
8	2	Al	25.000	1.000	1.000
9	2	Si	25.000	0.000	1.000
10	3	SiC	25.000	0.001	1.000
11	3	Si3N4	25.000	0.000	1.000
12	4	Al4C3	25.000	0.000	1.000
13	4	AlN	25.000	0.000	1.000

9 $(-4.048+5760/T) \cdot (1-x(9))^2$

X SiC	Y 1 Al	Y 2 Si	Y 3 SiC	Y 4 Al4C3
1.00000E-03	9.98670E-01	1.00000E-03	1.00000E-36	3.33330E-04
2.10000E-02	9.72000E-01	2.10000E-02	1.00000E-36	7.00000E-03
4.10000E-02	9.45330E-01	4.10000E-02	1.00000E-36	1.36670E-02
6.10000E-02	9.18670E-01	6.10000E-02	1.00000E-36	2.03330E-02
8.10000E-02	8.92000E-01	8.10000E-02	1.00000E-36	2.70000E-02
1.01000E-01	8.65330E-01	1.01000E-01	1.00000E-36	3.36670E-02
1.21000E-01	8.38670E-01	1.21000E-01	1.00000E-36	4.03330E-02
1.41000E-01	8.31160E-01	1.26630E-01	1.43690E-02	4.22100E-02
1.61000E-01	8.31160E-01	1.26630E-01	3.43690E-02	4.22100E-02
1.81000E-01	8.31160E-01	1.26630E-01	5.43690E-02	4.22100E-02

Input data saved as: a:\alsic.IGI

Effect of SiC/Al ratio

Temperature: 1000 C, Step = 0.000 C
 Pressure: 1.000 bar, Step = 0.000 bar
 Number of Steps: 10

Phase	Specie	Temp C	Input mol	Step mol	Activity coefficient	
1	1	Al (g)	25.000	0.000	0.000	1.000
2	1	Al2 (g)	25.000	0.000	0.000	1.000
3	1	AlC (g)	25.000	0.000	0.000	1.000
4	1	Ar (g)	25.000	1.000	0.000	1.000
5	1	N2 (g)	25.000	1.0000E-10	0.000	1.000
6	1	Si (g)	25.000	0.000	0.000	1.000
7	1	SiC (g)	25.000	0.000	0.000	1.000
8	2	Al	25.000	1.000	0.000	1.000
9	2	Si	25.000	0.000	0.000	f
10	3	SiC	25.000	0.001	0.100	1.000
11	3	Si3N4	25.000	0.000	0.000	1.000
12	4	Al4C3	25.000	0.000	0.000	1.000
13	4	AlN	25.000	0.000	0.000	1.000

9 (-4.048+5760/T)*(1-x(9))^2

X	Y 1	Y 2	Y 3	Y 4
SiC	Al	SiC	Si	Al4C3
1.00000E-03	9.98670E-01	1.00000E-36	1.00000E-03	3.33330E-04
1.01000E-01	8.65330E-01	1.00000E-36	1.01000E-01	3.36670E-02
2.01000E-01	8.31160E-01	7.43690E-02	1.26630E-01	4.22100E-02
3.01000E-01	8.31160E-01	1.74370E-01	1.26630E-01	4.22100E-02
4.01000E-01	8.31160E-01	2.74370E-01	1.26630E-01	4.22100E-02
5.01000E-01	8.31160E-01	3.74370E-01	1.26630E-01	4.22100E-02
6.01000E-01	8.31160E-01	4.74370E-01	1.26630E-01	4.22100E-02
7.01000E-01	8.31160E-01	5.74370E-01	1.26630E-01	4.22100E-02
8.01000E-01	8.31160E-01	6.74370E-01	1.26630E-01	4.22100E-02
9.01000E-01	8.31160E-01	7.74370E-01	1.26630E-01	4.22100E-02

Input data saved as: a:\alsic.igt

Effect of temperature
 Temperature: 700.000 C, Step = 50.000 C
 Pressure: 1.000 bar, Step = 0.000 bar
 Number of Steps: 10

Phase	Species	Temp C	Input mol	Step mol	Activity coefficient
1	Al(g)	25.000	0.000	0.000	1.000
2	Al2(g)	25.000	0.000	0.000	1.000
3	AlC(g)	25.000	0.000	0.000	1.000
4	Ar(g)	25.000	1.000	0.000	1.000
5	N2(g)	25.000	1.0000E-10	0.000	1.000
6	Si(g)	25.000	0.000	0.000	1.000
7	SiC(g)	25.000	0.000	0.000	1.000
8	Al	25.000	1.000	0.000	f
9	Si	25.000	0.000	0.000	1.000
10	SiC	25.000	1.000	0.000	1.000
11	Si3N4	25.000	0.000	0.000	1.000
12	Al4C3	25.000	0.000	0.000	1.000
13	AlN	25.000	0.000	0.000	1.000

$$9 \quad (-4.048+5760/T) \cdot (1-x(9))^2$$

X	Y 1	Y 2	Y 3	Y 4
Temperature	SiC	Al	Si	Al4C3
9.73150E+02	9.36770E-01	9.15690E-01	6.32300E-02	2.10770E-02
1.02315E+03	9.24600E-01	8.99460E-01	7.54030E-02	2.51340E-02
1.07315E+03	9.12720E-01	8.83630E-01	8.72770E-02	2.90920E-02
1.12315E+03	9.01510E-01	8.68680E-01	9.84910E-02	3.28300E-02
1.17315E+03	8.91170E-01	8.54890E-01	1.08830E-01	3.62770E-02
1.22315E+03	8.81790E-01	8.42390E-01	1.18210E-01	3.94030E-02
1.27315E+03	8.73370E-01	8.31160E-01	1.26630E-01	4.22100E-02
1.32315E+03	8.65850E-01	8.21140E-01	1.34150E-01	4.47150E-02
1.37315E+03	8.59160E-01	8.12220E-01	1.40840E-01	4.69450E-02
1.42315E+03	8.53210E-01	8.04280E-01	1.46790E-01	4.89300E-02

X	Y 1	Y 2
Temperature	Al	Si
9.73150E+02	9.35400E+01	6.45900E+00
1.02315E+03	9.22700E+01	7.73500E+00
1.07315E+03	9.10100E+01	8.98900E+00
1.12315E+03	8.98200E+01	1.01800E+01
1.17315E+03	8.87100E+01	1.12900E+01
1.22315E+03	8.76900E+01	1.23100E+01
1.27315E+03	8.67800E+01	1.32200E+01
1.32315E+03	8.59600E+01	1.40400E+01
1.37315E+03	8.52200E+01	1.47800E+01
1.42315E+03	8.45700E+01	1.54300E+01

Input data saved as: a:\alsic.IGI

Effect of temperature

Temperature: 1150.000 C, Step = 50.000 C
 Pressure: 1.000 bar, Step = 0.000 bar
 Number of Steps: 8

Phase	Species	Temp C	Input mol	Step mol	Activity coefficient
1	1	Al (g)	25.000	0.000	1.000
2	1	Al2 (g)	25.000	0.000	1.000
3	1	AlC (g)	25.000	0.000	1.000
4	1	Ar (g)	25.000	1.000	1.000
5	1	N2 (g)	25.000	1.0000E-10	1.000
6	1	Si (g)	25.000	0.000	1.000
7	1	SiC (g)	25.000	0.000	1.000
8	2	Al	25.000	1.000	1.000
9	2	Si	25.000	0.000	1.000
10	3	SiC	25.000	1.000	1.000
11	3	Si3N4	25.000	0.000	1.000
12	4	Al4C3	25.000	0.000	1.000
13	4	AlN	25.000	0.000	1.000

X	Y 1	Y 2	Y 3	Y 4
Temperature	SiC	Al	Si	Al4C3
1.42315E+03	8.53260E-01	8.04340E-01	1.46740E-01	4.89130E-02
1.47315E+03	8.58820E-01	8.11750E-01	1.41180E-01	4.70590E-02
1.52315E+03	8.63940E-01	8.18560E-01	1.36060E-01	4.53540E-02
1.57315E+03	8.68660E-01	8.24830E-01	1.31340E-01	4.37810E-02
1.62315E+03	8.73020E-01	8.30600E-01	1.26980E-01	4.23270E-02
1.67315E+03	8.77060E-01	8.35900E-01	1.22940E-01	4.09780E-02
1.72315E+03	8.73010E-01	8.30330E-01	1.26990E-01	4.23310E-02
1.77315E+03	8.66660E-01	8.21600E-01	1.33330E-01	4.44450E-02

X	Y 1	Y 2
Temperature	Al	Si
1.42315E+03	8.45700E+01	1.54300E+01
1.47315E+03	8.51800E+01	1.48200E+01
1.52315E+03	8.57500E+01	1.42500E+01
1.57315E+03	8.62600E+01	1.37400E+01
1.62315E+03	8.67400E+01	1.32600E+01
1.67315E+03	8.71800E+01	1.28200E+01
1.72315E+03	8.67300E+01	1.32700E+01
1.77315E+03	8.60400E+01	1.39600E+01

Input data saved as: a:\alsic.IGI

Effect of Si

Temperature: 800 C, Step = 0.000 C

Pressure: 1.000 bar, Step = 0.000 bar

Number of Steps: 10

Phase	Species	Temp C	Input mol	Step mol	Activity coefficient
1	Al(g)	25.000	0.000	0.000	1.000
2	Al2(g)	25.000	0.000	0.000	1.000
3	AlC(g)	25.000	0.000	0.000	1.000
4	Ar(g)	25.000	1.000	0.000	1.000
5	N2(g)	25.000	1.0000E-10	0.000	1.000
6	Si(g)	25.000	0.000	0.000	1.000
7	SiC(g)	25.000	0.000	0.000	1.000
8	Al	25.000	1.000	0.000	1.000
9	Si	25.000	1.0000E-04	0.020	f
10	SiC	25.000	0.200	0.000	1.000
11	Si3N4	25.000	0.000	0.000	1.000
12	Al4C3	25.000	0.000	0.000	1.000
13	AlN	25.000	0.000	0.000	1.000

9 (-4.048+5760/T)*(1-x(9))^2

X	Y 1	Y 2	Y 3	Y 4
Si	Al	SiC	Si	Al4C3
1.00000E-04	8.83750E-01	1.12810E-01	8.72890E-02	2.90630E-02
2.01000E-02	9.07310E-01	1.30480E-01	8.96160E-02	2.31720E-02
4.01000E-02	9.30880E-01	1.48160E-01	9.19440E-02	1.72810E-02
6.01000E-02	9.54440E-01	1.65830E-01	9.42710E-02	1.13900E-02
8.01000E-02	9.78000E-01	1.83500E-01	9.65980E-02	5.49950E-03
1.00100E-01	1.00000E+00	2.00000E-01	1.00100E-01	5.89090E-09
1.20100E-01	1.00000E+00	2.00000E-01	1.20100E-01	3.22840E-10
1.40100E-01	1.00000E+00	2.00000E-01	1.40100E-01	1.48720E-10
1.60100E-01	1.00000E+00	2.00000E-01	1.60100E-01	9.05570E-11
1.80100E-01	1.00000E+00	2.00000E-01	1.80100E-01	6.23260E-11

Input data saved as: a:\alsic.IGI

Effect of Si
 Temperature: 900 C, Step = 0.000 C
 Pressure: 1.000 bar, Step = 0.000 bar
 Number of Steps: 10

Phase	Species	Temp C	Input mol	Step mol	Activity coefficient
1	1	Al(g)	25.000	0.000	1.000
2	1	Al2(g)	25.000	0.000	1.000
3	1	AlC(g)	25.000	0.000	1.000
4	1	Ar(g)	25.000	1.000	1.000
5	1	N2(g)	25.000	1.0000E-10	1.000
6	1	Si(g)	25.000	0.000	1.000
7	1	SiC(g)	25.000	0.000	1.000
8	2	Al	25.000	1.000	1.000
9	2	Si	25.000	1.0000E-04	0.020
10	3	SiC	25.000	0.200	1.000
11	3	Si3N4	25.000	0.000	1.000
12	4	Al4C3	25.000	0.000	1.000
13	4	AlN	25.000	0.000	1.000

9 (-4.048+5760/T)*(1-x(9))^2

X	Y 1	Y 2	Y 3	Y 4
Si	Al	SiC	Si	Al4C3
1.00000E-04	8.55010E-01	9.12540E-02	1.08850E-01	3.62490E-02
2.01000E-02	8.77800E-01	1.08350E-01	1.11750E-01	3.05490E-02
4.01000E-02	9.00600E-01	1.25450E-01	1.14650E-01	2.48500E-02
6.01000E-02	9.23400E-01	1.42550E-01	1.17550E-01	1.91510E-02
8.01000E-02	9.46190E-01	1.59650E-01	1.20450E-01	1.34510E-02
1.00100E-01	9.68990E-01	1.76740E-01	1.23360E-01	7.75210E-03
1.20100E-01	9.91790E-01	1.93840E-01	1.26260E-01	2.05290E-03
1.40100E-01	1.00000E+00	2.00000E-01	1.40100E-01	6.94070E-10
1.60100E-01	1.00000E+00	2.00000E-01	1.60100E-01	2.41700E-10
1.80100E-01	1.00000E+00	2.00000E-01	1.80100E-01	1.35060E-10

Input data saved as: a:\alsic.IGI

Effect of Si

Temperature: 1000 C, Step = 0.000 C
 Pressure: 1.000 bar, Step = 0.000 bar
 Number of Steps: 10

Phase	Specie	Temp C	Input mol	Step mol	Activity coefficient
1	Al(g)	25.000	0.000	0.000	1.000
2	Al2(g)	25.000	0.000	0.000	1.000
3	AlC(g)	25.000	0.000	0.000	1.000
4	Ar(g)	25.000	1.000	0.000	1.000
5	N2(g)	25.000	1.0000E-10	0.000	1.000
6	Si(g)	25.000	0.000	0.000	1.000
7	SiC(g)	25.000	0.000	0.000	1.000
8	Al	25.000	1.000	0.000	1.000
9	Si	25.000	1.0000E-04	0.020	f
10	SiC	25.000	0.200	0.000	1.000
11	Si3N4	25.000	0.000	0.000	1.000
12	Al4C3	25.000	0.000	0.000	1.000
13	AlN	25.000	0.000	0.000	1.000

9 $(-4.048+5760/T)*(1-x(9))^2$

X	Y 1	Y 2	Y 3	Y 4
Si	Al	SiC	Si	Al4C3
1.00000E-04	8.31270E-01	7.34530E-02	1.26650E-01	4.21820E-02
2.01000E-02	8.53430E-01	9.00760E-02	1.30020E-01	3.66410E-02
4.01000E-02	8.75600E-01	1.06700E-01	1.33400E-01	3.11000E-02
6.01000E-02	8.97760E-01	1.23320E-01	1.36780E-01	2.55590E-02
8.01000E-02	9.19930E-01	1.39950E-01	1.40150E-01	2.00180E-02
1.00100E-01	9.42090E-01	1.56570E-01	1.43530E-01	1.44770E-02
1.20100E-01	9.64260E-01	1.73190E-01	1.46910E-01	8.93610E-03
1.40100E-01	9.86420E-01	1.89810E-01	1.50290E-01	3.39500E-03
1.60100E-01	1.00000E+00	2.00000E-01	1.60100E-01	1.31920E-03
1.80100E-01	1.00000E+00	2.00000E-01	1.80100E-01	3.28320E-10

Input data saved as: a:\alsic.IGI

Effect of carbon

Temperature: 1100.000 C, Step = 0.000 C
 Pressure: 1.000 bar, Step = 0.000 bar
 Number of Steps: 10

Phase	Specie	Temp C	Input mol	Step mol	Activity coefficient
1	Al (g)	25.000	0.000	0.000	1.000
2	Al2 (g)	25.000	0.000	0.000	1.000
3	AlC (g)	25.000	0.000	0.000	1.000
4	Ar (g)	25.000	1.000	0.000	1.000
5	N2 (g)	25.000	1.000E-10	0.000	1.000
6	Si (g)	25.000	0.000	0.000	1.000
7	SiC (g)	25.000	0.000	0.000	1.000
8	Al	25.000	0.700	0.000	1.000
9	Si	25.000	0.300	0.000	f
10	SiC	25.000	0.000	0.000	1.000
11	Si3N4	25.000	0.000	0.000	1.000
12	Al4C3	25.000	0.000	0.000	1.000
13	AlN	25.000	0.000	0.000	1.000
14	C	25.000	1.000E-04	0.040	1.000

9 $(-4.048+5760/T) \cdot (1-x(9))^2$

X C	Y 1 Al	Y 2 Si	Y 3 SiC	Y 4 Al4C3
1.00000E-04	7.00000E-01	2.99900E-01	1.00000E-04	1.28230E-11
4.01000E-02	7.00000E-01	2.59900E-01	4.01000E-02	2.09280E-11
8.01000E-02	7.00000E-01	2.19900E-01	8.01000E-02	3.80760E-11
1.20100E-01	7.00000E-01	1.79900E-01	1.20100E-01	8.50880E-11
1.60100E-01	7.00000E-01	1.39900E-01	1.60100E-01	3.67500E-10
2.00100E-01	6.76740E-01	1.17340E-01	1.82660E-01	5.81490E-03
2.40100E-01	6.33420E-01	1.09830E-01	1.90170E-01	1.66450E-02
2.80100E-01	5.90100E-01	1.02320E-01	1.97680E-01	2.74740E-02
3.20100E-01	5.46780E-01	9.48110E-02	2.05190E-01	3.83040E-02
3.60100E-01	5.03470E-01	8.73000E-02	2.12700E-01	4.91330E-02

X C	Y 1 Al	Y 2 Si
1.00000E-04	7.00100E+01	2.99900E+01
4.01000E-02	7.29200E+01	2.70800E+01
8.01000E-02	7.61000E+01	2.39000E+01
1.20100E-01	7.95500E+01	2.04500E+01
1.60100E-01	8.33400E+01	1.66600E+01
2.00100E-01	8.52200E+01	1.47800E+01
2.40100E-01	8.52200E+01	1.47800E+01
2.80100E-01	8.52200E+01	1.47800E+01
3.20100E-01	8.52200E+01	1.47800E+01
3.60100E-01	8.52200E+01	1.47800E+01

Input data saved as: a:\alsic.IGI

Effect of carbon

Temperature: 1100.000 C, Step = 0.000 C
 Pressure: 1.000 bar, Step = 0.000 bar
 Number of Steps: 10

Phase	Species	Temp C	Input mol	Step mol	Activity coefficient
1	1	Al(g)	25.000	0.000	1.000
2	1	Al2(g)	25.000	0.000	1.000
3	1	AlC(g)	25.000	0.000	1.000
4	1	Ar(g)	25.000	1.000	1.000
5	1	N2(g)	25.000	1.0000E-10	1.000
6	1	Si(g)	25.000	0.000	1.000
7	1	SiC(g)	25.000	0.000	1.000
8	2	Al	25.000	0.600	1.000
9	2	Si	25.000	0.400	1.000
10	3	SiC	25.000	0.000	1.000
11	3	Si3N4	25.000	0.000	1.000
12	4	Al4C3	25.000	0.000	1.000
13	4	AlN	25.000	0.000	1.000
14	5	C	25.000	1.0000E-04	1.000

9 $(-4.048+5760/T) \cdot (1-x(5))^{-2}$

X C	Y 1 Al	Y 2 Si	Y 3 SiC	Y 4 Al4C3
1.00000E-04	6.00000E-01	3.99900E-01	1.00000E-04	2.94300E-12
8.01000E-02	6.00000E-01	3.19900E-01	8.01000E-02	6.17390E-12
1.60100E-01	6.00000E-01	2.39900E-01	1.60100E-01	1.62140E-11
2.40100E-01	6.00000E-01	1.59900E-01	2.40100E-01	7.27510E-11
3.20100E-01	5.73860E-01	9.95060E-02	3.00490E-01	6.53520E-03
4.00100E-01	4.87220E-01	8.44830E-02	3.15520E-01	2.81940E-02
4.80100E-01	4.00580E-01	6.94600E-02	3.30540E-01	4.98530E-02
5.60100E-01	3.13950E-01	5.44380E-02	3.45560E-01	7.15130E-02
6.40100E-01	2.27310E-01	3.94150E-02	3.60580E-01	9.31720E-02
7.20100E-01	1.40670E-01	2.43930E-02	3.75610E-01	1.14830E-01

X C	Y 1 Al	Y 2 Si
1.00000E-04	6.00100E+01	3.99900E+01
8.01000E-02	6.52200E+01	3.47800E+01
1.60100E-01	7.14400E+01	2.85600E+01
2.40100E-01	7.89600E+01	2.10400E+01
3.20100E-01	8.52200E+01	1.47800E+01
4.00100E-01	8.52200E+01	1.47800E+01
4.80100E-01	8.52200E+01	1.47800E+01
5.60100E-01	8.52200E+01	1.47800E+01
6.40100E-01	8.52200E+01	1.47800E+01
7.20100E-01	8.52200E+01	1.47800E+01

Input data saved as: a:\alsic.IGI

Effect of carbon
 Temperature: 1100.000 C, Step = 0.000 C
 Pressure: 1.000 bar, Step = 0.000 bar
 Number of Steps: 10

Phase	Specie	Temp C	Input mol	Step mol	Activity coefficient	
1	1	Al(g)	25.000	0.000	0.000	1.000
2	1	Al2(g)	25.000	0.000	0.000	1.000
3	1	AlC(g)	25.000	0.000	0.000	1.000
4	1	Ar(g)	25.000	1.000	0.000	1.000
5	1	N2(g)	25.000	1.0000E-10	0.000	1.000
6	1	Si(g)	25.000	0.000	0.000	1.000
7	1	SiC(g)	25.000	0.000	0.000	1.000
8	2	Al	25.000	0.500	0.000	1.000
9	2	Si	25.000	0.500	0.000	1.000
10	3	SiC	25.000	0.000	0.000	1.000
11	3	Si3N4	25.000	0.000	0.000	1.000
12	4	Al4C3	25.000	0.000	0.000	1.000
13	4	AlN	25.000	0.000	0.000	1.000
14	5	C	25.000	1.0000E-04	0.080	1.000

$$9 \quad (-4.048+5760/T) * (1-x(9))^2$$

X C	Y 1 Al	Y 2 Si	Y 3 SiC	Y 4 Al4C3
1.00000E-04	5.00000E-01	4.99900E-01	1.00000E-04	7.52700E-13
8.01000E-02	5.00000E-01	4.15900E-01	8.01000E-02	1.35880E-12
1.60100E-01	5.00000E-01	3.39900E-01	1.60100E-01	2.75570E-12
2.40100E-01	5.00000E-01	2.59900E-01	2.40100E-01	6.71710E-12
3.20100E-01	5.00000E-01	1.79900E-01	3.20100E-01	2.33550E-11
4.00100E-01	5.00000E-01	9.99000E-02	4.00100E-01	3.68420E-10
4.80100E-01	4.27660E-01	7.41550E-02	4.25850E-01	1.80850E-02
5.60100E-01	3.41020E-01	5.91320E-02	4.40870E-01	3.97440E-02
6.40100E-01	2.54390E-01	4.41100E-02	4.55890E-01	6.14030E-02
7.20100E-01	1.67750E-01	2.90870E-02	4.70910E-01	8.30620E-02

X C	Y 1 Al	Y 2 Si
1.00000E-04	5.00000E+01	5.00000E+01
8.01000E-02	5.43500E+01	4.56500E+01
1.60100E-01	5.95300E+01	4.04700E+01
2.40100E-01	6.58000E+01	3.42000E+01
3.20100E-01	7.35400E+01	2.64600E+01
4.00100E-01	8.33500E+01	1.66500E+01
4.80100E-01	8.52200E+01	1.47800E+01
5.60100E-01	8.52200E+01	1.47800E+01
6.40100E-01	8.52200E+01	1.47800E+01
7.20100E-01	8.52200E+01	1.47800E+01

Input data saved as: a:\alsic3.IGI

Effect of carbon

Temperature: 1200.000 C, Step = 0.000 C
 Pressure: 1.000 bar, Step = 0.000 bar
 Number of Steps: 10

Phase	Specie	Temp C	Input mol	Step mol	Activity coefficient	
1	1	Al(g)	25.000	0.000	0.000	1.000
2	1	Al2(g)	25.000	0.000	0.000	1.000
3	1	AlC(g)	25.000	0.000	0.000	1.000
4	1	Ar(g)	25.000	1.000	0.000	1.000
5	1	N2(g)	25.000	1.0000E-10	0.000	1.000
6	1	Si(g)	25.000	0.000	0.000	1.000
7	1	SiC(g)	25.000	0.000	0.000	1.000
8	2	Al	25.000	0.500	0.000	1.000
9	2	Si	25.000	0.500	0.000	1.000
10	3	SiC	25.000	0.000	0.000	1.000
11	3	Si3N4	25.000	0.000	0.000	1.000
12	4	Al4C3	25.000	0.000	0.000	1.000
13	4	AlN	25.000	0.000	0.000	1.000
14	5	C	25.000	1.0000E-04	0.000	1.000

X C	Y 1 Al	Y 2 Si	Y 3 SiC	Y 4 Al4C3
1.00000E-04	4.99990E-01	4.99900E-01	1.00000E-04	4.09790E-13
8.01000E-02	4.99990E-01	4.19900E-01	8.01000E-02	8.14360E-13
1.60100E-01	4.99990E-01	3.39900E-01	1.60100E-01	1.81110E-12
2.40100E-01	4.99990E-01	2.59900E-01	2.40100E-01	4.85120E-12
3.20100E-01	4.99990E-01	1.79900E-01	3.20100E-01	1.88300E-11
4.00100E-01	4.99990E-01	9.99000E-02	4.00100E-01	3.58200E-10
4.80100E-01	4.27410E-01	7.43340E-02	4.25670E-01	1.81450E-02
5.60100E-01	3.40820E-01	5.92750E-02	4.40720E-01	3.97920E-02
6.40100E-01	2.54240E-01	4.42160E-02	4.55780E-01	6.14390E-02
7.20100E-01	1.67650E-01	2.91570E-02	4.70840E-01	8.30860E-02

X C	Y 1 Al	Y 2 Si
1.00000E-04	5.00000E+01	5.00000E+01
8.01000E-02	5.43500E+01	4.56500E+01
1.60100E-01	5.95300E+01	4.04700E+01
2.40100E-01	6.58000E+01	3.42000E+01
3.20100E-01	7.35400E+01	2.64600E+01
4.00100E-01	8.33500E+01	1.66500E+01
4.80100E-01	8.51800E+01	1.48200E+01
5.60100E-01	8.51800E+01	1.48200E+01
6.40100E-01	8.51800E+01	1.48200E+01
7.20100E-01	8.51800E+01	1.48200E+01

Input data saved as: a:\alsic3.IGI

Effect of carbon

Temperature: 1200.000 C, Step = 0.000 C
 Pressure: 1.000 bar, Step = 0.000 bar
 Number of Steps: 10

	Phase	Species	Temp C	Input mol	Step mol	Activity coefficient
1	1	Al (g)	25.000	0.000	0.000	1.000
2	1	Al2 (g)	25.000	0.000	0.000	1.000
3	1	AlC (g)	25.000	0.000	0.000	1.000
4	1	Ar (g)	25.000	1.000	0.000	1.000
5	1	N2 (g)	25.000	1.0000E-10	0.000	1.000
6	1	Si (g)	25.000	0.000	0.000	1.000
7	1	SiC (g)	25.000	0.000	0.000	1.000
8	2	Al	25.000	0.600	0.000	1.000
9	2	Si	25.000	0.400	0.000	1.000
10	3	SiC	25.000	0.000	0.000	1.000
11	3	Si3N4	25.000	0.000	0.000	1.000
12	4	Al4C3	25.000	0.000	0.000	1.000
13	4	AlN	25.000	0.000	0.000	1.000
14	5	C	25.000	1.0000E-04	0.080	1.000

X C	Y 1 Al	Y 2 Si	Y 3 SiC	Y 4 Al4C3
1.00000E-04	5.99990E-01	3.99900E-01	1.00000E-04	1.94950E-12
8.01000E-02	5.99990E-01	3.19900E-01	8.01000E-02	4.42290E-12
1.60100E-01	5.99990E-01	2.39900E-01	1.60100E-01	1.26780E-11
2.40100E-01	5.99990E-01	1.59900E-01	2.40100E-01	6.41660E-11
3.20100E-01	5.73530E-01	9.97470E-02	3.00250E-01	6.61550E-03
4.00100E-01	4.86940E-01	8.46870E-02	3.15310E-01	2.82620E-02
4.80100E-01	4.00350E-01	6.96280E-02	3.30370E-01	4.99090E-02
5.60100E-01	3.13770E-01	5.45690E-02	3.45430E-01	7.15560E-02
6.40100E-01	2.27180E-01	3.95100E-02	3.60490E-01	9.32030E-02
7.20100E-01	1.40590E-01	2.44510E-02	3.75550E-01	1.14850E-01

X C	Y 1 Al	Y 2 Si
1.00000E-04	6.00100E+01	3.99900E+01
8.01000E-02	6.52200E+01	3.47800E+01
1.60100E-01	7.14400E+01	2.85600E+01
2.40100E-01	7.89600E+01	2.10400E+01
3.20100E-01	8.51800E+01	1.48200E+01
4.00100E-01	8.51800E+01	1.48200E+01
4.80100E-01	8.51800E+01	1.48200E+01
5.60100E-01	8.51800E+01	1.48200E+01
6.40100E-01	8.51800E+01	1.48200E+01
7.20100E-01	8.51800E+01	1.48200E+01

Input data saved as: a:\alsic3.IGI

Effect of carbon

Temperature: 1200.000 C, Step = 0.000 C
 Pressure: 1.000 bar, Step = 0.000 bar
 Number of Steps: 10

Phase	Specie	Temp C	Input mol	Step mol	Activity coefficient	
1	1	Al (g)	25.000	0.000	0.000	1.000
2	1	Al2 (g)	25.000	0.000	0.000	1.000
3	1	AlC (g)	25.000	0.000	0.000	1.000
4	1	Ar (g)	25.000	1.000	0.000	1.000
5	1	N2 (g)	25.000	1.0000E-10	0.000	1.000
6	1	Si (g)	25.000	0.000	0.000	1.000
7	1	SiC (g)	25.000	0.000	0.000	1.000
8	2	Al	25.000	0.700	0.000	1.000
9	2	Si	25.000	0.300	0.000	1.000
10	3	SiC	25.000	0.000	0.000	1.000
11	3	Si3N4	25.000	0.000	0.000	1.000
12	4	Al4C3	25.000	0.000	0.000	1.000
13	4	AlN	25.000	0.000	0.000	1.000
14	5	C	25.000	1.0000E-04	0.040	1.000

X C	Y 1 Al	Y 2 Si	Y 3 SiC	Y 4 Al4C3
1.00000E-04	6.99990E-01	2.99900E-01	1.00000E-04	9.82660E-12
4.01000E-02	6.99990E-01	2.59900E-01	4.01000E-02	1.67210E-11
8.01000E-02	6.99990E-01	2.19900E-01	8.01000E-02	3.19430E-11
1.20100E-01	6.99990E-01	1.79900E-01	1.20100E-01	7.59150E-11
1.60100E-01	6.99990E-01	1.39900E-01	1.60100E-01	3.57280E-10
2.00100E-01	6.76350E-01	1.17630E-01	1.82370E-01	5.90970E-03
2.40100E-01	6.33060E-01	1.10100E-01	1.89900E-01	1.67330E-02
2.80100E-01	5.89760E-01	1.02570E-01	1.97430E-01	2.75570E-02
3.20100E-01	5.46470E-01	9.50410E-02	2.04960E-01	3.83800E-02
3.60100E-01	5.03180E-01	8.75110E-02	2.12490E-01	4.92040E-02

X C	Y 1 Al	Y 2 Si
1.00000E-04	7.00100E+01	2.59900E+01
4.01000E-02	7.29200E+01	2.70800E+01
8.01000E-02	7.61000E+01	2.39000E+01
1.20100E-01	7.95500E+01	2.04500E+01
1.60100E-01	8.33400E+01	1.66600E+01
2.00100E-01	8.51800E+01	1.48200E+01
2.40100E-01	8.51800E+01	1.48200E+01
2.80100E-01	8.51800E+01	1.48200E+01
3.20100E-01	8.51800E+01	1.48200E+01
3.60100E-01	8.51800E+01	1.48200E+01

Input data saved as: a:\alsic3.IGI

Effect of carbon

Temperature: 1300.000 C, Step = 0.000 C
 Pressure: 1.000 bar, Step = 0.000 bar
 Number of Steps: 10

Phase	Specie	Temp C	Input mol	Step mol	Activity coefficient	
1	1	Al(g)	25.000	0.000	0.000	1.000
2	1	Al2(g)	25.000	0.000	0.000	1.000
3	1	AlC(g)	25.000	0.000	0.000	1.000
4	1	Ar(g)	25.000	1.000	0.000	1.000
5	1	N2(g)	25.000	1.0000E-10	0.000	1.000
6	1	Si(g)	25.000	0.000	0.000	1.000
7	1	SiC(g)	25.000	0.000	0.000	1.000
8	2	Al	25.000	0.600	0.000	1.000
9	2	Si	25.000	0.400	0.000	1.000
10	3	SiC	25.000	0.000	0.000	1.000
11	3	Si3N4	25.000	0.000	0.000	1.000
12	4	Al4C3	25.000	0.000	0.000	1.000
13	4	AlN	25.000	0.000	0.000	1.000
14	5	C	25.000	1.0000E-C4	0.000	1.000

X	Y 1	Y 2	Y 3	Y 4
C	Al	Si	SiC	Al4C3
1.00000E-04	5.59970E-01	3.99900E-01	1.00000E-04	1.00000E-36
8.01000E-02	5.59970E-01	3.19900E-01	8.01000E-02	1.00000E-36
1.60100E-01	5.59960E-01	2.39900E-01	1.60100E-01	1.00000E-36
2.40100E-01	5.59960E-01	1.59900E-01	2.40100E-01	1.00000E-36
3.20100E-01	5.82760E-01	9.27970E-02	3.07200E-01	4.29890E-03
4.00100E-01	4.54770E-01	7.87860E-02	3.21210E-01	2.62950E-02
4.80100E-01	4.06790E-01	6.47760E-02	3.35220E-01	4.82920E-02
5.60100E-01	3.18800E-01	5.07650E-02	3.49240E-01	7.02880E-02
6.40100E-01	2.30820E-01	3.67540E-02	3.63250E-01	9.22850E-02
7.20100E-01	1.42830E-01	2.27440E-02	3.77260E-01	1.14280E-01

X	Y 1	Y 2
C	Al	Si
1.00000E-04	6.00000E+01	4.00000E+01
8.01000E-02	6.52200E+01	3.47800E+01
1.60100E-01	7.14400E+01	2.85600E+01
2.40100E-01	7.89600E+01	2.10400E+01
3.20100E-01	8.62600E+01	1.37400E+01
4.00100E-01	8.62600E+01	1.37400E+01
4.80100E-01	8.62600E+01	1.37400E+01
5.60100E-01	8.62600E+01	1.37400E+01
6.40100E-01	8.62600E+01	1.37400E+01
7.20100E-01	8.62600E+01	1.37400E+01

Input data saved as: a:\alsic3.IGI

Effect of carbon

Temperature: 1300.000 C, Step = 0.000 C
 Pressure: 1.000 bar, Step = 0.000 bar
 Number of Steps: 10

Phase	Species	Temp C	Input mol	Step mol	Activity coefficient	
1	1	Al(g)	25.000	0.000	0.000	1.000
2	1	Al2(g)	25.000	0.000	0.000	1.000
3	1	AlC(g)	25.000	0.000	0.000	1.000
4	1	Ar(g)	25.000	1.000	0.000	1.000
5	1	N2(g)	25.000	1.00000E-10	0.000	1.000
6	1	Si(g)	25.000	0.000	0.000	1.000
7	1	SiC(g)	25.000	0.000	0.000	1.000
8	2	Al	25.000	0.500	0.000	1.000
9	2	Si	25.000	0.500	0.000	1.000
10	3	SiC	25.000	0.000	0.000	1.000
11	3	Si3N4	25.000	0.000	0.000	1.000
12	4	Al4C3	25.000	0.000	0.000	1.000
13	4	AlN	25.000	0.000	0.000	1.000
14	5	C	25.000	1.00000E-04	0.000	1.000

X C	Y 1 Al	Y 2 Si	Y 3 SiC	Y 4 Al4C3
1.00000E-04	4.99970E-01	4.99900E-01	1.00000E-04	1.00000E-36
8.01000E-02	4.99970E-01	4.19900E-01	8.01000E-02	1.00000E-36
1.60100E-01	4.99970E-01	3.39900E-01	1.60100E-01	1.00000E-36
2.40100E-01	4.99970E-01	2.59900E-01	2.40100E-01	1.00000E-36
3.20100E-01	4.99960E-01	1.79900E-01	3.20100E-01	1.00000E-36
4.00100E-01	4.99960E-01	9.99000E-02	4.00100E-01	1.00000E-36
4.80100E-01	4.34280E-01	6.91540E-02	4.30850E-01	1.64180E-02
5.60100E-01	3.46300E-01	5.51430E-02	4.44860E-01	3.84140E-02
6.40100E-01	2.56310E-01	4.11330E-02	4.58870E-01	6.04120E-02
7.20100E-01	1.70320E-01	2.71220E-02	4.72860E-01	8.24070E-02

X C	Y 1 Al	Y 2 Si
1.00000E-04	5.00000E+01	5.00000E+01
8.01000E-02	5.43500E+01	4.56500E+01
1.60100E-01	5.95300E+01	4.04700E+01
2.40100E-01	6.58000E+01	3.42000E+01
3.20100E-01	7.35400E+01	2.64600E+01
4.00100E-01	8.33500E+01	1.66500E+01
4.80100E-01	8.62600E+01	1.37400E+01
5.60100E-01	8.62600E+01	1.37400E+01
6.40100E-01	8.62600E+01	1.37400E+01
7.20100E-01	8.62600E+01	1.37400E+01

Input data saved as: a:\alsic3.igt

Effect of carbon

Temperature: 1300.000 C, Step = 0.000 C
 Pressure: 1.000 bar, Step = 0.000 bar
 Number of Steps: 10

Phase	Species	Temp C	Input mol	Step mol	Activity coefficient	
1	1	Al(g)	25.000	0.000	0.000	1.000
2	1	Al2(g)	25.000	0.000	0.000	1.000
3	1	AlC(g)	25.000	0.000	0.000	1.000
4	1	Ar(g)	25.000	1.000	0.000	1.000
5	1	N2(g)	25.000	1.0000E-10	0.000	1.000
6	1	Si(g)	25.000	0.000	0.000	1.000
7	1	SiC(g)	25.000	0.000	0.000	1.000
8	2	Al	25.000	0.700	0.000	1.000
9	2	Si	25.000	0.300	0.000	1.000
10	3	SiC	25.000	0.000	0.000	1.000
11	3	Si3N4	25.000	0.000	0.000	1.000
12	4	Al4C3	25.000	0.000	0.000	1.000
13	4	AlN	25.000	0.000	0.000	1.000
14	5	C	25.000	1.0000E-04	0.040	1.000

X C	Y 1 Al	Y 2 Si	Y 3 SiC	Y 4 Al4C3
1.00000E-04	6.99960E-01	2.99900E-01	1.00000E-04	1.00000E-36
4.01000E-02	6.99960E-01	2.59900E-01	4.01000E-02	1.00000E-36
8.01000E-02	6.99960E-01	2.19900E-01	8.01000E-02	1.00000E-36
1.20100E-01	6.99960E-01	1.79900E-01	1.20100E-01	1.00000E-36
1.60100E-01	6.99960E-01	1.39900E-01	1.60100E-01	1.00000E-36
2.00100E-01	6.87240E-01	1.09430E-01	1.90570E-01	3.17810E-03
2.40100E-01	6.43250E-01	1.02430E-01	1.97570E-01	1.41760E-02
2.80100E-01	5.99260E-01	9.54240E-02	2.04580E-01	2.51750E-02
3.20100E-01	5.55260E-01	8.84190E-02	2.11580E-01	3.61730E-02
3.60100E-01	5.11270E-01	8.14130E-02	2.18590E-01	4.71710E-02

X C	Y 1 Al	Y 2 Si
1.00000E-04	7.00100E+01	2.99900E+01
4.01000E-02	7.29200E+01	2.70800E+01
8.01000E-02	7.60900E+01	2.39100E+01
1.20100E-01	7.95500E+01	2.04500E+01
1.60100E-01	8.33400E+01	1.66600E+01
2.00100E-01	8.62600E+01	1.37400E+01
2.40100E-01	8.62600E+01	1.37400E+01
2.80100E-01	8.62600E+01	1.37400E+01
3.20100E-01	8.62600E+01	1.37400E+01
3.60100E-01	8.62600E+01	1.37400E+01

APPENDIX 2

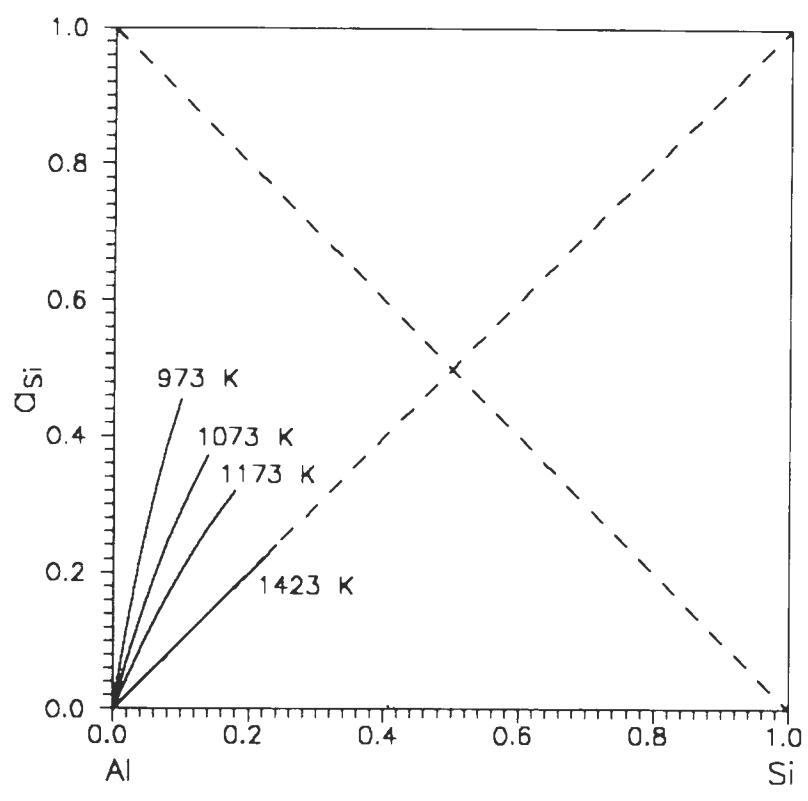


Figure 81 Activity of Si in dilute Al-Si solution